Distribution Agreement

In presenting this thesis or dissertation as a partial fulfillment of the requirements for an advanced degree from Emory University, I hereby grant to Emory University and its agents the non-exclusive license to archive, make accessible, and display my thesis or dissertation in whole or in part in all forms of media, now or hereafter known, including display on the world wide web. I understand that I may select some access restrictions as part of the online submission of this thesis or dissertation. I retain all ownership rights to the copyright of the thesis or dissertation. I also retain the right to use in future works (such as articles or books) all or part of this thesis or dissertation.

_____ _____

James Muse Davis, III Date

The role of the granuloma in bacterial expansion and dissemination during early tuberculosis

James Muse Davis, III
Doctor of Philosophy

Graduate Division of Biological and Biomedical Sciences
Immunology and Molecular Pathogenesis Program

_____ _____

Rafi Ahmed, PhD
Co-advisor

Lalita Ramakrishnan, MBBS, PhD
Co-advisor

_____

Linda R. Gooding, PhD
Committee Member

_____

Iain Shepherd, PhD
Committee Member

_____

Ifor R. Williams, MD/PhD
Committee Member

Accepted:

_____

Lisa A. Tedesco, PhD
Dean of the Graduate School

_____

Date

THE ROLE OF THE GRANULOMA IN BACTERIAL EXPANSION AND DISSEMINATION DURING EARLY TUBERCULOSIS

By

James Muse Davis III
B. Arch., Mississippi State University, 1996

Advisors:
Rafi Ahmed, PhD
Lalita Ramakrishnan, MBBS, PhD

An Abstract of a dissertation submitted to the
Faculty of the Graduate School of Emory University in partial fulfillment of the
requirements for the degree of Doctor of Philosophy

in
Immunology and Molecular Pathogenesis
Graduate Division of Biological and Biomedical Sciences

2009

ABSTRACT

The role of the granuloma in bacterial expansion and dissemination during early tuberculosis

by James Muse Davis III

Despite decades of research, tuberculosis (TB) remains a major human health threat, responsible for approximately 1.5 million deaths each year. An effective vaccine remains elusive despite continuous efforts, and the existing vaccine, BCG, is of questionable efficacy. An additional grave concern is the increased prevalence of multiple-drug resistant strains of Mycobacterium tuberculosis (Mtb), the causative agent of tuberculosis. Most TB research has focused on later, adaptive immune aspects, while less attention has been paid to the early, innate immune reactions. In early infection, infected macrophages aggregate to form immune structures called granulomas, hallmark lesions of tuberculosis. Just prior to graduate school, I established the embryonic zebrafish to model tuberculosis in real-time using fluorescence and Differential Interference Contrast (DIC) microscopy. With this model we found that granuloma formation can be initiated in the context of innate immunity alone. The research detailed here centers on the mechanisms and steps of granuloma formation, which have been difficult to study in other model systems. By comparing mycobacterial pathogenesis in thto embryonic zebrafish infections with other bacterial pathogens, we have confirmed that the host-pathogen interactions observed in this model are each specific to the infecting organism, and quite similar to corresponding human infections with similar pathogens.

Turning to the question of how granulomas form and what consequence they have to early infection, we used intravital microscopy to reveal the distinct steps of granuloma formation and assess their consequence for infection. Intracellular mycobacteria use the ESX-1/RD1 virulence locus to induce recruitment of new macrophages to, and their rapid movement within, nascent granulomas. This motility enables multiple arriving macrophages to efficiently find and phagocytose

infected macrophages undergoing apoptosis, leading to rapid, iterative expansion of infected macrophages and thereby bacterial numbers. Thus, although the cellular responses which make up early granuloma formation--cell migration, chemotaxis, phagocytosis, and apoptosis--might individually restrict bacterial growth, together they are induced by mycobacteria to provide an excellent growth environment. The primary granuloma then seeds secondary granulomas via egress of infected macrophages. Our direct observations provide mechanisms whereby pathogenic mycobacteria exploit the granuloma during the innate immune phase for local expansion and systemic dissemination.

THE ROLE OF THE GRANULOMA IN BACTERIAL EXPANSION AND DISSEMINATION DURING EARLY TUBERCULOSIS

By

James Muse Davis III
B. Arch., Mississippi State University, 1996

Advisors:
Rafi Ahmed, PhD
Lalita Ramakrishnan, MBBS, PhD

A dissertation submitted to the
Faculty of the Graduate School of Emory University in partial fulfillment of the requirements for the degree of
Doctor of Philosophy

in
Immunology and Molecular Pathogenesis
Graduate Division of Biological and Biomedical Sciences

2009

ACKNOWLEDGEMENTS

I would like to acknowledge the late Dr. H. Kirk Ziegler, without whom this research would not have come to fruition. I also thank the Emory MDPhD Program, for the flexibility to allow me to pursue a bicoastal research course. My parents, Muse and Linda Davis are ultimately responsible for the core attitudes, sensibilities, and perseverance I have needed to complete this process. I also thank the labmates and friends, too numerous to name here, who have made the journey possible and worthwhile.

TABLE OF CONTENTS

INDEX OF FIGURES

INDEX OF TABLES

Chapter 1

Introduction to tuberculosis[1]

[1]A portion of this chapter (section 1.7) has been published: Davis JM and Ramakrishnan L (2008). "The very pulse of the machine": the tuberculous granuloma in motion. Immunity **28**(2): 146-8

Despite over a century of medical research, tuberculosis (TB) remains a major human health threat, responsible for approximately 1.5 million deaths worldwide each year (Corbett et al., 2003). Hit hardest by disease are residents of third world countries, immunosuppressed individuals such as AIDS patients, and young children (Corbett et al., 2003). An effective vaccine remains elusive despite continuous efforts (McShane, 2004), and the existing vaccine, BCG, is of questionable efficacy (Fine, 1995). Tuberculosis is treatable with a prolonged regimen of multiple antibiotics, but consistent patient adherence to the full course of therapy is difficult to achieve. An additional grave concern is the increased prevalence of multiple-drug resistant strains of *Mycobacterium tuberculosis* (Mtb), the causative agent of tuberculosis (Espinal, 2003). Given the vast impact of TB to global health, we must gain a better understanding of the immune response to infection with Mtb. The bulk of TB research has focused on later, adaptive immune aspects, while less attention has been paid to the early, innate immune reaction to Mtb in vivo. Because of the nature of those most biologically susceptible—immunosuppressed and pediatric patients, who presumably rely more than others on the innate immune system—a better understanding these earliest events and the immune factors relevant to them is imperative. In addition, it is now clearly understood that innate immune mechanisms are critical in the efficacious development of the subsequent adaptive response.

1.1 Pathogenesis of tuberculosis

Mtb is spread in aerosolized droplets from the sputum of an actively infected person. The inhaled droplets find their way to the terminal alveoli, where the bacteria are phagocytosed by alveolar macrophages. Although some of the mycobacteria are killed, many grow well inside these cells (Dannenberg, 1993; van Crevel et al., 2002). The infected macrophages then migrate out of the airway into interstitial lung tissue, where bacterial replication continues until the death of the host macrophage (Dannenberg, 1993). New macrophages and other cells are recruited to these interstitial sites, and it is thought that these loci develop into granulomas, the characteristic lesions of tuberculosis (Dannenberg, 1993; Glickman and Jacobs, 2001). Classically described, mature granulomas are multicellular structures composed of infected and uninfected macrophages, epithelioid cells (macrophages with tightly apposed membranes circling the lesion), giant cells (multinucleated cells with mostly secretory functions, derived from fused macrophages), T cells and B cells (Flynn and Chan, 2001a).

Outcomes following exposure to Mtb vary. It is presumed a cohort of exposed individuals do not develop infection or disease because the mycobacteria are eradicated by the first encounter with the innate immune system (suggested by epidemiological evidence, but not proven). The vast majority of people infected with TB (as evidenced by a positive tuberculin skin test) are asymptomatic, potentially because their granulomas are effective in preventing active tuberculosis. Those who are asymptomatic and still carry the

bacterium have a 5-10% chance of reactivation disease later in life (Young and Stewart, 2002); in these individuals bacterial replication is held in check for long periods, even years, before active tuberculosis develops (Flynn and Chan, 2001b). Only about five percent of exposed individuals develop active disease shortly after exposure (Young and Stewart, 2002). In these susceptible individuals, granulomas never gain control of the pathogen, and the infection rapidly proceeds to active tuberculosis, with large cavitary lesions in the lungs and release of more infective droplets through coughing. Thus, those exposed to aerosolized Mtb have three possible fates: active disease, control of the pathogen (either by clearing of the initial infection or development of lifelong latent infection), or reactivation following a period of latency.

Research into the pathogenesis of TB has focused broadly on two stages of the infection: the first encounter of the pathogen with host macrophages, studied primarily in cell culture, and the adaptive immune stage of infection control, studied in rabbits, guinea pigs, mice, and non-human primates (Flynn et al., 2005; Orme and Collins, 1994). Studies in vitro have provided a wealth of information about the receptors macrophages use to recognize TB and the mechanism by which this pathogen evades host killing mechanisms after phagocytosis (Ernst, 1998; Flynn and Chan, 2003). In vivo models have been used to elucidate which cytokines and other host factors are most required for general protection in terms of end-stage measures of infection such as bacterial burden and histopathology. In mammalian models of tuberculosis it has proven

difficult to study the phases of infection following initial phagocytosis by macrophages, in particular the early events of granuloma establishment, before the onset of the adaptive immune response. This period lasts roughly 14 days in mice, but since the lesions at this time are difficult to find histologically and the bacteria are so sparse, observations of this period are seldom made (Flynn et al., 2005). In general, it has been assumed that the innate immune system is ineffective in controlling infection since bacterial numbers increase exponentially during the first two weeks of TB infection of mice (Musa et al., 1987) and rabbits (Dannenberg, 1993). However, the steps by which granulomas arise and the mechanisms of bacterial dissemination remain poorly understood.

1.2 The macrophage in tuberculosis

Macrophages are both the first cell type to encounter mycobacteria and the primary host cell for mycobacterial replication. The study of cultured macrophages has been key to understanding early events of TB including phagocytosis, evasion of intracellular killing and pathogen recognition.

Phagocytosis Mtb enters macrophages by binding to a variety of receptors (Ernst, 1998), and is readily phagocytosed in vitro. Complement receptors (CR) are the major entry point for Mtb, as shown by in vitro experiments with human macrophages and monocytes. In the absence of CR3, phagocytosis of Mtb by these cells is reduced by 70-80% (Schlesinger, 1993; Schlesinger et al., 1990). Mtb also binds directly to C2a, allowing entry via CR1 (Schorey and Cooper,

2003), and unopsonized Mtb can bind to CR3 (Cywes et al., 1997) and CR4 (Zaffran and Ellner, 1997). The macrophage Mannose Receptor (MR) is another major entry point for Mtb (Schlesinger, 1993; Schlesinger et al., 1996), along with the type A scavenger receptor (Zimmerli et al., 1996). The receptor of entry makes a difference in cellular response, as Fcγ receptors, though they play a relatively minor role in Mtb phagocytosis (Armstrong and Hart, 1975), induce a stronger inflammatory response when used compared to other receptors (Aderem and Underhill, 1999). More virulent strains are more likely to enter via MR (Schlesinger, 1993). This difference is likely to be meaningful, as signaling by this receptor on binding Mtb is anti-inflammatory (Nigou et al., 2001) and does not result in production of reactive oxygen intermediates (Astarie-Dequeker et al., 1999). Also, Mtb phagocytosed via CR1 shows better intracellular survival than Mtb taken in by CR3 or CR4 (Da Silva et al., 1989).

Virulent strains of Mtb replicate inside macrophages and epithelial cells (Shepard, 1957a; Shepard, 1957b) in part by modifying their phagocytic compartment to prevent phago-lysosomal fusion (Hart et al., 1972) and acidification (Sturgill-Koszycki et al., 1994) (reviewed in (Russell et al., 2002)). Mtb-containing phagosomes interact with other host cell membranes, and carry a mixture of membrane components of the cell surface and of early endosomes (Russell et al., 2002). This customized compartment is also somewhat permeable, as proteins and lipids of Mtb are able to diffuse into the cytosol (Beatty and Russell, 2000). These molecules may be extruded from the cell by

exocytosis, and also appear in uninfected cells nearby (Beatty et al., 2000; Beatty et al., 2001). The pathway by which these mycobacterial products are dispersed likely plays a role in the processing and presentation of epitopes of Mtb on MHC I (Flynn and Chan, 2001a).

Pathogen Recognition Toll-Like Receptors (TLRs) have been thought to represent a major link between the innate and adaptive immune responses to MTB, but the details of how this family of pathogen receptors might impact TB pathogenesis are still being worked out (Krutzik et al., 2001; Salgame, 2005). To date, there is evidence only for TLR2, and perhaps TLR9 having a measurable role in the TB immunity; mice lacking MyD88, the conserved intracellular adaptor for all TLRs, are also severely susceptible to mycobacterial infection (Fremond et al., 2004; Scanga et al., 2004). TLR2-deficient mice succumb to infection somewhat more rapidly than wild-type mice (Drennan et al., 2004). TLR2 participates in recognition of many gram-positive bacterial cell wall components, but the mechanism by which the loss of this gene results in susceptibility to TB is under debate. It is thought that particular lipids and the 19kDa lipoprotein of MTB produce a pro-inflammatory signal via TLR2 (Krutzik et al., 2001). However, recent studies suggest an anti-inflammatory role for this signal, as IL-10 upregulation after infection is lost by dendritic cells derived from TLR2-/- mice, although IL-12 upregulation remains intact (Jang et al., 2004). In accordance with this observation, the histopathology of TLR2-/- mice suggests an excessively inflammatory response (Drennan et al., 2004). There is new evidence that TLR9

has an important role in TB, as TLR9 knockout and TLR2/TLR9 double knockout mice are increasingly susceptible (Bafica et al., 2005). In contrast to TLR2 and TLR9, mice deficient in TLR4 or TLR6 are as susceptible to infection as wild-type animals (Reiling et al., 2002; Sugawara et al., 2003). It is likely that different TLR family members are important at distinct stages of infection (e.g. pathogen recognition as well as modulation of the adaptive immune response) which has made interpretation of the knockout mouse experiments even more complicated. Despite the considerable excitement generated over the role of TLRs in immunity, more recent evidence in humans suggests that this group of receptors may have a very narrow or redundant role in human disease (Picard et al., 2003; von Bernuth et al., 2008), in contrast to their fascinating importance and specificity in mice.

Beyond TLRs, other receptors have been shown to be involved in the recognition of MTB and determining the ensuing immune response. Plasma LPS-binding protein (LBP) recognizes lipoarabinomannan (LAM) and transfers it to CD14 on the cell surface (Fenton and Golenbock, 1998). There is also evidence that DC-SIGN, the C-type lectin receptor, provides a privileged site of entry to dendritic cells (Tailleux et al., 2003) and alveolar macrophages (Tailleux et al., 2005).

1.3 Granuloma Formation

1.3.1 Granuloma Formation—the Transition from Innate to Adaptive Immunity to Mtb

During the first ten to fourteen days of infection, intracellular bacteria expand in numbers, and the alveolar macrophages originally containing the invading bacteria die, either by mycobacteria-induced apoptosis (Kornfeld et al., 1999) or by expansion of intracellular bacteria followed by lysis (van Crevel et al., 2002). The bacteria, now in greater numbers, are re-phagocytosed by recently arrived macrophages recruited to the site by chemokines (see below), and the lesion grows. TNF expression by the increasing number of infected macrophages in turn is thought to induce even more chemokine expression, and influx of monocyte-derived macrophages continues (Algood et al., 2003). This cycle of macrophage infection and recruitment is thought to continue until the advent of an adaptive immune response. Work in the zebrafish model of tuberculosis suggests that granuloma formation is not impaired by loss of TNF, and its primary role is in preventing bacterial growth and macrophage death (Clay et al., 2008). By this reasoning, another upstream initiator of chemokine expression must be found.

Dendritic cells called to the site of infection eventually migrate to local lymph nodes to initiate T cell activation, and killing of mycobacteria in significant numbers is thought to occur only after CD4+ lymphocytes arrive to activate granuloma macrophages with IFN-γ. The granulomas have matured by this time

and contain a variety of cells, including epithelioid macrophages and giant cells, both thought to be derived from monocytes. Other cells include T cells of both CD4+ and CD8+ subtype, γδ T cells, B cells, NK cells, and eosinophils (Adams, 1976; Dannenberg, 1993). The ultrastructure of the granuloma evolves as well, developing a layer of epithelioid macrophages surrounding a caseous center presumed to contain dead macrophages and both living and dead bacteria. It is unclear when these architectural changes occur relative to the arrival of lymphocytes and other cells, what signals they require, and how they contribute to bacterial containment.

The finding that inhibition of TNFα after granuloma formation results in their disorganization (Moreira et al., 1997) suggests that these lesions require active maintenance. This complicates the interpretation of in vivo studies which use granuloma morphology at necropsy to infer what host factors are important for granuloma formation, since deficits in granuloma formation and maintenance cannot be distinguished. Supporting this contention that the mature granuloma is dynamic are observations that granulomas in adult fish and frogs readily incorporate new bacteria, and even phagocytosed beads (Cosma et al., 2004). This suggests that granuloma maintenance is not as simple as maintaining a static structure. The zebrafish embryo has proven an excellent model for answering these questions.

1.3.2 Granuloma formation—the role of cytokines and chemokines

The transition from single infected macrophage to nascent granuloma has long been difficult observe directly, but it is generally believed that single infected macrophages travel into the parenchymal tissue before settling at the location that will become a granuloma (Dannenberg, 1993). Mtb induces macrophages to upregulate many genes, most notably TNF, IL-10 and IL-12 (Flynn and Chan, 2001a) (although there is evidence for virulent strains downregulating IL-12 as well (Post et al., 2001)). TNF is critically important in the immune response to Mtb; deficiency (Mohan et al., 2001) or excess (Moreira et al., 1997) can both lead to increased susceptibility to mycobacterial infection. Specifically, deficiency of TNF leads to poorly formed granulomas in late pathogenesis, suggesting it is a key factor in the formation and/or maintenance of granulomas. IL-12-deficient mice succumb rapidly to TB (Moreira et al., 1997), and this cytokine is extremely important in invoking the Th1 type immune response essential to a protective response (Salgame, 2005). IL-12 synergizes with TNF to induce IFNγ induction in T cells (van Crevel et al., 2002), and there are several instances of increased human susceptibility to TB based on genetic changes in the IL-12-IFNγ signal transduction pathways (Casanova and Abel, 2002).

Mycobacterial uptake induces macrophages to transcribe a variety of chemokines, including CCL2 (MCP-1), CCL3 (MIP1α), CCL4 (MIP1β), CCL5 (RANTES), CCL7 (MCP-3), and CXCL10 (IP10) (Algood et al., 2003; Orme and Cooper, 1999; Rhoades et al., 1995). In vivo, these chemokines are responsible for the recruitment additional cells, including monocyte-derived macrophages and

eventually T cells expressing CCR2 (which binds CCL2, CCL8, CCL7, CCL12 and CCL13) and CCR5 (which binds CCL3, CCL4, and CCL5). TNF also induces macrophages to transcribe chemokines, amplifying the chemokine induction initiated by infection. CCR2 knockout mice are more susceptible to Mtb than wild-type mice and show a delay in the arrival of T lymphocytes to the lungs (Peters et al., 2001; Scott and Flynn, 2002). Knockouts of other chemokine receptors have not resulted in Mtb-sensitive phenotypes. CCR5-/- mice were no more susceptible than wild-type mice, although they did produce more extensive cellular infiltrate in the lungs (Algood and Flynn, 2004). CXCR3-/- mice were also unaltered in their susceptibility to infection, but featured fewer and smaller granulomas (Seiler et al., 2003). The redundancy of chemokines and their receptors, the histopathological differences described in their response to Mtb, and the difficulty of isolating which stage of infection is affected, suggests these chemokine receptors may still impact early pathogenesis.

1.3.3 Granuloma formation—the role of regulated cell-cell adhesion

Cell adhesion molecules play roles in many microbial infections (Kerr, 1999). Genes involved in cell-cell adhesion are also induced by phagocytosis of Mtb and by subsequent exposure to TNF. ICAM-1 and LFA-1 are both upregulated during mycobacterial infection (DesJardin et al., 2002), and E-cadherin is expressed in innate granulomas in the zebrafish embryo (Tobin and Ramakrishnan, unpublished results). Regulation of cell-cell adhesion, by expression and post-

translational modification of adhesion molecules, is likely to be central to the ontogeny of granulomas, but research in this area of tuberculosis is just beginning. Proteolysis of adhesion molecules may be particularly salient to granuloma remodeling and dissemination of infection (Volkman, Pozos and Ramakrishnan, unpublished). Matrix metalloproteinases (MMPs), endopeptidases produced by a variety of cell types, are likely candidate proteases to regulate a variety of adhesion events important in tuberculosis. These enzymes cleave both extracellular matrix (ECM) products as well as adhesion molecules such as E and N-cadherin (Parks et al., 2004), facilitating cell migration (Parks et al., 2004). Relevant to granuloma dynamics, various members of the MMP family cleave chemokines, in some cases activating them and in others inactivating them (Li et al., 2002; McQuibban et al., 2002). They can also activate or inhibit cytokines such as TNF and IL-1β (Black et al., 1997; Gearing et al., 1994; Ito et al., 1996). Another report shows that treating TB-infected mice with an MMP inhibitor disrupts granuloma formation (Izzo et al., 2004). Finally, several MMPs are upregulated in response to Mtb infection (Keller et al., 2004; Quiding-Jarbrink et al., 2001). Research in our laboratory uses *Mycobacterium marinum* infection of zebrafish embryos as a model of early TB pathogenesis, and we have found MMPs upregulated during infection in this model as well (Volkman, Pozos and Ramakrishnan, unpublished).

Another adhesion molecule implicated in granuloma formation and mycobacterial pathogenesis is CD44. CD44 is expressed on many cells which

arrive to the lungs during TB pathogenesis, including macrophages and T lymphocytes (Griffin and Orme, 1994). Macrophages use CD44 as a receptor for mycobacteria (Leemans et al., 2003) as well as for the ECM protein hyaluronate (Ponta et al., 2003), suggesting a role for this molecule in both phagocytosis and trafficking of macrophages and other cells to granulomas. CD44-/- mice form poorly organized granulomas in TB infection (Schmits et al., 1997).

1.4 The embryonic zebrafish model of tuberculosis

The following is a brief introduction to the zebrafish as a model host for studying tuberculosis. A more detailed account of the model appears in Chapter Two. The development in our laboratory of the zebrafish embryonic model of infection has given new access to the earliest events of TB pathogenesis and granuloma formation. Embryonic macrophages capable of phagocytosis and killing of nonpathogenic bacteria appear in the zebrafish by 28 hours post-fertilization (pf) (Herbomel et al., 1999). Despite their capacity to kill *E. coli* and *B. subtilis* (Herbomel et al., 1999) they phagocytose but seldom kill *M. marinum* (Davis et al., 2002), which is a close genetic relative of Mtb (Tonjum et al., 1998).

M. marinum is a natural pathogen of a variety of cold-blooded animals, including the zebrafish (Clark and Shepard, 1963). Pathogenesis of the infection in aquaria is not worked out in detail, but the resulting pathology bears many striking resemblances to human tuberculosis. Like human TB, and unlike that of mice, mature granulomas formed in the adult zebrafish contain a center of

caseous necrosis. Lesions appear most in the liver, kidney, spleen and neural tissue, and even light doses prove fatal in approximately four months (Swaim et al., 2006). Horizontal spread is efficient, as entire tanks can be affected in a short time (Westerfield, 2000).

1.5 M. marinum Infection of Zebrafish Embryos

When *M. marinum* is injected into the caudal vein of zebrafish embryos shortly after the onset of circulation (~32 hours pf), they are phagocytosed within hours and carried throughout the tissues of the embryo within migrating macrophages (Davis et al., 2002). After two to five days (depending on the amount of bacteria introduced), infected macrophages begin to coalesce, along with uninfected macrophages, into lesions with many similarities to classical mammalian granulomas, with multinucleated giant cells and cells with tightly apposed membranes like those of epithelioid macrophages (Davis et al., 2002). In addition, the activation of *gaps*–granuloma activated promoters—by the bacteria in these zebrafish lesions further supports the similarity of these zebrafish lesions to classical granulomas (Davis et al., 2002). The gaps, which are not induced in vitro, were discovered in a promoter trap screen using *M. marinum* infection of adult frogs (Ramakrishnan et al., 2000). Lymphocytes do not appear in the circulation of embryonic zebrafish until approximately 21 days post-fertilization (Trede et al., 2001; Willett et al., 1997). Induction of gaps in zebrafish embryos

before the developmental appearance of adaptive immunity suggests that the bacterial response to granulomas does not require adaptive immune cells.

Not only do mycobacteria have genes expressed specifically in granulomas, they also have genes which cue the initiation of granuloma formation. RD1 (region of difference 1) is the largest of the genetic loci missing in the nonpathogenic BCG strain of *M. bovis* (the existing TB vaccine) but present wild-type, virulent strains of Mtb (Mahairas et al., 1996). Mtb strains lacking RD1 are attenuated for growth in mice, but the mouse experiments did not clarify the temporal stage of infection affected (Lewis et al., 2003). Using *M. marinum* lacking RD1 to infect zebrafish embryos, Volkman et. al. demonstrated that loss of RD1 greatly reduced the ability of *M. marinum* to elicit granuloma formation (Volkman et al., 2004). Co-infection with wild type bacteria, or the addition of wild-type bacteria later in pathogenesis, rescued the granuloma-forming phenotype, suggesting that the mutant strain cannot produce a secreted bacterial factor or factors important for granuloma formation. Furthermore, the dramatic increase in bacterial replication which begins shortly after granuloma formation in wild-type infection does not occur in infections with the RD1 strain. Therefore bacterial growth appears to be facilitated by early granuloma formation. These observations raise important questions as to the nature of the early granuloma, since a variety of non-living and even inorganic materials are capable of initiating macrophage aggregation (Epstein and Fukuyama, 1989). First, do the granulomas that result from the mere irritation of foreign bodies differ

significantly from granulomas induced by live bacteria? Second, are there unique features of mycobacterial granulomas that are specifically favorable to the mycobacterial growth, i.e. do granulomas provide a niche for enhanced bacterial replication in addition to their known role in controlling the spread of disease throughout the host? This particular question is confronted in Chapter Five.

Other experiments using *M. marinum*, infecting both adult zebrafish and adult frogs, have uncovered another unexpected aspect of the tuberculous granuloma. While granulomas are considered to be efforts by the host to 'wall off' infections or materials which cannot be eradicated, Cosma et al (Cosma et al., 2004) have shown that granulomas in fish and frogs freely allow the entrance of macrophages infected with mycobacteria from the outside. Previous work in rabbits had shown that macrophages continually arrive at established granulomas (Dannenberg, 1993), but this was thought to represent maintenance of the lesion in the face of macrophage death. The ramifications of this permeability in granulomas await further investigation in the zebrafish embryo model. One implication, as stated above, is that the granuloma provides a haven for mycobacteria adapted to them, and further attracts infected macrophages, continuing the expansion of the lesion. I will examine this possibility in Chapter Five.

1.6 Questions in granuloma formation, maintenance, and spread

The current understanding of granuloma formation is based entirely upon in vitro studies and mammalian infection studies. As such there are areas of investigation that have not been technically possible, and parts of the story are incomplete. Mammalian studies thus far have relied upon fixed tissue for investigations of granuloma formation, allowing each animal and each lesion to be visualized only once. A host of questions remains which require the study of granuloma dynamics in vivo.

The original inoculum of Mtb in natural human infection is likely quite small, constrained in part by the size the droplets capable of reaching the deep tissues where alveolar macrophages are. Because of this, each original infected macrophage contains only one or two bacteria. In the aerosol route of experimental Mtb infection of mice, each mouse receives ~100 CFU of bacteria. According to the current view of granuloma formation, each of those would result in one infected macrophage, which would migrate and each establish one granuloma. However, many hundreds of granulomas are found when the disease has run its course. How do the lesions multiply and disseminate?

Another conundrum lies in the location of lesions. Inhaled foreign bodies like the droplets required for spread of TB typically settle in the lower lobes of the lung, but the classic location for most TB lesions on X-ray is the upper lobes. The expansion in number of granulomas may be explained by tissue rupture and

hematogenous spread but the paucity of lesions in the original site of implantation has no such answer.

The zebrafish model provides direct observation of early granuloma formation and continual tracking of the same lesion over a period of days. Thus far we have shown that morphologic differentiation of macrophages within granulomas occurs prior to the arrival and activity of activated lymphocytes. What further similarity innate granulomas have with later, mature granulomas is still under investigation. We have observed that innate granulomas are dynamic, with departure of infected macrophages from some lesions, and complete dissolution of others. These observations contradict expectations that that bacterial growth is completely unchecked in the period of innate immunity. Also suggested are mechanisms by which granulomas may proliferate and spread to new locations away from the sites of implantation.

1.7 In vivo imaging of tuberculosis pathogenesis

Ilya Metchnikov published his observations of macrophages in action 116 years ago, ten years after Robert Koch had established *Mycobacterium tuberculosis* (Mtb) as the causative agent of tuberculosis (TB). These findings have since become linked by the appreciation that mycobacteria are inveterate macrophage pathogens, having evolved to circumvent and even exploit these key immune effector cells (Clay et al., 2007). Direct observation of immune cells in action has since become far more detailed, thanks to the invention of new microscope

technology and the software necessary to explore image data in three and even four dimensions (Bajenoff and Germain, 2007). During the same time frame, tuberculosis has been under more or less continuous study, but despite advances in antibiotic therapy, remains as intractable a global health problem as ever with the advent of increasingly drug-resistant Mtb strains. Setting aside the obvious public health, social and economic failures to control TB, its continued status as the "Captain of all Men of Death" stems from the inexplicable persistence of Mtb in the face of an apparently solid immune response and vaccination with *Mycobacterium bovis* Bacillus Calmette-Guérin (BCG), the world's most widely used yet relatively ineffective vaccine. An emerging body of work utilizing the power of in vivo imaging has begun to shed light on the arguable center of the mystery: the granuloma (Bajenoff and Germain, 2007; Davis et al., 2002; Volkman et al., 2004). The recent study by Egen et al., (Egen et al., 2008) further cracks open the secrets of TB. It extends the previous studies on early granuloma formation to examine the granuloma live as adaptive immunity develops .

What then are granulomas? These complex organized immunological structures are comprised of differentiated, interdigitated macrophages (the so called epithelioid cells) that are subsequently joined by other immune cells such as T and B lymphocytes and NK cells (Adams, 1976). Granulomas form in humans in response to a variety of persistent stimuli, be they pathogens (e.g. *Mycobacteria* and *Brucella*) or foreign bodies, as well as in certain mystery

diseases such as sarcoidosis. Tuberculosis is by far the most prevalent cause of human granulomas world-wide, such that the pathologist's finding of granulomas promptly sets off a search for signs of tuberculosis. Tuberculous infection is initiated in humans by airborne Mtb within cough droplets that gain access to the deepest alveoli of a victim's lungs, where the bacterium is phagocytosed by alveolar macrophages and dendritic cells (Dannenberg, 1993). Frequently failing to kill their new cargo, these cells serve as effective transporters of the bacteria from the airway into deeper tissues (Clay et al., 2007), where they soon aggregate into granulomas. Live imaging studies in the transparent developing zebrafish infected with *Mycobacterium marinum*, a close genetic relative of Mtb, have shown that granulomas can form as a result of mycobacterial interactions with innate immunity alone (Davis et al., 2002). Adaptive immune elements then come into play but mysteriously even the resultant bolstered response can fail to eradicate these organisms, suggesting that mycobacteria may counter or even usurp a full range of host defenses (Flynn, 2006). For years it has been thought that tuberculous granulomas, like foreign body granulomas, at least serve as an encircling barrier to 'wall off' material which cannot be destroyed--a view that this study, along with other recent ones, shows is simplistic (Cosma et al., 2004; Davis et al., 2002; Egen et al., 2008; Volkman et al., 2004).

Granuloma formation and maintenance is an area ripe for in vivo imaging studies. First, it is not clear exactly how infected macrophages give rise to granulomas. The initial inoculum of Mtb can be exceedingly small, perhaps even

fewer than 10 organisms, so that infection of a single macrophage might well be sufficient to establish infection. How would single macrophages so lightly infected give rise to granulomas which contain hundreds of immune cells and many more bacteria? Do single infected macrophages simply attract more macrophages to achieve a critical mass of infectable cells? What induces these infected macrophages to become “granulomagenic?” The mycobacterial RD1 secretion system, a virulence determinant, is required to induce granuloma formation but the mode (e.g. cell migration, infection, or adhesion) and mechanism are not clear (Volkman et al., 2004). Moreover the source of new macrophages (local versus systemic, tissue versus blood-borne) is not clear. The picture becomes increasingly murky as the granuloma matures and other immune cell types appear in the granuloma. When and in what numbers do they arrive? Is their order and number critical to the maturation of the lesion, or to the outcome of infection? Are granulomas permanent structures, or do they come and go in different locations during the years in which the average infected human is thought to harbor infection? Finally, which, if any, of these steps are susceptible to intervention? Visual evidence, and especially live, timelapsed evidence, will be key to asking and answering these questions.

The developing zebrafish has provided insights into the early innate immune phases of macrophage migration and granuloma formation (Clay et al., 2007; Davis et al., 2002; Volkman et al., 2004) but the later adaptive immune phase of infection has until now not been visualized. For this later stage of

granuloma formation, the mouse with its plentiful immunological reagents and strains has distinct advantages as a model organism. In an impressive technical display, Egen et al have used the mouse to produce the first live images of mycobacterial infection in a mammalian host. Although the lung is generally the subject of study in the mouse model of tuberculosis, its constant movement, practically a condition for physiologic normalcy, makes it unsuitable for timelapsed imaging under the microscope. To overcome this problem, these authors used intravenous infection to initiate granulomas in the liver. Also, Mtb work requires dedicated biosafety level 3 (BSL3) facilities so these authors have resorted to using a large inoculum of the attenuated BCG vaccine strain (requiring only BSL2 containment) to produce a persistent infection with granulomas numerous enough to be found under the microscope without difficulty.

In a series of intricately clever manipulations of transgenic mice and 3D timelapse microscopy, Egen et al. demonstrate that bloodborne BCG is rapidly taken up by Kupffer cells, the resident macrophages of the liver (Figure 1.1 part 1). Both the infected cells and the invading bacteria appear to survive well over time, and after several days, aggregates consisting of the original infected Kupffer cells, recruited Kupffer cells and monocyte-derived macrophages are visible (Figure 1.1 part 2). These myeloid cells are not very motile, although their membranes do appear to be in constant flux. The precise details of this phase must be interpreted with caution as BCG is attenuated and lacks the RD1

determinant that has been found to enhance macrophage aggregation into granulomas (Volkman et al., 2004). Consistent with its attenuation, there is little or no net bacterial growth in the first three weeks of infection, a period when pathogenic mycobacteria grow logarithmically in their hosts, exemplified by Mtb in mice (Flynn, 2006).

To probe granuloma dynamics further, the authors perform TNF blockade of established granulomas and within four days find smaller lesions with reduced macrophage numbers. Immunofluorescence histology reveals that TNF blockade does not alter the number of infected macrophages in the lesion. The selective loss of uninfected macrophages has several possible explanations: the treatment could lead to a reduced migration of new uninfected macrophages to the lesion, or differentially affect the retention or survival of infected vs. uninfected macrophages. These possible mechanisms and their effects on pathogenesis can be explored further using this and other in vivo models.

It is the movement and behavior of T lymphocytes in granulomas which provide the most intriguing findings of this study. These cells, which arrive at the granulomas within days (Figure 1.1 part 2), are in constant motion throughout the lesion. Their motion is such that each lymphocyte appears to wander through the entire granuloma, likely making direct contact with most of its macrophages (Figure 1.1 part 3). This finding begs the question of how antigen-specific T lymphocytes would behave. Would they make more prolonged contacts with macrophages expressing the relevant antigen? The mechanics of the interaction

between arriving T cells and the macrophage matrix are of particular interest. Activated T lymphocytes readily enter lesions but they appear restrained from leaving so that they accumulate therein. Egen et al. propose that this retention of T cells is due to the macrophages acting as a scaffold upon which the lymphocytes crawl, rather than to a physical barrier to departure (Figure 1.1 part 4). This model is similar to that proposed by this same group for T cells migrating within lymph nodes (Bajenoff and Germain, 2007). It has been suggested that the granuloma may serve as a form of tertiary lymphoid organ (Ulrichs et al., 2004), and these new data add to that discussion. After TNF blockade, T lymphocytes are still found in granulomas in reduced numbers. This reduction may be due to the overall reduction in granuloma size after anti-TNF treatment.

The emerging picture of the granuloma as a tight accumulation of macrophages which serves to support T cell migration and contact—with infected cells, with each other, with some unseen cell type—is a revealing one indeed. Observations of early, innate immune granuloma formation have suggested a highly dynamic lesion, with constant innate cell motility (Davis et al., 2002). Egen et al. similarly find an adaptive immune-stage granuloma in constant motion. The ultimate contribution of all this motion and action to pathogenesis will only be known after further study; however, this report adds convincingly to the argument that the granuloma cannot be thought of as simply a barricade to contain mycobacteria, even after adaptive immunity is established.

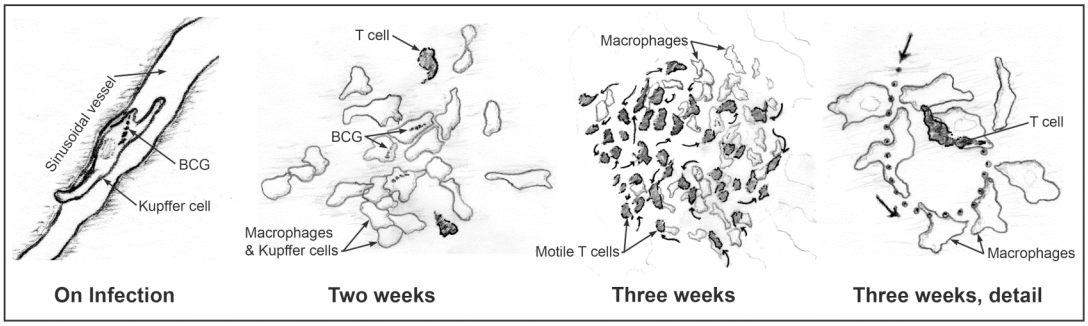

Figure 1.1 Stages of BCG granuloma formation in the mouse liver. Upon infection, blood-borne bacteria are phagocytosed by resident Kupffer cells. At two weeks after infection, infected Kupffer cells have attracted local resident macrophages and monocyte-derived macrophages. Arriving T lymphocytes are also seen. By three weeks after infection, T cells are plentiful among the macrophages. T cells migrate in constant contact with a 'scaffold' of macrophages.

Chapter 2

Introduction to the zebrafish as a model of host-pathogen interaction[1]

[1] This chapter has been submitted as a chapter in *Phagocyte-Pathogen Interactions*, Russell and Gordon, eds., ASM Press, in preparation.

2.1 Why Zebrafish? Strengths and weaknesses as a model of host-pathogen interactions.

As with any new model system, the sheer novelty is initially enough to excite great enthusiasm (or disdain), often out of proportion to what the system has to offer. The zebrafish as a model for host-pathogen interactions has now matured to the point that we can reflect on what it truly has to offer, where it is helpful, and how it complements other models. As a model for the study of early development, the zebrafish came to prominence because of the easy access to early events (hundreds of developing embryos developing outside the mother, in simple conditions), and the speed with which they take place (from fertilization to a semi-motile organism in 36 hours, to a feeding larva in five days) (Westerfield, 2000). Seizing on these advantages, huge strides have been made to propel the zebrafish model forward through the development of imaging and fixation techniques, and forward and reverse genetics. Only after these vast amounts of work had been done by developmental biologists did the study of infection in the zebrafish become so attractive. As it stands now, the chief advantages afforded by this model range from the practical, to the genetic, to the observational.

Practical advantages mainly relate to the relatively low cost and ease of husbandry and breeding. Thousands of fish can be kept in a room that would hold only one or two hundred mice. Importantly, many different strains can be housed efficiently in these small spaces by using small tanks that can fit along side large tanks in the same racks. A female fish can lay several hundred eggs

at once, most of which develop to maturity. Several breeding pairs can be set up in a small space so that progeny of different fish mutant or reporter lines can be obtained or crossed at one time. Ethical and regulatory issues can be less constraining than for mouse research especially when fish embryos and larvae are involved. The zebrafish embryo is not considered to be a vertebrate until after hatching or even beyond, the exact window of time for this dispensation varying between institutions.

The genetic advantages of zebrafish are often considered the strongest. Forward genetic screens are relatively easy again due to the large number of progeny derived and the speed with which they can be assessed. Chemical mutagenesis with N-ethyl-N-nitrosourea (ENU) is the most popular method but some laboratories have developed techniques for retroviral insertion mutagenesis (Patton and Zon, 2001). Additional screening techniques, such as the creation of gynecogenetic diploids (the production of offspring from only maternal DNA) allow for the screening of recessive mutations in the second generation, cutting down on one generation from the classical Mendelian screens. The more recent availability of transgenic technologies and resultant lines with fluorescently marked cells of different lineages has allowed for the full use of visualization techniques for more rapid and increasingly sophisticated screens, such as for cell migration phenotypes. The zebrafish genome is in the final stages of annotation (www.sanger.ac.uk/Projects/D_rerio), so that mutant mapping is progressively easier. Excelling thus in forward genetics, the zebrafish had thus far

complemented the mouse model which offers reverse genetics by homologous recombination into and implantation of embryonic stem cells. However, new tricks are being employed to correct this deficiency in the zebrafish: mutants in desired genes are produced by a variety of methods (Skromne and Prince, 2008). In addition, transient gene knock-downs are readily created by injecting modified antisense oligonucleotides (Morpholinos) into very early stage embryos (Nasevicius and Ekker, 2000). Morpholino technology makes for a rapid and relatively inexpensive tool for the study of gene function for up to seven to ten days of life.

With chemical biology and genetics coming to the forefront as ways to probe biological processes including host pathogen interactions (Hung et al., 2005), we note that the zebrafish is eminently suited for such small molecule screens. Their aquatic habitat allows for the small molecule to simply be placed in the water. This advantage is highlighted when using larvae that can be placed in 96-well plates for a high throughput screen, and a variety of reagents with known molecular actions are in use (Skromne and Prince, 2008). Such an approach has been elegantly used to find and characterize a small molecule that reverses a genetic defect leading to coarctation of aorta even when administered for six hours during early development (Peterson et al., 2004). The power of this model to find relevant drugs for both developmental abnormalities and pathogenic processes has extraordinary potential.

The zebrafish embryo is naturally pigmentless for the first 24 hours of life, and this see-through state can be extended for seven to ten days by treatment with phenylthiourea (Westerfield, 2000) that has few other discernible consequences. It is this transparency that has allowed the direct viewing of development both normal and abnormal (Kimmel et al., 1995) and has allowed the detailed studies of hematopoietic and immune cell development as will be detailed in the following sections (Traver et al., 2003). This transparency alone allowed the excellent early studies of the zebrafish embryonic macrophage (Herbomel et al., 1999; Herbomel et al., 2001), but when combined with fluorescent reagents or with transgenic fish strains, it allows an unprecedented view into the pathogenesis of a variety of diseases (Langenau et al., 2003; Mathias et al., 2007; Mathias et al., 2006; Meijer et al., 2007). Because both the overall organism and also small areas can be imaged repeatedly with minimal harm to the embryo, this model goes far beyond the endpoint bacterial counts and postmortem morphology available in more conventional animal models. In addition, some vital dyes are capable of penetration by simple soaking (Cooper et al., 2005; Santos et al., 2006), or intravenous injection, allowing in vivo high resolution visualization of structures previously seen only in cultured cells. The observational advantages come mostly with the use of the transparent early stages, though transparent adults are being developed as they have been for medaka (Broussard and Ennis, 2007; Wakamatsu et al., 2001; White et al., 2008).

The zebrafish model presents notable difficulties as well. One issue plaguing the use of the zebrafish to study immunology is the relative paucity of immunological reagents. While the available genetic tools, as mentioned above, are impressive, fish-specific antibodies have been slow in coming. Some existing mouse antibodies do identify homologous fish proteins, but the zebrafish is a long way from enjoying the number of reagents available for mouse work. Publication of successful monoclonal production (Crosnier et al., 2005) and the efforts of private companies (e.g. Phylonics) show that this deficiency may not be permanent. Owing to the small size of zebrafish and the lack of inbred lines, cell transfer and reconstitution experiments that have been the backbone of cellular immunology in the mouse model are not yet facile although some techniques have been developed (Langenau et al., 2004). Finally, it is thought that the remnants of at least one whole genome duplication exist in many fishes including zebrafish. The large number of *hox* genes present in zebrafish is a famous example of this (Amores et al., 1998; Jozefowicz et al., 2003), as is the duplication of granulin and interferon gamma genes discussed below. When taking advantage of the genetic accessibility of this species therefore, it is important to beware of duplicates.

2.2 Overview of the immune system of the zebrafish

Zebrafish immunology as a field is only about fifteen years old, but researchers can also draw upon functional immunology studies in other teleost

fish[taxonomy footnote] such as trout, catfish, and sea bass which appear to have very similar immune systems and have been under study for decades. The zebrafish immune system has been reviewed in detail (Traver et al., 2003; Trede et al., 2004). The major features of mammalian innate and adaptive immunity are represented in fish including the complement system, chemokines, cytokines and adhesion molecules. The different types of phagocytes and B and T lymphocytes are found as are MHC Class I and II molecules. Some components, such as T lymphocyte subset markers, have as yet only been identified in silico. Innate immunity develops earlier in ontogeny than adaptive immunity, similar to the case with mammals. Because the early innate-only stages of the zebrafish are accessible to experimentation, one can use this aspect of the developmental program to isolate the contribution of innate and adaptive immunity to pathogenesis (Davis et al., 2002). As expected there may well be differences in the relative contribution of some immune determinants to immune function in mammals and fish. For instance, the complement system is more polymorphic in fish than in mammals and components such as C3 and B are present as multiple copies in the zebrafish, leading to the speculation that complement may allow the recognition of a broader range of pathogens by innate immunity in the fish and compensate for the relatively minor (as compared to mammals) antibody response which fish generate. In this context it is interesting to note that there is no evidence of isotype switching per se in fish, although the zebrafish AID protein is capable of mediating this process in human cells (Wakae et al., 2006). Fish B

cells produce IgM, IgD, and the fish-specific IgZ classes of heavy chain immunoglobulin components, but the details of expression are still being worked out (Danilova et al., 2005). There is also evidence that the B lymphocytes have phagocytic potential, a feature that may distinguish the fish or one that has simply not yet been identified in mammals (Li et al., 2006). Where antigen presentation occurs has posed another intriguing question as no lymph nodes are obvious and the spleen consists of mixed pulp without the discrete zones of mammalian spleens. Lymphatics have been identified recently, reducing the intrigue surrounding this matter (Kuchler et al., 2006; Yaniv et al., 2006).

In summary, most immune mechanisms are common to fish and mammals and the study of phagocytes and their pathogens appears to be on particularly solid ground in its relevance to mammalian systems as will be discussed in the sections below.

2.3 Phagocytes of the zebrafish

2.3.1 Macrophages

Macrophages are the first phagocytes, and indeed the first immune cells, to appear in zebrafish development. The origins and capabilities of these earliest phagocytic cells have been reviewed extensively (Traver et al., 2003), and here we shall attempt only an overview. Both developmental and inflammatory responses of early macrophages can be studied in exquisite detail. The first macrophage precursors are identified in the anterior-most lateral mesoderm at

around the seven-somite stage (about 12 hours post fertilization (hpf)) from where they migrate laterally toward the anterior surface of the yolk sac (figure 2.1A) and express CSF-1 receptor and L-plastin (Herbomel et al., 1999; Herbomel et al., 2001). Once they arrive at the yolk sac, they change shape to become small, active "pre-macrophages," with scant cytoplasm, which further differentiate into macrophages by around 22hpf. This location on the surface of the yolk sac is below the outer periderm and the dermis of the embryo, but within the blood flow, and will become the yolk circulation valley, or duct of Cuvier (figure 2.1C). As development continues this space becomes enclosed by vascular epithelium and remains part of the circulatory pathway. It is this detail of yolk sac-associated circulation (specific only to a few teleosts) which makes the viewing of early macrophages at high resolution so convenient in zebrafish (Herbomel et al., 1999) (see figure 2.2A-C).

Although the heart has been beating since 22hpf, it is not until after the proerythroblasts have made their way to the yolk sac at 24-26 hours that systemic circulation begins, allowing the macrophages to circulate into a variety of tissues. Some of the macrophages find other tissues without traveling in the blood, however. Starting by 26 hpf, some embryonic macrophages migrate into the head mesenchyme, where no vasculature is yet formed (figure 2.1B). By 36 hpf the vasculature of the head is still scarce (Isogai et al., 2001), but this area is populated with roughly 100 macrophages (Herbomel et al., 1999). By this time in development the embryonic macrophages are capable of eradicating

nonpathogenic bacteria injected into the bloodstream, and the introduction of bacteria into the hindbrain ventricle (figure 2.1C) accelerates their appearance in this space (Herbomel et al., 1999). Once the embryonic macrophages move into various tissues they begin to modify their gene expression and phagocytic capacities (Traver et al., 2003). The best studied example of this is the upregulation of apolipoprotein E (apoE) by macrophages colonizing the brain and other neural tissues. It is possible that these cells become or give rise to microglia in the adult (Herbomel et al., 2001).

How these embryonic macrophages (or those of any species) compare functionally to the later adult macrophages, and how long they remain active in the organism, are still unknown.

Hematopoiesis

Although the kidney is the site of hematopoiesis in the adult fish (figure 2.1E), the predecessors of the stem cells responsible for definitive hematopoiesis first appear in a region of the trunk call the aorta-gonad-mesonephros (AGM) at around 24hpf, whence they move to another temporary hematopoietic site in the ventral tail called the caudal hematopoietic tissue (CHT) (figure 2.1C). The migrations of these cells have been shown by an elegant series of experiments from the Herbomel group (Murayama et al., 2006). By four days post fertilization, hematopoietic stem cells begin to populate the kidney and thymus (figure 2.1D), but new cells are still produced in the CHT until around day 14. Thus, by five to

seven days post fertilization, there may be macrophages of three different origins sharing the same tissues: true embryonic macrophages that are derived from anterior mesoderm, macrophages originating from the CHT, and full adult macrophages from the kidney. The monocyte stage of development of the latter two has not yet been described in zebrafish, although monocytes have been identified in the adult (Trede et al., 2004). More study of the monocyte/macrophage distinction has been done in the goldfish *Carassius auratus*, where Belosevic and colleagues have shown that the adult goldfish kidney contains three subsets of macrophage-like cells (Barreda et al., 2000; Neumann et al., 2000). The first, called R1, is a hematopoietic precursor cell, which is capable of giving rise to the other two types. R2 is phenotypically most like an adult macrophage, and the development of R1 cells to R2 cells suggests a pathway for macrophage maturation with no monocyte intermediate. The R3 subset is monocyte-like and can give rise to R2 cells, approximating the usual mammalian system of monocyte-derived macrophages (Neumann et al., 2000). Surprisingly the most differentiated R2 cells are also capable of replication (Barreda et al., 2000). The appearance of replicating macrophages has also been noted in some cases in mammals (Alliot et al., 1991; Sorokin and Hoyt, 1987). The unexpected appearance of dual differentiation pathways in the primary hematopoietic tissue of goldfish may occur in the zebrafish as well.

Another unexpected finding in goldfish myelopoiesis is the role of granulin as a growth factor (Hanington et al., 2006), a role also suggested by studies in

carp (Belcourt et al., 1993). The granulin in question was found to be expressed only in the kidney and spleen (figure 2.1E), in contrast to the more ubiquitous expression seen in mammals. The confusion has been somewhat relieved by the discovery of four granulins in zebrafish, with only one (granulin a) expressed in a way that suggests a hematopoietic role (Cadieux et al., 2005). Of the other three, one (granulin b), an ortholog of the mammalian gene, and two paralogs (granulin 1 and 2) showed more ubiquitous expression. Granulin a, which appears to be a hematopoietic growth factor, does not appear necessary for embryonic development, while the others do. Thus, it is thought that partial genome duplication (perhaps more than once) is responsible for multiple copies of what is in the mammalian line a single gene.

Molecular markers

CSF1R remains the major molecular marker for macrophages in zebrafish and other teleosts. A line of zebrafish mutant in the *fms* gene that encodes CSF1R was originally discovered as a stripeless variety in a pet store (Parichy and Turner, 2003). Strains of fish associated with loss of function mutations in this gene have been called *panther* (Parichy and Turner, 2003). The functional status of the gene in this and related lines remains uncertain, as the main distinguishing points of the panther mutant are altered pigment patterns and an altered macrophage migration pattern in early development (Herbomel et al., 2001). More recently, a deficiency in resistance to *Mycobacterium marinum* has also

been found (Swaim, and Ramakrishnan, unpublished). Whether there is a duplicate gene which is preventing the severe phenotype seen in the *csf1r* knockout mouse (Dai et al., 2002), or whether the M-CSF pathway plays a role more restricted to hematopoiesis in the fish is not clear. A distinct possibility is that the lack of bone marrow in teleost fish may simply make osteoclast deficiency and the ensuing metabolic and bony structural defects that dominate in M-CSF pathway defects in mammals less important in the fish.

A major impetus for finding a molecular marker of zebrafish macrophages has been the hope of producing a transgenic line with fluorescent macrophages, thereby taking advantage of the excellent optical characteristics of the embryo in studying infection. Some studies of embryonic macrophages have taken advantage of neutral red accumulation in macrophages (Davis et al., 2002; Herbomel et al., 2001), but this dye is toxic within hours of administration. Pilot studies with injected PKH26 (Sigma) have also shown bright but incomplete fluorescent marking of phagocytic cells (Lesley and Ramakrishnan, unpublished). As for genetic means, whole-mount in situ hybridization shows csfr1 to be a reliable marker of macrophages at least in the embryo, but efforts by multiple laboratories to produce a transgenic line using the promoter have been fruitless thus far. Existing transgenic zebrafish lines with some macrophage expression include *Tg(fli1::EGFP)*^{y1} (Lawson and Weinstein, 2002) (in which all vasculature expresses EGFP, as do macrophages for the first 24-36 hours) and *TG(zpu.1:EGFP)* (Hsu et al., 2004) (in which all myeloid cells express EGFP in

the embryo). Due to transient expression, expression in other tissues, or a combination of both, neither of these have proven broadly useful. More recently, transgenic lines based upon the lysozyme C promoter (*lysC::EGFP* and *lysC::dsRED2*) has been introduced (Hall et al., 2007). As published, this line has shown great promise, but with caveats: expression patterns show incomplete overlap with csfr1 expression (still the gold standard), suggesting incomplete coverage of all macrophages, and overlap with *mpo* expression, suggesting some neutrophils are also marked (Hall et al., 2007). Our own recent studies with these transgenic lines suggest that lysozyme C expression is restricted to granulocytes, and any overlap with macrophage-like gene expression likely occurs only in early primitive hematopoiesis (Davis and Ramakrishnan, unpublished). For this reason, we consider lysozyme C not a viable macrophage marker. Another proposed marker molecule is l-plastin, which appears to be expressed by all macrophages and at least some neutrophils, but expression dies out in the first 2-4 days of life (Herbomel et al., 1999) (a more rapid downregulation in neutrophils may account for the apparent incomplete coverage of this group).

Chemotaxis

In the zebrafish embryo, bacteria such as *E. coli* and *Mycobacterium marinum* can be injected into the hindbrain ventricle at 21-24 hpf, and macrophages will be attracted to the site to phagocytose the foreign matter (Clay et al., 2007; Davis et

al., 2002; Herbomel et al., 1999; Volkman et al., 2004). At this point in normal development, the hindbrain ventricle is devoid of macrophages, so the arriving cells have come from some distance. Injections of PBS or untreated latex beads do not attract this response, suggesting that it is not due to the trauma of wounding (Clay et al., 2007). The exact nature of the signal is not known, although csf1r is not absolutely required (Davis et al., 2002). Genes encoding a number of chemokines and chemokine receptors have been detected and cloned in the zebrafish, including Sdf1a and CXCR4b (Knaut et al., 2003; Miyasaka et al., 2007), Sdf1b and CXCR4a (Chong et al., 2007), CXCR7 (Dambly-Chaudiere et al., 2007), and these have roles in germ cell migration and neural development. A large number of CC chemokines have been detected in the zebrafish and catfish genomes (Peatman et al., 2005; Peatman et al., 2006; Peatman and Liu, 2006), but functional studies of any chemokines in the service of immunity have yet to be published. The effect of pertussis toxin, which blocks all G_i proteins including all chemokine receptors, on zebrafish development has been studied (Hammerschmidt and McMahon, 1998) and pilot studies in our laboratory are ongoing to learn its effect on infectious processes. The importance of microtubules in zebrafish macrophage motility was shown by visualization studies after laser-induced wounding (Redd et al., 2006). Work with zebrafish CXCR4 and SDF-1 has led to other experiments concerning sub-cellular mechanics of cell motility (Blaser et al., 2006). Overall, the zebrafish,

presenting the unique view of cell movements that it does, is only beginning to be exploited for the study of the chemokine networks that direct these movements.

Phagocytosis

Functionally, thus far much more is known about macrophages of the zebrafish embryo than those of the adult. As noted above, there are macrophages derived from 'definitive' myelopoiesis present in the stages used for embryonic observations of infection, but it is not certain how similar these are to later adult macrophages, or how they can be distinguished (if at all) from the still numerous true embryonic macrophages. Nevertheless, the cells present by 48 hpf, whatever their origin, are readily capable of phagocytosis of both living and heat-killed organisms, including Gram positive and Gram negative bacteria (Herbomel et al., 1999), spirochetes (Davis and Ramakrishnan, in preparation), and yeast (Traver et al., 2003). Studies with adult goldfish macrophages also show uptake of *Leishmania major* (Stafford et al., 1999), so the general classes of pathogens are all documented as being taken in by fish macrophages. Given that there is no functional adaptive immune system in the zebrafish embryos of the former studies, the phagocytosis is not antibody-mediated. A study of trout head kidney macrophages exposed to mycobacteria suggested that some form of opsonization is needed for efficient uptake of bacteria (Chen et al., 1998), and that trout serum and trout antibody both perform well. Opsonization by complement is quite possible in the 48 hpf zebrafish, as multiple complement

components are induced by *M. marinum* infection at this time (Pozos, T., Volkman, H.E., Rawls, J.F. and L.R., unpublished data).

Receptors

The presence of complement receptor and mannose receptor have been identified in other teleosts (Rodriguez et al., 2003; Schraml et al., 2006; Sorensen et al., 2001) although they have yet to be definitively found in zebrafish. Many TLR-related genes have been found in the genome, including TLRs 1-5 and 7-9, MyD88, MAL, TRIF, TRAF6 and IRAK-4 (Jault et al., 2004; Meijer et al., 2004; Phelan et al., 2005a). In both embryonic and adult infections, TLR3 and TRAF6 were shown to be upregulated in response to snakehead rhabdovirus infection, and TLR3, TRAF6 and IRAK-4 were upregulated upon infection with *Edwardsiella tarda* (Phelan et al., 2005b). The TLR genes are not only upregulated but also functioning, as shown by the reduced ability of zebrafish embryos to clear *Salmonella enterica* when MyD88 function was blocked (van der Sar et al., 2006). Work on intracellular receptors is also beginning, and NOD2 has been identified in the fugu and zebrafish genomes (Ogura et al., 2003).

Effector pathways

Microbial killing by reactive oxygen or nitrogen species is well documented in fish macrophages (reviewed in (Neumann et al., 2001)), and uses a familiar set of enzymes. One interesting feature of fish macrophages shown in trout and goldfish is their relative autonomy in initiating antimicrobial free radicals. In vitro studies with cultured or explanted macrophages showed that LPS alone can induce an oxidative burst and/or nitric oxide species (NOS) within six hours (Chen et al., 1998; Neumann et al., 2000). This is in contrast to the general need for interferon gamma in mammals, although two interferon gamma homologues are present in the zebrafish genome (Igawa et al., 2006). Another contrast to mammalian systems is the use of cleaved transferrin as an activator of macrophages to produce NO (Stafford and Belosevic, 2003; Stafford et al., 2001).

2.3.2 Melanomacrophages

Melanomacrophages are a subset of macrophages found in fish, amphibians and reptiles. They are most commonly found as a part of melanomacrophage centers (MMCs) in the spleen, liver, and sometimes kidney (as reviewed in (Agius and Roberts, 2003)), but are also seen singly. Specific studies of zebrafish melanomacrophages have not been published, but there is plentiful literature on those of other teleost species.

It is very likely that macrophages and melanomacrophages are in fact the same cell type, and the latter has happened to ingest pigmented material

(predominantly lipofuscin, melanin, and hemosiderin (Agius and Roberts, 2003)) and are henceforth associated with MMCs. However it has been asserted (Sichel et al., 1997; Zuasti et al., 1989) that these cells actually produce melanin by a unique pathway. The majority view, however, is that melanomacrophages, and MMCs, are storage and destruction sites for hazardous materials, resistant bacteria, and excess iron from dead erythrocytes. This view is supported by evidence that indigestible materials such as India ink and thorium hydroxide traffic to MMCs after intraperitoneal injection (Ellis et al., 1976; Herraez and Zapata, 1991). Also older fish, or fish enduring toxic environments, have more and larger MMCs.

Vaccine antigens also traffic to MMCs, suggesting an antigen storage/presentation role for these structures. The assertion that MMCs were sites of antigen presentation was first made by Ellis and deSousa in 1974 (Ellis and De Sousa, 1974), and since then other evidence has accrued to suggest that these structures represent functional homologs of mammalian germinal centers. The recent finding that melanomacrophages, both single and within MMCs, stain with CNA-42, (an antibody specific for human follicular dendritic cells) supports this relationship (Vigliano et al., 2006). A homolog of CD83, a dendritic cell marker in humans, has been found expressed on the SHK-1 line of Atlantic salmon macrophages; this same cell line was found to possess the machinery for melanin production (Haugarvoll et al., 2006). Thus further research will be

required to determine the specific identity of melanomacrophages and their possible relationship to dendritic cells and other macrophages.

2.3.3 Neutrophils

In earlier publications on the subject, the neutrophil-like granulocytes of some fish, including zebrafish, have been termed ‘heterophils', based on the fact that their cytoplasmic granules are not uniform but of two distinct shapes. This term has gradually given way to ‘neutrophils’ and we will refer to them as such here.

Hematopoiesis

Neutrophils in the zebrafish embryo appear only slightly later in development than do macrophages. By electron microscopy, they were first detected at 48 hpf (Willett et al., 1999), but studies relying on gene expression show neutrophils as early as 18 hpf (Bennett et al., 2001). MPO-expressing cells in the transgenic model (see below) are reported by others to be on the yolk surface amongst the embryonic macrophages as early as 22hpf (Mathias et al., 2006). Evidence from the Herbomel group (Le Guyader et al., 2008), and our own observations, suggest that at least some of the earliest phagocytes seen in the yolk circulation valley at 25-30hpf possess granules and will become neutrophils. It is intriguing that 32 hpf is the only timepoint published at which the macrophage marker fms and Lysozyme C (which we find expressed only by granulocytes) are seen expressed in the same cell. Also, we find all of the yolk surface macrophages to

express the mpo transgene (see below) at this time. Based on these observations, we suspect that the macrophage or neutrophil identity of these cells is not fully determined until after 32hpf.

Molecular markers

The primary molecular marker for neutrophils in the zebrafish is myeloperoxidase (MPO), also called myeloid-specific peroxidase. Two different lines of MPO transgenic zebrafish have been derived (Mathias et al., 2006; Renshaw et al., 2006), with apparently equivalent results in neutrophil-specificity (although the line from Renshaw et al appears brighter in our hands). As mentioned above, L-plastin and lysozyme C have been considered imperfect candidates for marking neutrophils, although our own observations suggest the lysozyme C is a very good neutrophil marker indeed. A recent report of a promoter trap transgenic in which a subset of neutrophils express YFP (Meijer et al., 2007) offers another, as yet unidentified candidate, but once again expression is transient and is best at 3 to 4 dpf. Transient expression may again explain the apparent expression by only a subset of mpo^{+} neutrophils.

Chemotaxis

Expression of specific chemotactic receptors by neutrophils has not yet been addressed. Thanks to the existence of transgenic embryos, compelling studies have been published showing that neutrophilic inflammation may resolve either

by apoptosis of neutrophils (Renshaw et al., 2006) or, surprisingly, their return to the vasculature (Mathias et al., 2006). Molecular mechanisms for this or other neutrophil movements have not been well studied. One group has implicated the zebrafish homolog of CD31, acting through the membrane channel ERG (Ether-a-go-go like gene), is responsible for the attraction of neutrophils to fin wounds (Brown et al., 2007).

Phagocytosis

It has been proposed that the zebrafish neutrophil is highly attracted to infection and inflammation, but is very rarely phagocytic (Le Guyader et al., 2008). Our own observations show that embryonic neutrophils are capable of phagocytosing *M. marinum*, though this is a relatively rare event (JMD and LR, unpublished). *Streptococcus iniae* (LR, unpublished) and *Pseudomonas aeruginosa* (Brennan, Davis et al, in preparation—see Chapter Three) are predominantly taken up by neutrophils, but specific studies on the molecular features and mechanisms of neutrophil phagocytosis, as distinct from macrophage phagocytosis, have yet to be done.

Effector pathways

There is evidence for a strong oxidative burst (Kemenade et al., 1994) and degranulation (Neumann et al., 2001) by fish neutrophils, and recently detailed accounts of neutrophil extracellular trap release and degranulation in zebrafish

(Palic et al., 2007a) and fathead minnows (Palic et al., 2007b). The visual access provided by zebrafish embryos offers an excellent opportunity for studying such phenomena.

2.3.4 Dendritic Cells

As stated above (see 'Melanomacrophages'), the two main dendritic cell markers for which homologs have been identified in fish are CD83, in Atlantic salmon (Haugarvoll et al., 2006) and trout (Ohta et al., 2004), and three C-type lectins similar to DC-SIGN in Atlantic salmon (Soanes et al., 2004). The zebrafish embryo, in which macrophages and neutrophils have been so well observed, is not likely to contain dendritic cells or their equivalent, as mammalian species do not develop this cell type until late in development (Dakic et al., 2004). Therefore, although genomic evidence in other fish suggests their presence, more study with adult zebrafish blood cells will be required to determine if dendritic cells function in this organism as they do in mammals.

2.4 Zebrafish Models of Infection

Despite some of the immunological tools and reagents lagging behind the mouse, the power of real-time visualization in the zebrafish has opened up the black box of host-pathogen interactions leading to critical end stage pathologies such as granuloma formation. Our laboratory first started to use the zebrafish to study *Mycobacterium marinum* and *Salmonella arizonae* infection in 2000 (Davis

et al., 2002) and the model has since been used to study the pathogenesis of other bacteria as well as bacterial toxins (Hamm et al., 2006; Neely et al., 2002; van der Sar et al., 2003; Voth et al., 2005). The pathogenesis of the diseases caused by these organisms in the zebrafish is remarkably similar to the ones caused by the related mammalian pathogens in their hosts, highlighting the idea that a organism might have first evolved into a pathogen in the context of a particular host species and then adapted to other hosts by further evolution leading to speciation. In the following we will highlight the work done thus far with the various pathogen species.

2.4.1 Mycobacteria

The zebrafish had long been known to be a natural host to *Mycobacterium marinum* infection. Fish tuberculosis, as it is commonly referred to, is a dreaded disease by fish fanciers and zebrafish facility managers alike (Westerfield, 2000). A detailed analysis of the infection and pathology demonstrates that *M. marinum* infection in the zebrafish produces a caseating granulomatous disease with pathology very similar to that of active human tuberculosis (Swaim et al., 2006). Furthermore, control of infection is dependent on adaptive immunity as *rag1* mutant zebrafish are hypersusceptible to infection similar to the case with mammals. The close genetic relationship of *M. marinum* and *M. tuberculosis* and their similar pathology and pathogenesis in their respective natural hosts (ectotherms and humans) has made the *M. marinum*-zebrafish model an ideal

one in which to gain a clearer understanding of the host pathogen interactions that lead to the ultimate pathology and outcomes of tuberculosis.

Human tuberculosis is a systemic disease that most frequently involves the lungs but can involve virtually any other organ of the body. It is postulated to occur in distinct steps, with the infecting bacteria being phagocytosed by macrophages and gaining entry into tissues via these phagocytic cells (Clay et al., 2007; Dannenberg, 1993). Pathogenic mycobacteria have devised strategies for host survival that may range from avoiding phagosomal acidification to a subset of the bacteria entering the cytoplasm and being propelled within the cell and into others by host actin (Honer zu Bentrup and Russell, 2001; Stamm et al., 2003; van der Wel et al., 2007). Indeed, mycobacteria have been thought to be such well-adapted macrophage pathogens that they grow optimally within these cells. Additional macrophages are next recruited to the site of infection to form a granuloma, a complex immune structure that ultimately consists of a variety of immune cells and highly differentiated macrophages that have undergone epithelioid transformation. The granuloma was previously thought to require adaptive immunity for its formation. Functionally, infection is often eradicated within a granuloma but can persist indefinitely therein. Therefore, the granuloma has been considered solely a host beneficial structure even though it is not fully effective in this capacity. Indeed, immune defects associated with poor granuloma formation such as T lymphocyte deficiencies are associated with a worse outcome from *M. tuberculosis* infection (Cooper et al., 1993; Flynn et al.,

1995). One paradox of human tuberculosis has been the growing recognition that re-infection occurs despite a seemingly effective adaptive immune response with good granuloma formation (Chiang and Riley, 2005; Cosma et al., 2004). This was attributed to the re-infecting mycobacteria surviving by avoiding pre-existing granulomas where adaptive immunity was concentrated (Cosma et al., 2003).

The zebrafish model has proved most telling in matters pertaining to the cellular movements and cell-cell interactions that abound in the pathogenesis of tuberculosis. Macrophages respond very quickly to infection by arriving at infection sites and phagocytosing bacteria within an hour (Cosma et al., 2003; Davis et al., 2002). Cytokines are induced and the macrophages carry the bacteria back into the deeper tissues (figure 2.3A). Macrophage depletion using a morpholino directed against the myeloid transcription factor PU.1 showed that macrophages curb bacterial growth from the very earliest stages of infection so that the macrophage is not a preferred mycobacterial niche if growth alone is considered (Clay et al., 2007). However, the bacteria require macrophages to transport them across epithelial barriers and blood vessels (detailed by the use of the *Tg(fli1::EGFP)*^{y1}line) (Clay et al., 2007) so that they appear to tolerate a suboptimal growth niche in order to establish systemic infection. This work exemplifies one type of discovery that is feasible to make in the zebrafish (versus in the mouse) using morpholino and transgenic technologies in combination with real-time visualization. Once infected macrophages reach the tissues, other

macrophages arrive and undergo the characteristic epithelioid transformation to form granulomas despite the lack of adaptive immunity at this stage (Davis et al., 2002) (figure 2.3B). This discovery was possible only because the zebrafish embryo can be readily infected at a stage when adaptive immunity has not yet come into play. The visual clarity of the embryo also allowed unprecedented microscopic access to the pathogenic events. The model has proved useful in defining the exact role played by individual bacterial determinants as well. For instance, the *M. tuberculosis* Erp virulence determinant, a secreted protein, was the first one to be identified (Berthet et al., 1998) and by examining the *M. marinum* Erp mutant in the zebrafish in the presence and absence of macrophages, it has been possible to show that this determinant exerts its effects on virulence by specifically endowing the bacteria with the capacity to grow within macrophages (Clay et al., 2007; Cosma et al., 2006b). In contrast, the RD1 virulence locus, famously the cause of attenuation of the vaccine strain BCG and also encoding a secretion system, does not appear to impact bacterial growth within individual macrophages (Volkman et al., 2004). Rather, it enhances granuloma formation and by so doing increases the number of infected macrophages and the total number of bacteria. Thus, the use of the zebrafish has shown that the granuloma, heretofore considered a host protective structure, is co-opted by the bacteria to enhance infection at least at its early stages (Volkman et al., 2004). Furthermore, even mature granulomas developing in the context of adaptive immunity in adult animals appear to benefit mycobacteria

(Cosma et al., 2004). Superinfecting bacteria home rapidly to pre-existing granulomas and survive within them to the same extent as the bacteria that were present right from the inception of the granuloma. These discoveries made in a relatively young model give hope that a yet deeper understanding of tuberculosis will come from the zebrafish with the use of forward and reverse genetics and more sophisticated imaging tools.

2.4.2 Salmonella

Salmonella comprise another genus of intramacrophage pathogens that occupy a distinct phagosomal compartment from mycobacterium (Linehan and Holden, 2003) and can produce either acute or chronic infection. *Salmonella enterica* sv. Typhi is the cause of typhoid fever, a systemic disease of the reticuloendothelial system in humans. *Salmonella enterica* sv. Typhimurium is commonly used to model human typhoid infection in the mouse. *Salmonella enterica* sv. Arizonae, a pathogen of ectotherms, is lethal to zebrafish embryos even at very small inoculae (5-20 bacteria/embryo). In the embryo, it infects macrophages (figure 2.4A) where it produces the typical spacious phagosomes seen in other models (figure 2.4B) and soon overhwelms and causes lysis of macrophages very early after infection (figure 2.4C), thus reproducing the features of *Salmonella* encounters with mammalian cells (Davis et al., 2002). *S.* Typhimurium also causes a lethal infection of zebrafish embryos that is dependent on key virulence determinants of mammalian infection (van der Sar et al., 2003). Therefore, it is

possible that the zebrafish will similarly provide new insights about *Salmonella* pathogenesis.

2.4.3 Streptococcus

Streptococci are pyogenic organisms and therefore would be expected to interact with neutrophils during infection. Our laboratory has observed in the zebrafish embryo the readiness with which neutrophils engulf *S. iniae*. This is in contrast to our findings with *M. marinum*, which is taken in far more often by macrophages than neutrophils (JMD, O. Humbert and LR, unpublished; (Clay et al., 2007)). Published studies to date have focused on adult zebrafish infection with *S. iniae*, a fish pathogen, and *S. pyogenes*, the notorious human pathogen causing pyogenic pharyngitis ("strep throat"), necrotizing fasciitis and toxic shock syndrome (Neely et al., 2002). Inoculation of adult fish intramuscularly at the dorsal muscle results in distinct courses of infection with these two pathogens. While both species are lethal within a few days, *S. iniae* spreads systemically by around 26 hours post infection (hpi), and is fully disseminated by 40hpi. At the site of injection, inflammatory cells (of uncertain identity) and necrosis are plentiful; systemically, bacteria are copious in the bloodstream, and notably appear intracellularly in Kupffer cells of the liver and in endothelial cells of the central nervous system (Miller and Neely, 2004; Neely et al., 2002). *S. pyogenes*, on the other hand, induces very little inflammatory cell recruitment to the injection site, but induces death within 12 to 24 hours, possibly as a result of

the systemic introduction of toxins from the rapidly growing initial lesion (Miller and Neely, 2004; Neely et al., 2002). Because of these variations in pathogenesis, *S. iniae* infection of adult zebrafish has been proposed as a model for systemic human pathogens such as *S. pneumoniae*, while *S. pyogenes* in the zebrafish mimics human necrotizing fasciitis caused by the same organism (Miller and Neely, 2004). In *S. iniae*, a large-scale mutant screen for bacterial virulence factors (Lowe et al., 2007; Miller and Neely, 2005), has found a preponderance of factors directly related to capsule formation, and suggested that while growth in the injection site was less dependent on this structure, the transition to systemic infection required it. These findings demonstrate that the capsule is important during zebrafish infection as it has long been held to be for avoidance of phagocytosis and ensuing bloodborne dissemination, a completely different strategy from that used by mycobacteria (Clay et al., 2007).

Lending credence to the *S. pyogenes*-zebrafish model is the finding that several bacterial genes suspected to play a role in virulence have been confirmed as important in pathogenesis in the adult zebrafish (Bates et al., 2005; Brenot et al., 2004; Montanez et al., 2005). Germane to the pathogen-phagocyte relationship are the findings that *S. pyogenes* actually survives within macrophages and that this ability is a major factor in its virulence. In recent work, Phelps and Neely (Phelps and Neely, 2007) have described an attenuated *S. pyogenes* mutant (SalY) which induces far more inflammatory infiltration than wildtype, and is far less resistant to killing by macrophages. Depletion of

macrophages in zebrafish before infection induced a major recovery in virulence in the mutant, compared to a mild one in the wildtype (Phelps and Neely, 2007). How this relates to the relative paucity of macrophages in wild-type *S. pyogenes* lesions awaits further study, and exploitation of the zebrafish as a genetically tractable host.

2.4.4 Edwardsiella

Edwardsiella tarda is a relatively common pathogen of fish, and more rarely humans. Pressley et al (Pressley et al., 2005) established baseline data for infection of embryos and adults through a variety of exposure routes, and more recently the same group has examined the effect of low levels of arsenic on the immune response of zebrafish embryos to this pathogen (Nayak et al., 2007). Control of bacteria was significantly reduced concurrent with a loss of oxidative burst by macrophages and neutrophils. Chemokine levels were also affected. This reduction in effector function appears to be due to the combination of blunted TNF and IL-1β production along with a direct effect on the respiratory burst itself. Use of the embryo in these experiments allowed isolation of the innate immune response as affected by arsenic. Another study demonstrated the upregulation of TLR3 and parts of the TLR signaling pathway during *E. tarda* infection (Phelan et al., 2005a) (see macrophage receptor section above).

2.4.5 Other microbial pathogens

Several other pathogens, bacterial and viral, have been subject to studies in zebrafish infection. Lin and colleagues (Lin et al., 2007) studied the acute phase reaction of adult zebrafish to *Staphylococcus aureus* and *Aeromonas salmonicida*, gram-positive and –negative pathogens, respectively, in a gene expression study. Several viruses, including snakehead rhabdovirus (Phelan et al., 2005a; Phelan et al., 2005b; Pressley et al., 2005), spring viremia of carp virus (Sanders et al., 2003), and viral hemorrhagic septicemia virus (Novoa et al., 2006) have also been featured in studies using zebrafish. These studies have focused mainly on establishing susceptibility and survival baselines and on the use of TLRs in the recognition of pathogens. Thus far none of these models have expanded to address the role of phagocytes in host-pathogen interactions.

2.5 Summary

The zebrafish offers several unique advantages for the study of host pathogen interactions. The optical transparency of the larvae allows easy whole-embryo examinations of specific steps in pathogenesis. We have found that the zebrafish embryo is a magnificent host for studying the innate immune system in virtual isolation, since a functional adaptive immune system does not arise for at least two weeks after fertilization. The isolation of innate immunity along with the close visual access allowed by the larvae make for an excellent opportunity to witness pathogen-phagocyte interactions first hand. Working with embryos also allows use of morpholino technology, the effects of which only last for the first ten

days of life. The genetic tractability of the organism and its fully ramified adaptive immune system also makes the adult fish a promising model host. However, given the relative lack of immunological reagents and inbred lines, it is important to choose appropriate questions for study to minimize the disadvantages of the model while capitalizing on its strengths. In this way one can take advantage of the best attributes of the zebrafish—optical transparency, fecundity, and genetic tools—to make discoveries in phagocyte biology that complement those being made in other models.

Acknowledgements

The authors would like to thank David Tobin for critical review of the manuscript. This work is supported by a National Defense Science and Engineering Fellowship (to J.M.D.), by grants from the National Institutes of Health (to L.R.), and by a Burroughs Wellcome award to L.R.

Taxonomy footnote:

The variety of fish species is phenomenal, and their taxonomy can be difficult to grasp. Since the terminology is often lightly used in the discussion of fish immunology, a brief explanation is appropriate here. There are 3 main groups of fish—jawless, cartilaginous and bony—all of which share common external features such as a mouth, gill openings, fins, nostrils, and a muscular trunk and tail. The jawless fish (Agnatha), such as the lamprey have a sucker mouth and median fin folds. The cartilaginous group (chondroichthyes) includes sharks and rays, which have immune systems somewhat different from the third group, osteichthyes. Osteichthyes, the bony fish group, is incredibly diverse, and

contains fish with both bony and cartilaginous features. The major subgroup of bony fish are the ray-finned fishes (actinopterygii—with fins structured by rays of bony material). The teleosts are the largest group of ray-finned fish, and also the largest group of bony fish. Teleosts are strictly bony, and the defining feature is fully moveable upper and lower jaws. The vast majority of familiar fish are teleosts. Here are the major species listed in immune and genomics literature, by their subgroup:

Cyprinids:

Goldfish (*Carrasius auratus*), Common carp (*Cyprinus carpio*), Zebrafish (*Danio rerio*)

Salmonids:

Rainbow trout (*Oncorhynchus mykiss*) Atlantic salmon (*Salmo salar*).

Perciforms:

Sea Bream (*Sparus aurata*), Sea bass (*Dicentrarchus labrax*)

Siluriforms:

Channel catfish (*Ictalurus punctatus*)

Tetraodons:

Pufferfish, “fugu” (*Takifugu rubripes*)

2.6 Figures

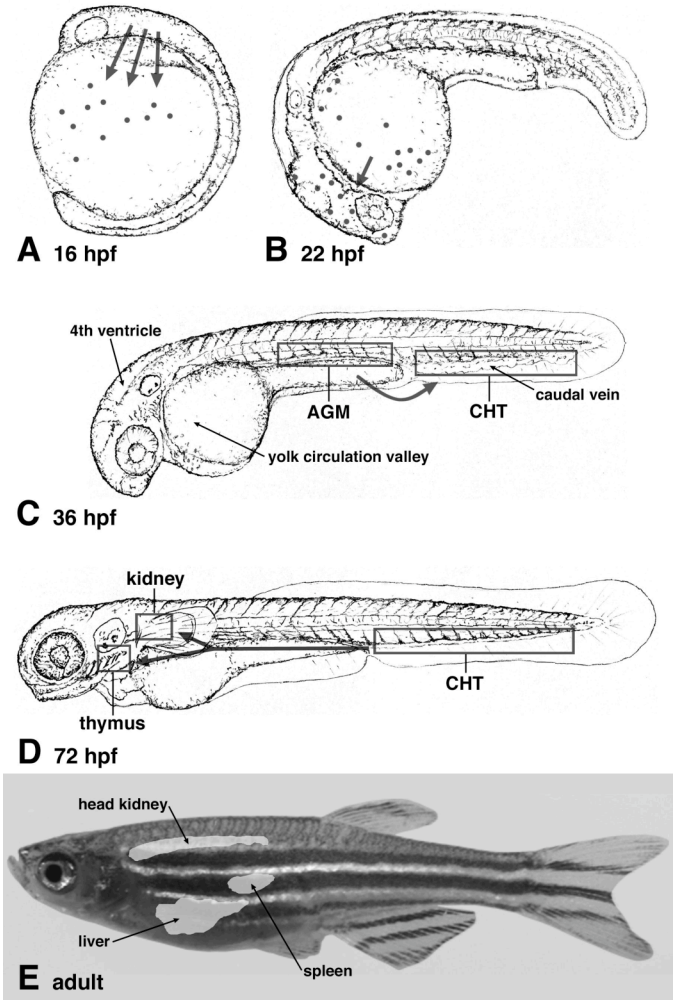

Figure 2.1

General anatomy and location of myelopoiesis during progressive stages of development. (A-D), line drawings based on sketches from (Kimmel et al., 1995). Path of hematopoietic cells as reported in (Herbomel et al., 1999) and (Murayama et al., 2006). (A) Path of embryonic macrophages from lateral mesoderm to anterior yolk. B) Before the onset of circulation, embryonic macrophages have spread over the yolk and begun to infiltrate the brain. (C) Definitive hematopoiesis begins in the aorta-gonad-mesonephros (AGM), but hematopoietic precursors soon migrate to the caudal hematopoietic tissue (CHT). (D) By four days post-fertilization, hematopoiesis is taking place in the CHT, but

hematopoietic cells are also transferring to the thymus and kidney. (E) Location of organs important to hematopoiesis and infection in the adult.

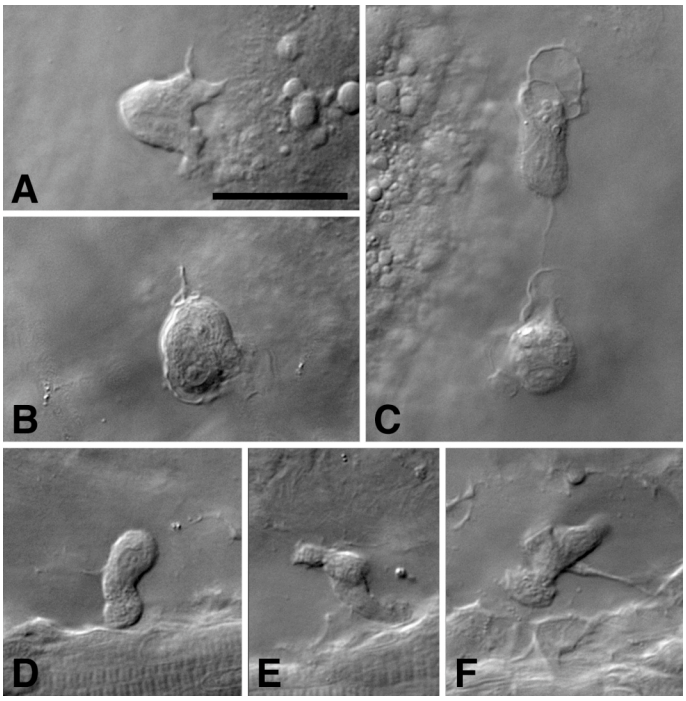

Figure 2.2

Examples of macrophages and neutrophils visible with DIC microscopy during embryonic and larval development. (A-C) Embryonic macrophages. (A) Early embryonic macrophage at yolk surface, ~30 hpf, just before the onset of circulation. Scale bar, 20μm, all panels same scale. (B) More mature embryonic macrophage in yolk circulation valley at ~48 hpf. (C) Two embryonic macrophages in yolk circulation valley, with many cellular processes and connected by a 'tether.' (D-F) Neutrophils. Note the more slender proportions and plentiful cytoplasmic granules. (A, C) located near caudal vein (ventral is up), with muscle tissue nearby. (D) Located just superficial to caudal hematopoietic tissue.

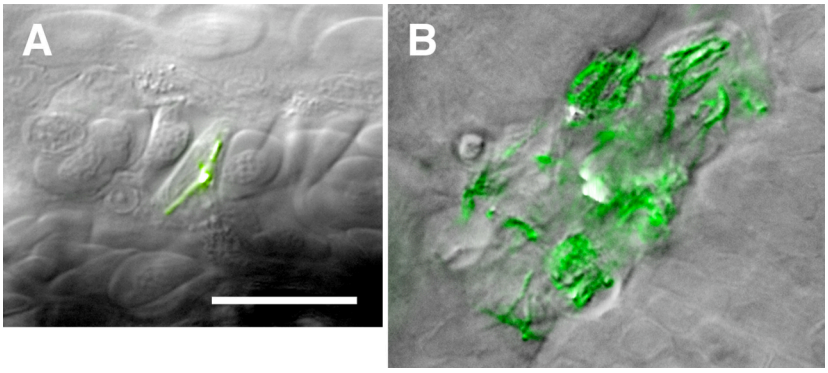

Figure 2.3

Larval zebrafish macrophages infected with *M. marinum* in vivo. (A) Single macrophage infected with green fluorescent *Mycobacterium marinum*, surrounded by caudal hematopoietic tissue (dorsal is up). Immediately below is the caudal vein, where nucleated erythrocytes are flowing to the left (anterior). ~24 hours post infection (hpi). (B) Granuloma in the brain of a five day embryo. Green fluorescent *M. marinum* seen inside both living and dead (nonmotile) macrophages. Neuronal tissue is visible to the lower right. Scale bar 20μm, both panels same scale

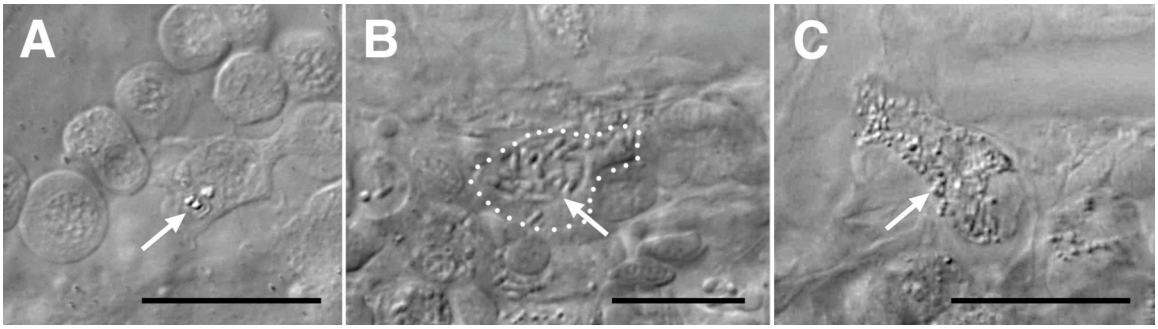

Figure 2.4

Larval zebrafish macrophages infected with *Salmonella* arizonae in vivo. (A) A macrophage in the yolk circulation valley contains three bacteria (white arrow) in a phagosome, ~one hour post intravenous infection. (B) ~18 hours post infection a macrophage (outlined with white dots) near the CHT contains many bacteria, most within a large phagosome (white arrow). (C) ~24 hours post infection a

macrophage crawling in a venule in the tail is overrun with intracellular bacteria. All scale bars 20μm.

Chapter 3

Specificity of infection phenotype in the zebrafish embryo[1]

[1]Portions of this chapter have been accepted or submitted for publication. Section 3.2 is accepted for publication at Cellular Microbiology as Brennan et al 2009 (see References). I am listed as co-first author Of the work described there, I am responsible for the analysis and microscopy of infected zebrafish, for intellectual contributions to planning and analyzing experiments, and for some writing. I was directly responsible for Figures 3.3 and 3.4, and all supplemental movies. Section 3.3 is comprised of a submitted manuscript for which I am first author. I was directly responsible for all figures and movies.

3.1 Introduction

As we have proceeded beyond the establishment of the embryonic zebrafish model of tuberculosis, toward using it to answer basic questions about tuberculous pathogenesis, it has been necessary on several fronts to provide evidence that the embryo response to *M. marinum* is specific to that pathogen. To that end, this chapter describes detailed studies of the infection phenotype produced by other bacteria, to reinforce the results of infection with *Salmonella enteritica* sv. arizonae we have published in the past (Davis et al., 2002). Beyond providing evidence for pathogen-specific outcomes, more that once we have made new discoveries concerning these other pathogens, and proceeded partway to establishing the zebrafish embryo as a model for other infections.

3.2 *Pseudomonas aeruginosa* Type III secretion system interacts with phagocytes to modulate systemic infection of zebrafish embryos

3.2.1 Introduction

Pseudomonas aeruginosa (PA) is a ubiquitous Gram-negative bacterium that can infect a wide variety of plants and animals. It is an important opportunistic pathogen in humans, producing serious infections that can be localized or systemic depending on the clinical setting. Localized infections include keratitis, otitis externa, and most notably, chronic lung infection in patients with cystic fibrosis, in which defective clearance of airway secretions and concomitant impairment of host phagocyte function creates a permissive environmental niche

(Knowles and Boucher, 2002; Lyczak et al., 2000; Matsui et al., 2005). In contrast, acute systemic infection occurs principally in neutropenic hosts undergoing chemotherapy and in those with serious burns (Lyczak et al., 2000).

Because PA produces diverse disease, multiple animal models are useful to elucidate the factors and mechanisms of pathogenesis relevant to specific clinical settings. Murine models include corneal infection, burn-wound infection, and acute pneumonia and sepsis (Lee et al., 2005; Stevens et al., 1994; Vance et al., 2005; Zolfaghar et al., 2006). Genetically tractable invertebrate models such as *Caenorhabditis elegans* (roundworm) and *Drosophila melanogaster* (fruit fly), as well as the plant model *Arabidopsis thaliana* (thale cress), have also been developed to study PA virulence factors and pathogenesis (D'Argenio et al., 2001; Darby et al., 1999; Fauvarque et al., 2002; Mahajan-Miklos et al., 1999; Rahme et al., 2000).

While several PA factors are required for virulence across these diverse models (Rahme et al., 2000), others appear to be important only in specific models and clinical contexts. One example is the PA Type III secretion system (T3SS), which translocates exotoxins into host cell cytoplasm and is associated with poor clinical outcomes in acute systemic infection and pneumonia (Hauser et al., 2002; Lee et al., 2005; Roy-Burman et al., 2001). The T3SS is a key virulence factor in *Galleria mellonella* (greater wax moth), fruit fly, and mouse, but not in roundworm or thale cress (Fauvarque et al., 2002; Laskowski et al., 2004; Lee et al., 2005; Miyata et al., 2003; Vance et al., 2005).

Danio rerio (zebrafish), perhaps best known as a model for investigating the cellular and genetic mechanisms of vertebrate development, is rapidly gaining favor as a model for the study of host-bacterial interactions (Bates et al., 2006; Clay et al., 2008; Davis et al., 2002; Lin et al., 2007; Neely et al., 2002; Prajsnar et al., 2008; Pressley et al., 2005; Rawls et al., 2006; van der Sar et al., 2003). Its genetic tractability and optical transparency early in development make it useful for studying aspects of infectious diseases not accessible in more traditional models. Moreover, while the adult zebrafish has a complex immune system similar to that of humans, with both innate and adaptive arms (Traver et al., 2003), at early developmental stages only innate immunity is operant, allowing for the dissection of innate and adaptive immune responses (Clay et al., 2007; Clay et al., 2008; Davis et al., 2002). Studies of zebrafish development have demonstrated that neutrophils and macrophages are present during this time (Herbomel et al., 1999; Le Guyader et al., 2008; Traver et al., 2003), and have shown the ability of these cells to phagocytose both Gram-negative and Gram-positive bacteria (Lin et al., 2007; Neely et al., 2002; Prajsnar et al., 2008; Pressley et al., 2005; van der Sar et al., 2003).

In this study, we developed the zebrafish embryo as a model for the study of systemic PA infection, and examined the virulence of a PA T3SS mutant in this model. We used Differential Interference Contrast (DIC) and fluorescence microscopy to monitor PA infection in real time in transgenic zebrafish lines with fluorescent phagocytes (Hall et al., 2007; Mathias et al., 2006). Finally, we

defined the effects of phagocyte depletion on embryos during subsequent infection with wild-type and T3SS-deficient PA strains. Our results show that bacterial T3SS-phagocyte interactions are critical determinants of PA pathogenesis in this model, and suggest that macrophages as well as neutrophils provide protection against systemic PA infection.

3.2.2 Materials and methods

Bacterial strains and culture methods

PA strains used in this study were PAO1 (Ochsner laboratory strain), kindly provided by E. P. Greenberg, University of Washington, PAK, and PAK*exsA*::Ω, both kindly provided by D. Frank, Medical College of Wisconsin (Frank et al., 1994). To confer constitutive expression of GFP or red fluorescent protein (RFP), each strain was transformed with plasmid pMF230, containing the *GFPmut2* gene and a carbenicillin resistance marker, kindly provided by M. Franklin, Montana State University, Bozeman (Nivens et al., 2001), or plasmid pMKB1::mCherry, a derivative of pMF230 constructed by replacing the *GFPmut2* gene with the mCherry *RFP* gene, kindly provided by R. Tsien, University of California San Diego (Shu et al., 2006). To obtain log-phase bacteria for injection, single colonies of each strain were inoculated into Luria-Bertani (LB) broth supplemented with 200 mg/L carbenicillin, grown overnight at 37°C, subcultured 1:100 in the same medium, and grown at 37°C to an optical density reading at 600 nm of 0.6 – 0.7. To prepare the final inoculum, 1 mL of cultured bacteria was

pelleted by centrifugation at 1500 × *g* for 5 minutes, resuspended in 0.4 mL of 1x phosphate-buffered saline (PBS), then diluted in additional 1x PBS as needed to achieve the desired bacterial density. To heat-kill bacteria, 20-μl aliquots were incubated in a 50°C water bath for 30 minutes. Phenol red tracking dye (5% solution) was added to bacterial aliquots (1:20 vol / vol) prior to injection. To enumerate CFU in the inoculum before, during, and after microinjection of each set of embryos, aliquots of the inoculum were spread on LB-agar plates containing 200 mg/L carbenicillin and incubated overnight at 37°C.

Maintenance, manipulation, and infection of zebrafish embryos

Zebrafish were maintained and handled as described (Davis et al., 2002; Volkman et al., 2004). Animal protocols for this study were compliant with laboratory standards outlined by the University of Washington Institutional Animal Care and Use Committee. Zebrafish embryos used in these experiments included wild-type strain AB, as well as strain AB carrying the myelomonocyte-specific transgenic marker *Tg(lyz:EGFP)* as a transcriptional fusion (Hall et al., 2007), and strain AB carrying the neutrophil-specific transgenic marker *Tg(mpx:GFP)* as a transcriptional fusion (Mathias et al., 2006). Embryos were harvested at 3 hpf and incubated overnight in fish water containing 0.01% methylene blue. At 24 hpf, embryos were dechorionated and sorted in fish water containing 0.003% phenylthiourea to prevent melanization. At 50–52 hpf, groups of 15–20 embryos were anesthetized in 0.1% 3-aminobenzoic acid ethyl ester

(tricaine), placed in a depression slide, and microinjected into the axial vein near the urogenital opening. For morpholino experiments, zygotes at the 1–2 cell stage were treated with *pu.1* or control morpholino using previously described concentrations and methods (Clay et al., 2007; Rhodes et al., 2005). Morpholino-treated embryos were then infected as described above.

Microscopy of embryos

Microscopy was performed on a Nikon E600 (Tokyo, Japan) equipped with DIC optics, a Nikon D-FL-E fluorescence unit with a 100-watt mercury lamp, and an MFC-1000 z-step controller (Applied Scientific Instrumentation). Objectives used included 4x Plan Fluor (0.13 NA), 10x Plan Fluor (0.3 NA), 20x Plan Fluor (0.5 NA), 40x Plan Fluor (0.75 NA), and 60x Water Fluor (1.0 NA). Wide-field fluorescence and DIC images were captured on a Photometrics CoolSnap HQ CCD camera (Roper Scientific, Trenton, NJ) using MetaMorph 7.1 image acquisition software (Molecular Devices Corporation, Sunnyvale, CA).

Image processing

Where indicated, z-stacks were deconvolved using AutoDeblur Gold CWF, Version X1.4.1 (Media Cybernetics, Bethesda, MD), with default settings for blind deconvolution. Dataset analysis and visualization was performed using MetaMorph 7.1 and Imaris x64 6.0 (Bitplane, Inc., Zurich, Switzerland). Figure processing and assembly was performed using MetaMorph 7.1 and Adobe

Photoshop CS2.

Determination of whole embryo bacterial counts

Infected embryos were randomly assigned to one of two sub-pools: an enumeration sub-pool and a survival monitoring sub-pool. At each time point from 0 to 48 hpi, groups of five embryos were randomly removed from the enumeration sub-pool, rinsed in 1x PBS, anesthetized in tricaine, placed in 1.5 mL centrifuge tubes containing 100 μl of 1x PBS with 1% Triton X-100, and homogenized together for 1–2 minutes with a sterile micropestle (Eppendorf, Westbury, NY). This homogenate was diluted in 1x PBS based on expected CFU, spread in triplicate on LB-agar plates containing 200 mg/L carbenicillin, and incubated overnight at 37°C. The mean value of triplicate counts for each group of five embryos was expressed as the mean (+/- standard deviation) bacterial count per embryo.

Statistical methods

For selected experiments, groups of zebrafish embryos were compared with respect to mean number of days alive, restricted to the first four dpi. In instances where subsequent pair-wise comparisons between experimental and control groups were performed, the resulting p-values were adjusted for multiple comparison testing using the Bonferroni method. For all analyses, embryos that were alive on a given day but no longer alive the following day were assumed to have died at the midpoint between days (e.g. embryos alive on day 2 but no

longer alive on day 3 were assigned a value of 2.5 for number of days alive).

3.2.3 Results

Zebrafish embryos are relatively resistant to intravenously injected PA

To determine the effects of introducing PA into the bloodstream, we microinjected a range of doses of two green fluorescent protein (GFP)-expressing laboratory strains (PAO1 and PAK) into the caudal vein of zebrafish embryos (Fig. 3.1A) at 50-52 hrs post fertilization (hpf), and assessed infected embryos for survival, and for bacterial burdens via serial fluorescence microscopy and quantitative plating (Davis et al., 2002; van der Sar et al., 2003; Volkman et al., 2004). At two hrs post infection (hpi) the embryos displayed bacterial burdens that were proportional to the initial inoculum (Fig. 3.1Bi-iii). Embryos were resistant to 150-200 colony-forming units (CFU) of either strain; bacteria were invariably cleared within two days (Fig. 3.1Biv) with no embryo mortality (Fig. 3.1C-D; the sole 200-CFU-injected embryo that died in Fig. 3.1C contained no fluorescent bacteria, suggesting that its death was not a direct consequence of PA infection). Dose-dependent mortality was observed with larger inocula (~800-2400 CFU per embryo) of either strain (Fig. 3.1C-D). While 2400 CFU of PAO1 was uniformly lethal by the first day post infection (dpi) (Fig. 3.1C), injection with an equivalent amount of heat-killed PAO1 produced no mortality (data not shown), indicating that live PA or heat-labile bacterial products, rather than heat-stable products such as endotoxin, mediated this effect. Infected embryos that survived the four-

day observation period continued to develop normally thereafter and cleared the infection (data not shown). Thus, zebrafish embryo survival following infection with PA reflected a binary outcome at the individual embryo level (i.e., survival with bacterial clearance or death with rampant bacteraemia) that was superimposed on the graded dose-dependent mortality observed at the population level.

Embryos infected with 75 CFU of the PAO1 strain cleared 75% of the inoculum within 15 minutes and continued to clear the remaining bacteria, albeit at a slower rate, during the eight-hour observation period (Fig. 3.1E), confirming the microscopic analysis of fluorescent bacteria (Fig. 3.1Bi and data not shown). In contrast, embryos infected with 2400 CFU of PAO1 supported rapid bacterial growth (a 19-fold increase in CFU per embryo over eight hours; Fig. 3.1E), consistent with their increased mortality (Fig. 3.1C). The PAK strain, when inoculated at 2200 CFU per embryo, also expanded rapidly (4-fold increase at eight hours) (Fig. 3.2A). However, in contrast to PAO1, this strain was cleared rapidly in the first two hours (78% of the inoculum of ~ 2200 bacteria) before achieving rapid growth between four and eight hpi (doubling time, ~60 minutes, compared to ~40 minutes in log-phase nutrient broth culture). Thereafter, growth from the nadir at four hours to the eight-hour time point (25-fold) was similar to that of the PAO1 strain.

These experiments show that zebrafish embryos can consistently clear PA doses of up to 200 CFU with minimal mortality, depending solely on innate

immunity, whereas doses of >800 CFU result in rapid proliferation of the inoculum and are frequently fatal. While the initial kinetics of growth varied between the two strains examined, the overall growth of the strains within embryos and the resultant host mortality were remarkably consistent.

The PA T3SS is required for virulence in zebrafish embryos

We next assessed the role of the PA T3SS, a key virulence determinant in acute infection of humans as well as in mammalian infection models (Hauser et al., 2002; Laskowski et al., 2004; Lee et al., 2005; Roy-Burman et al., 2001; Vance et al., 2005), by comparing infection with PAK strains that had or lacked the T3SS. The T3SS mutant strain PAK*exsA*::Ω was cleared rapidly in the first four hours, identical to the parent PAK strain (Fig. 3.2A). However, its growth rate thereafter was quite different, increasing only 2.5 fold between four and eight hours, compared to the 25-fold increase seen with the parent strain (Fig. 3.2A). Consistent with these reduced bacterial burdens, 90% of embryos infected with 2400 CFU of PAK*exsA*::Ω were alive at four dpi, compared to survival at one dpi of only 30% of embryos infected with 2200 CFU of wild-type PAK (Fig. 3.2B). In a separate experiment in which embryos were initially infected with ~2600 CFU of PAK*exsA*::Ω per embryo, the 95% of survivors at two dpi had nearly cleared the infection, with residual bacterial burdens of only 19 +/- 5 CFU per embryo. These experiments showed that the PA T3SS is a critical virulence determinant in the zebrafish embryo model impacting bacterial burdens and host survival.

PA infection causes blood cell aggregation and circulatory blockage

In microscopically monitoring live infected zebrafish, we observed that in contrast to *Mycobacterium marinum* and *Salmonella arizonae* (Davis et al., 2002), PA infection resulted in immediate accumulation of bacteria near the site of injection (Fig. 3.1Bii). Bacterial aggregates were also observed at sites adjacent to the caudal artery and vein (Fig. 3.3A and B). Detailed microscopy revealed that these aggregates contained both bacteria and blood cells (Fig. 3.3B-E). Among the cells present were erythrocytes and occasional infected phagocytes that completely occluded blood flow in the vessel (Fig. 3.3B and C; Movie 3.1). Although the duration of this phenomenon was dependent on the dose of injected PA, with aggregation typically resolved within minutes following low doses of PA but minimally if at all following higher doses, cellular aggregates also formed at anatomic sites with fewer bacteria, and appeared to result from adhesions between blood cells and the vascular endothelium (Fig. 3.3D and Movie 3.2). This cellular aggregation was observed upon injection of heat killed wild-type PA as well as live PAK*exsA*::Ω, but not following mock injections (data not shown).

Both neutrophils and macrophages rapidly phagocytose and kill PA

Our initial results suggested that zebrafish embryos are similar to humans in their capacity to clear systemic PA infection solely through innate immunity. In humans and other mammals, neutrophils are known to provide critical protection against

PA infection, although macrophages are also involved (Cheung et al., 2000; Lyczak et al., 2000; McClellan et al., 2003). The zebrafish embryo has functional macrophages and neutrophils (Clay et al., 2007; Clay et al., 2008; Herbomel et al., 1999; Le Guyader et al., 2008), and DIC microscopy suggested that bacteria could be phagocytosed early in infection by cells with the morphological appearance of macrophages (Fig. 3.3C and Movie 3.1). To identify types of phagocytes interacting with PA, we used two transgenic zebrafish lines. In the *Tg(lyz:EGFP)nz117* line, the lysozyme (*lyz*) gene promoter drives expression of enhanced GFP in neutrophils and possibly some macrophages (Hall et al., 2007). In contrast, in the *Tg(mpx:GFP)uwm1* line, the myeloperoxidase (*mpx*) gene promoter drives neutrophil-specific expression of enhanced GFP in a GFP-bright population of cells, while a GFP-dim population likely represents a subset of macrophages (Mathias et al., 2006).

We injected these green fluorescent transgenic strains with red fluorescent protein-expressing strains of PA. *Tg(lyz:EGFP)*-expressing cells were seen to phagocytose a substantial proportion of the bacteria within two hours of infection (Fig. 3.4A and B, and data not shown). To assess the relative contribution of macrophages and neutrophils to this phagocytic clearance mechanism, we used embryos of the *Tg(mpx:GFP)uwm1* zebrafish line and observed co-localization of bacteria with GFP-bright phagocytes (neutrophils) and with GFP-dim and non-fluorescent phagocytes (Fig. 3.4C and Movie 3.3); the latter were confirmed as macrophages by morphology based on motility, phagocytic capacity, and lack of

cytoplasmic granules (Davis et al., 2002; Herbomel et al., 1999; Le Guyader et al., 2008). At two hpi, most bacteria were intracellular and had been phagocytosed by neutrophils and macrophages (Fig. 3.4D and E; Movie 3.3). Moreover, a substantial number of bacteria had been degraded even within this short time, as indicated by the presence of red debris without clear bacterial morphology within some phagocytes (Fig. 3.4B, E, and F). Both intact PA and degraded remnants were seen within vacuole-shaped compartments in phagocytes, often corresponding to the DIC appearance of bacteria (Fig. 3.4B and D-F). We did not observe any differences in the phagocytosis of the PAK*exsA*::Ω T3SS mutant as compared to the PAK or PAO1 wild-type strains within transgenic zebrafish embryos at two hpi (data not shown). These data show that neutrophils and macrophages can rapidly phagocytose and destroy PA.

Phagocyte depletion renders zebrafish embryos hypersusceptible to PA infection and restores the virulence of the attenuated T3SS mutant

The differentiation and growth of macrophages and neutrophils in the developing zebrafish embryo are dependent on the myeloid transcription factor gene *pu.1* (Clay et al., 2007; Rhodes et al., 2005). To explore the functional relevance of phagocytes to interactions between PA and host cells, we depleted phagocytes from embryos by injection of a modified antisense oligonucleotide (morpholino) directed against *pu.1*, creating embryos we refer to as *pu.1* morphants. The *pu.1*

morphants succumbed rapidly to infection when injected with ~383 CFU PAK; 65% survived at one dpi, as compared to 100% of control embryos (Fig. 3.5A). These results show that phagocytes play a critical role in protection of zebrafish embryos against PA infection; however the relative role of macrophages and neutrophils could not be discerned as both cell types are depleted with this morpholino (Clay et al., 2007).

Given the attenuation of the T3SS mutant in wild-type embryos, we next examined whether this bacterial determinant was involved in the phagocyte-pathogen interaction. We found that whereas ~2400 CFU of PAK*exsA*::Ω had failed to kill wild-type embryos (Fig. 3.2B), doses of this strain as small as ~384 CFU per *pu.1* morphant embryo caused mortality equivalent to that of wild-type PAK; only 60% of embryos survived at two dpi, as compared to 100% of control embryos (Fig. 3.5B). The finding that phagocyte depletion restored the virulence of a T3SS mutant suggests that the T3SS acts to protect wild-type PA against phagocytes.

Consistent with this decreased survival of PA-infected *pu.1* morphants, by eight hpi bacterial counts in the PAK-infected *pu.1* morphants increased to 4491 +/-143 CFU per embryo, or 1173% of the inoculum, while control embryos essentially cleared the infection (8 +/-1 CFU per embryo, or 2% of the inoculum). Bacterial counts in the PAK*exsA*::Ω-infected *pu.1* morphants also increased over this interval, but to only 1077 +/-68 CFU per embryo, or 280% of the inoculum, one-fourth that of the wild-type strain. Thus, even after phagocyte depletion the

attenuated T3SS mutant still exhibited a relative in vivo growth defect, suggesting that phagocytes are not the sole targets of the PA T3SS.

3.2.4 Discussion

This work suggests that the zebrafish embryo is a relevant and tractable model for the study of systemic PA infections in the neutropenic host, allowing for live examination of bacterial interactions with different blood cell types. PA rarely causes systemic infection of humans unless they are neutropenic or have had a substantial integumentary breach as in the case of severe burns (Lyczak et al., 2000). Similarly, we have found the zebrafish embryo to be remarkably resistant to PA infection, requiring >2000 CFU of intravenously injected bacteria to produce sustained infection and consistent mortality. This stands in sharp contrast to the low infectious inoculum of <10 CFU of *M. marinum* or *S. arizonae* in this model (Davis et al., 2002; van der Sar et al., 2003). Yet PA is relatively pathogenic when compared to non-pathogenic laboratory strains of bacteria such as *Escherichia coli* K12 or *Bacillus subtilis*, which are rapidly eradicated by zebrafish embryos (Herbomel et al., 1999). Together, these data indicate that zebrafish embryos possess effective defense mechanisms against systemic PA infection that depend solely on innate immunity. This modest degree of virulence in the zebrafish embryo model is consistent with the reputation of PA as an opportunistic pathogen of humans (Lyczak et al., 2000).

Further validation of this model comes from our finding that key host

(phagocyte) and bacterial (T3SS) determinants in systemic PA infection of humans (Hauser et al., 2002; Lyczak et al., 2000; Roy-Burman et al., 2001) also play essential roles in zebrafish pathogenesis. Genetic ablation of the bacterial T3SS attenuated bacterial virulence, while phagocyte depletion rendered this host more susceptible to PA infection. Importantly, this work has directly demonstrated the central role of the bacterial T3SS-phagocyte interaction in determining the outcome of PA infection in vivo, as has been previously suggested through in vitro studies (Coburn and Frank, 1999; Dacheux et al., 2000; Vance et al., 2005). The first effect of Type III secretion in this infection model was observed between four and eight hpi, when the PAK strain (but not a T3SS mutant) began to grow rapidly despite an initial phase of bacterial clearance. Our data suggest that if the initial inoculum exceeds the phagocytic capacity of the host such that sufficient numbers of bacteria survive the initial burst of clearance, induction of T3SS expression in the surviving bacteria results in resistance to phagocytes, bacterial growth, and host mortality. This scenario may occur in severe neutropenia when a relatively small inoculum of PA may exceed the capacity of the few phagocytes present and thus initiate an acute systemic infection.

The *P. aeruginosa* strains used in this study, PAO1 and PAK, possess three known Type III secreted exotoxins (ExoS, ExoT, and ExoY) but lack a fourth exotoxin (ExoU) that confers cytotoxicity (Finck-Barbancon et al., 1997; Ichikawa et al., 2005; Lee et al., 2005; Vance et al., 2005). The biochemical functions and

virulence effects of these exotoxins suggest multiple mechanisms for affecting phagocyte function. In addition to their ADP-ribosyltransferase activity, the bifunctional exotoxins ExoS and ExoT are also GTPase-activating proteins that target Rho-like GTPases essential for receptor-mediated phagocytosis; ExoT additionally targets CrkI and CrkII, host kinases involved in cell adhesion and phagocytosis (Caron and Hall, 1998; Goehring et al., 1999; Sun and Barbieri, 2003). The adenylate cyclase activity of ExoY has not been shown to have a significant virulence effect in vivo (Vance et al., 2005); nonetheless, considering that it causes rounding of CHO cells, it could conceivably inhibit phagocyte microbicidal mechanisms (Yahr et al., 1998). Yet, how these effectors act in vivo is not entirely clear, with conflicting data from different models. In combination these exotoxins exert complex synergistic effects on the transcriptional responses of cultured pneumocytes (Ichikawa et al., 2005), but separable and largely non-synergistic effects on virulence in a mouse model of acute pneumonia (Shaver and Hauser, 2006). Activation of the T3SS and ExoS-dependent inhibition of hemocyte phagocytic function characterizes acute PA infection of fruit fly (Avet-Rochex et al., 2005; Fauvarque et al., 2002); in contrast, inhibition of phagocytosis during in vitro PA infection of a murine macrophage-like cell line is ExoT-dependent (Garrity-Ryan et al., 2000).

However, PA strains lacking ExoS, ExoU, or even all known Type III effector proteins can kill murine macrophages, with lysis requiring only the presence of a functional Type III translocase (Coburn and Frank, 1999; Dacheux et al., 2000;

Vance et al., 2005). Type III effectors are important for systemic spread and survival in blood in a cyclophosphamide-induced leukopenic mouse model of competitive PA infection, but host defenses can nonetheless clear PA T3SS mutants from the blood of these mice even after use of a neutrophil-specific monoclonal antibody to induce absolute neutropenia (Vance et al., 2005). In contrast, we observed that depletion of phagocytes in zebrafish embryos markedly hindered the clearance of a PA T3SS mutant. The distinct behavior of PA T3SS mutants in these models may be attributable to residual macrophages or lymphocytes in the neutropenic mouse. The dramatic dependence of PA on the T3SS to overcome normal phagocyte defenses in the absence of adaptive immunity suggests that the zebrafish may be a useful and relevant model to understand the details of T3SS-phagocyte interactions.

A central advantage of the zebrafish embryo model is the ability to monitor infection at a detailed cellular level in real-time. Using detailed microscopy of infected embryos, we have made two potentially important observations regarding pathogenesis. First, we found that neutrophils and macrophages seem to have similar capabilities with respect to phagocytosis and killing of PA. Indeed, the numbers of each cell type seen to interact with bacteria in this model seemed roughly proportional to their numbers in the caudal hematopoietic tissue, close to the injection site (Murayama et al., 2006). Thus, the relative role of the two cell types in PA phagocytosis and killing may simply be a function of their relative numbers. The greater prominence of neutrophils in acute bactericidal responses

in humans may largely reflect their greater abundance in the circulation and more rapid accumulation at sites of acute inflammation (Stossel and Babior, 2003).

Alternatively, macrophages may play a more general role in phagocytosis in zebrafish embryos than in adult mammals. However, this seems unlikely given that embryonic and adult macrophages are similar with respect to production of cytokines, cell surface receptors, and the inducible isoform of nitric oxide synthetase (Clay et al., 2007; Clay et al., 2008; Herbomel et al., 1999). Also, zebrafish embryonic macrophages have distinct interactions with different pathogens that parallel those of mammalian macrophages. For example, embryonic macrophages challenged with *M. marinum* form epithelioid granulomas, but are most likely to undergo pyroptosis upon phagocytosis of *S. arizonae* (Clay et al., 2007; Davis et al., 2002; Fink and Cookson, 2005). These responses are clearly distinct from the pattern of phagocytosis and digestion that occurs in response to PA, and all three pathogen-specific responses are similar to the corresponding macrophage-pathogen interactions observed in adult mammals, suggesting that embryonic and adult macrophages function similarly across a wide range of vertebrate organisms.

Our finding that embryonic zebrafish neutrophils can phagocytose and kill PA suggests that they are functionally competent even at this early developmental stage. Recent studies examining interactions of embryonic neutrophils with bacteria have shown that while they are capable of chemotactic attraction to infection sites, they do not phagocytose or kill non-pathogenic *E. coli* as

efficiently as macrophages do (Le Guyader et al., 2008), and do not associate with mycobacteria (Clay et al., 2007). However, in zebrafish embryos as in adults, these phagocytic functions are pathogen-specific, since in addition to our observations related to PA, others have recently shown that both embryonic neutrophils and macrophages efficiently phagocytose *Staphylococcus aureus* in an acute systemic infection model (Prajsnar et al., 2008). As with PA, resistance of zebrafish embryos to *S. aureus* is myeloid cell dependent, since phagocyte depletion with *pu.1* morpholino render embryos much more susceptible to systemic infection with *S. aureus* wild-type strains and restore the virulence of attenuated mutants of this opportunistic pathogen (Prajsnar et al., 2008).

Our real-time observations of PA-infected zebrafish embryos also revealed an erythroid aggregation phenomenon that appears to be transient at lower doses. We have not observed this phenomenon in either *S. arizonae* or *M. marinum* infection, suggesting that it is specific to certain bacteria, including PA. The consistent occurrence of this phenomenon intrigued us, because thrombotic complications are associated with PA infections in humans (Gupta et al., 1993). While these cellular aggregates are comprised principally of erythrocytes and proerythroblasts, we also noted the presence of phagocytes within them. However, these aggregates formed even in *pu.1*-depleted embryos (data not shown), suggesting that phagocytes may be bystander cells trapped within what is fundamentally a PA-erythrocyte interaction. Several features of these cellular aggregates are noteworthy. While they are entirely infection-dependent, the

number of bacteria present within any given aggregate may be minimal. Second, they occur even in the absence of the T3SS and can be induced by heat-killed bacteria, suggesting that they are not the result of the heat-labile PA phospholipase C that has been reported to induce platelet aggregation in vitro (Coutinho et al., 1988). Host and bacterial mutational analyses similar to ones that we performed to investigate T3SS-phagocyte interactions in this model could determine what role, if any, these cellular aggregates play in pathogenesis.

Various animal and plant models have been used to study host-pathogen interactions in acute PA infection. Interestingly, the T3SS is an important virulence factor of PA in hosts that possess professional phagocytes, such as vertebrates and insects, but not in those that lack such cells, such as worms and plants (Alper et al., 2007; Fauvarque et al., 2002; Laskowski et al., 2004; Lee et al., 2005; Miyata et al., 2003; Vance et al., 2005). The fruit fly has been used to examine the role of T3SS in lethal PA infection and modulation of hemocyte function (Avet-Rochex et al., 2005; D'Argenio et al., 2001; Fauvarque et al., 2002), and the greater wax moth caterpillar has similarly been used to demonstrate redundancy of ExoT and ExoU and dispensability of ExoY with respect to virulence in this host (Miyata et al., 2003). Advantages of these and other invertebrate models are the feasibility of using large numbers of animals for each test condition, the relative ease of infection, and well-established techniques for genetic manipulation and screening to identify host defense factors. However, these invertebrates have relatively rudimentary innate immune

systems that rely heavily on antimicrobial peptide expression as controlled through Toll-like receptor-dependent and -independent signaling cascades (Tanji and Ip, 2005). Given the fundamental nature of such innate immune mediators and the presence of homologues in fish and mammals (Barton and Medzhitov, 2002; van der Sar et al., 2006), invertebrate models can provide important insights into host-pathogen interactions in vertebrates, but the zebrafish embryo model of innate immune interactions with PA should provide more accurate simulation of human infection.

In summary, we have developed the zebrafish as a valid and tractable model of acute PA infection. This model provides useful tools for exploring the detailed interactions of PA with the vertebrate immune system. Experimental tools that are becoming available for zebrafish will further enhance the direct visualization and detailed analysis of innate immune responses to PA infection that this model enables. Because the zebrafish is genetically tractable, screens for mutants with aberrant responses to PA infection should be feasible. Also, the amenability of zebrafish to small molecule screens should allow for discovery of drugs with anti-pseudomonal activity in the context of a whole vertebrate animal (Peterson et al., 2000). On the pathogen side, this model should enable investigators to define additional factors that influence PA virulence through the use of PA clinical isolates and mutant libraries. The use of PA strains containing translational fusions of Type III effectors or transcriptional fusions of specific regulatory sequences to fluorescent protein genes (Pederson et al., 2002) should also

enable investigators to define cellular targets of Type III secretion and anatomic regions of regulated PA gene expression within the host. Such experimental approaches are expected to provide a richly detailed picture of host-pathogen interactions in vertebrate PA infection.

3.2.4 Figures

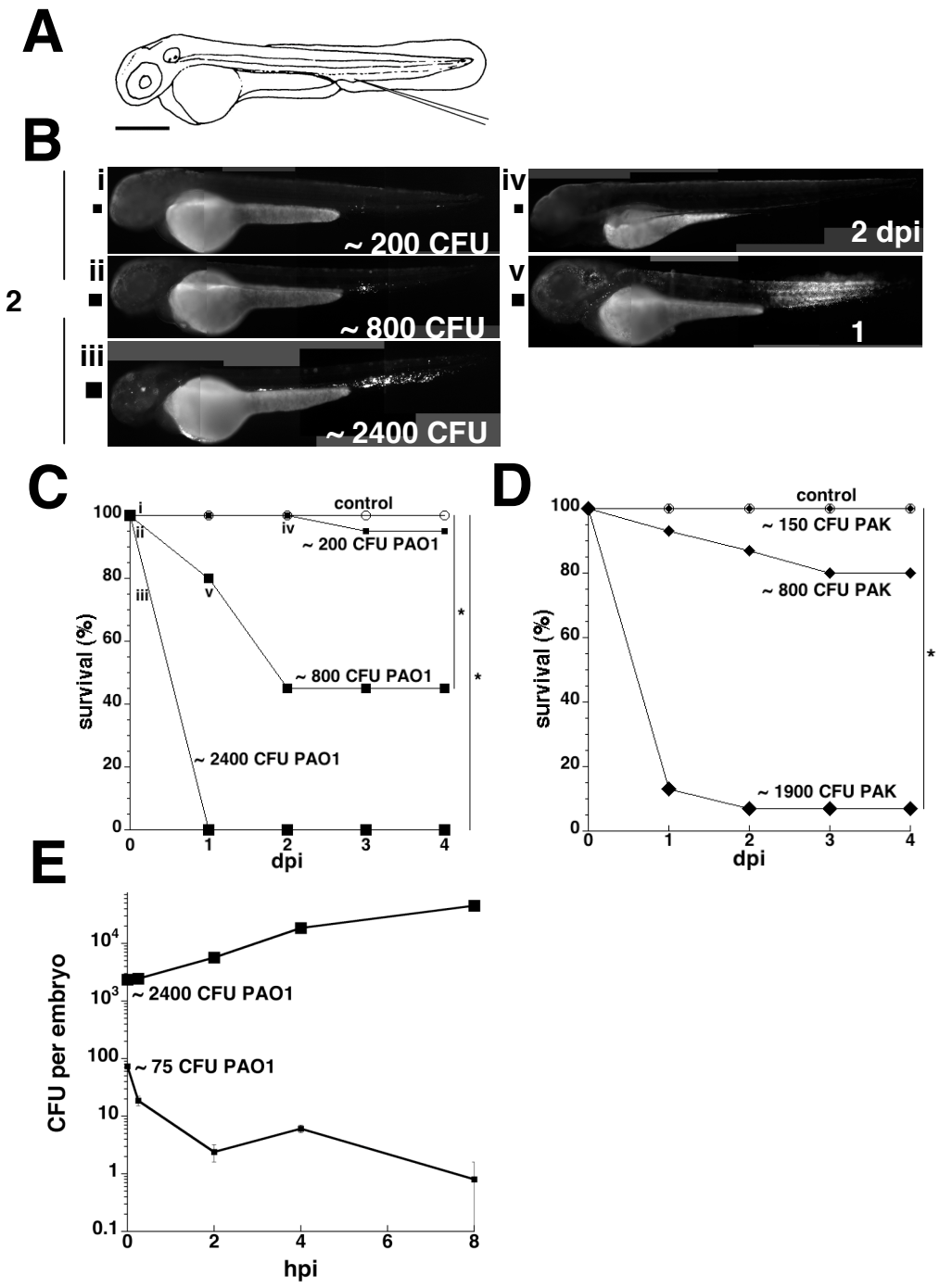

Figure 3.1. Effect of PA inoculum size on host survival and bacterial growth in zebrafish embryos. Embryo survival and bacterial enumeration experiments were repeated at least three times; representative results are shown.

A. Diagram of a zebrafish embryo at 48 hpf. Injection site (at the axial vein near the urogenital opening) is as indicated. Scale bar, 300 μm.

B. Photomicrographs of embryos infected with GFP-labeled strain PAO1. Embryos infected with a low dose (i, small square), intermediate dose (ii, medium square), or high dose (iii, large square) were imaged at two hpi. Several embryos that received the intermediate dose were highly infected at one dpi (v, medium square) and had died by two dpi (not shown). With one exception, embryos receiving the low or intermediate dose that survived to two dpi had cleared the infection (iv, small square) and were indistinguishable from each other and the controls. Scale same as for panel A.

C. Embryo survival following infection with GFP-labeled strain PAO1. Groups of embryos (n = 20 each) were inoculated with a low dose (~200 CFU per embryo, small squares), an intermediate dose (~800 CFU per embryo, medium squares), or a high dose (~2400 CFU per embryo, large squares) of bacteria at 50–52 hpf and monitored daily for survival over four days. Uninfected controls are shown as open circles. Roman numerals (i through v) correspond to photomicrographs (panel B) of representative embryos. There was an overall significant effect of inoculum size on mean survival during the first four days post-infection ($p<0.0001$). Pairwise comparisons showed no significant difference in mean survival for the 200 CFU group relative to the uninfected control group, but significant differences (indicated by *) in mean survival for the 800 and 2400 CFU groups relative to control (adjusted p-values of $p=1.0$, $p<0.0001$, and $p<0.0001$, respectively).

D. Embryo survival following infection with GFP-labeled strain PAK. Groups of embryos (n = 15 each) were inoculated with the indicated number of CFU per embryo (small, medium, and large diamonds) at 50—52 hpf and monitored daily for survival over 4 days. There was an overall significant effect of inoculum size on mean survival during the first four days post-infection ($p<0.0001$). Pairwise comparisons showed no significant differences in mean survival for the 150 CFU and 800 CFU groups relative to the uninfected control group (open circles), but a

significant difference (indicated by *) in mean survival for the 1900 CFU group relative to control (adjusted p-values of p=1.0, p=0.185, and p<0.0001, respectively).

E. Enumeration of bacteria in PAO1-infected embryos. In experiments separate from the survival curves shown above, groups of embryos (n = 45 each) were inoculated with a low dose (~75 CFU per embryo, small squares) or high dose (~2400 CFU per embryo, large squares) of PAO1 at 50—52 hpf, then sorted into sub-pools for enumeration (n = 25 each) and monitoring of survival (n = 20 each).

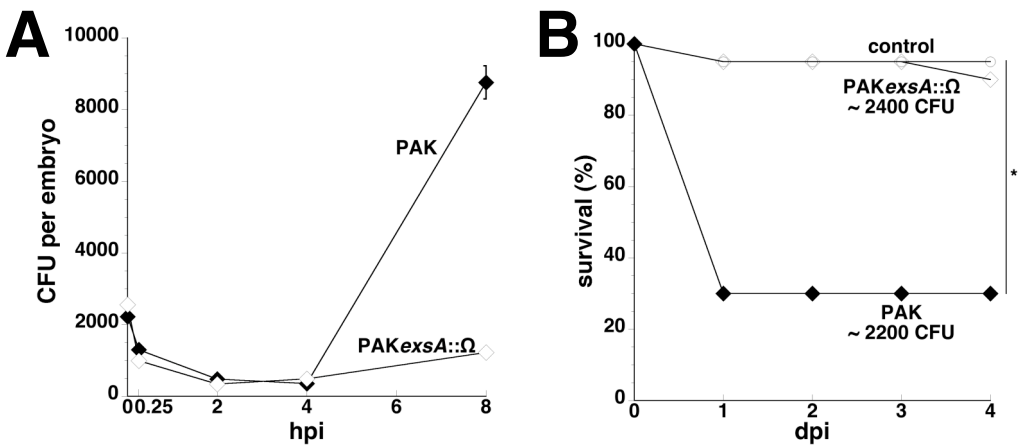

Error bars indicate standard deviation of CFU per embryo.

Figure 3.2. Infection of zebrafish embryos with PAK*exsA*::Ω, a T3SS mutant. Embryo survival and bacterial enumeration experiments were repeated at least three times; representative results are shown.

A. Enumeration of bacteria in PAK- and PAK*exsA*::Ω-infected embryos at 0.25—8 hpi. In a separate experiment, two groups of embryos (n = 45 each) were inoculated with PAK (~2200 CFU per embryo, solid diamonds) or PAK*exsA::Ω* (~2500 CFU per embryo, open diamonds) at 50—52 hpf, then sorted into sub-pools for enumeration (n = 25 each) and monitoring of survival (n = 20 each). Note the initial rapid drop in CFU of PAK and PAK*exsA*::Ω. Error bars indicate standard deviation of CFU per embryo.

B. Attenuated virulence of a PAK*exsA*::Ω T3SS mutant. Groups of 20 embryos were inoculated with a high dose of PAK (wild-type strain; ~2200 CFU per

embryo) or PAK*exsA*::Ω (T3SS mutant; ~2400 CFU per embryo) at 50–52 hpf and monitored for survival over four days. There was an overall significant effect of inoculum size on mean survival during the first four days post-infection ($p<0.0001$). Pairwise comparisons showed no significant difference in mean survival for the PAK*exsA*::Ω group relative to the uninfected control group, but a significant difference in mean survival for the wild-type PAK group relative to control (adjusted p-values of $p=1.0$ and $p<0.0001$, respectively).

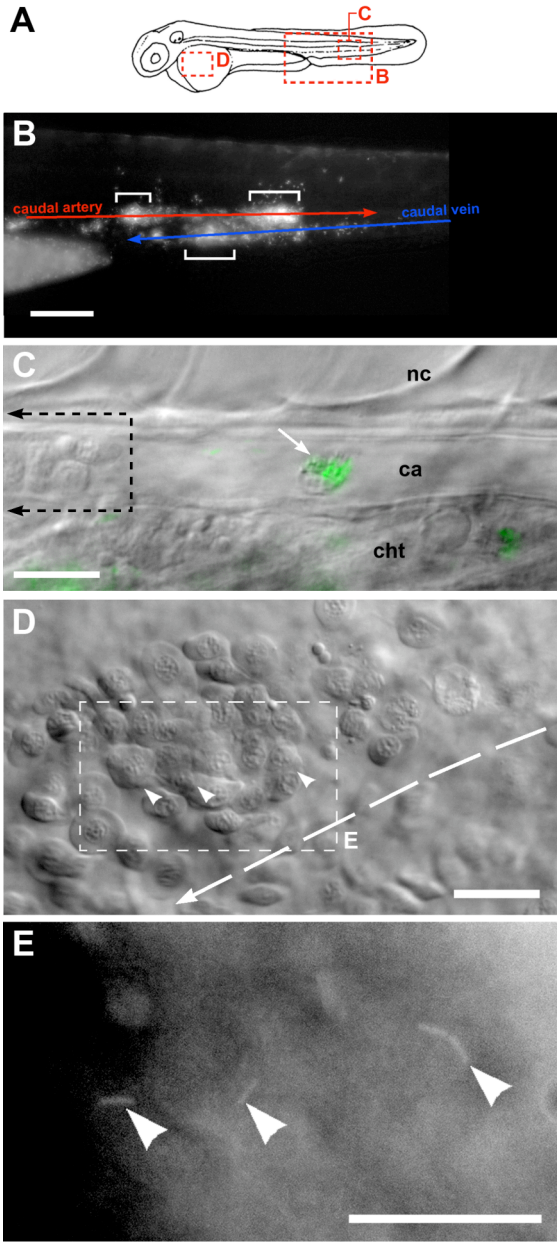

Figure 3.3. Aggregation of blood cells after intravenous injection of PA.

A. Overview of embryo at 48 hpf showing locations of other panels in this figure.

B. Tail region of a zebrafish embryo 1-2 hours post injection with fluorescent PA. Highly fluorescent areas (white brackets) show cell aggregates in the vasculature containing many bacteria. Scale bar, 100μm.

C. PA-infected macrophage (white arrow) within the caudal artery (ca). The artery is devoid of other blood cells due to the upstream cellular aggregates (black dashed box/arrows). nc = notochord; cht = caudal hematopoietic tissue. Scale bar, 20μm. See Movie 3.1.

D. Aggregated blood cells in the yolk circulation valley of the same embryo. White arrowheads indicate locations of fluorescent bacteria. Long dashed arrow shows blood flow past aggregation. Dashed box indicates area shown in panel E. Scale bar, 20μm. See Movie 3.2.

E. Fluorescent PA (white arrowheads) present as indicated in panel D. Scale bar, 20μm.

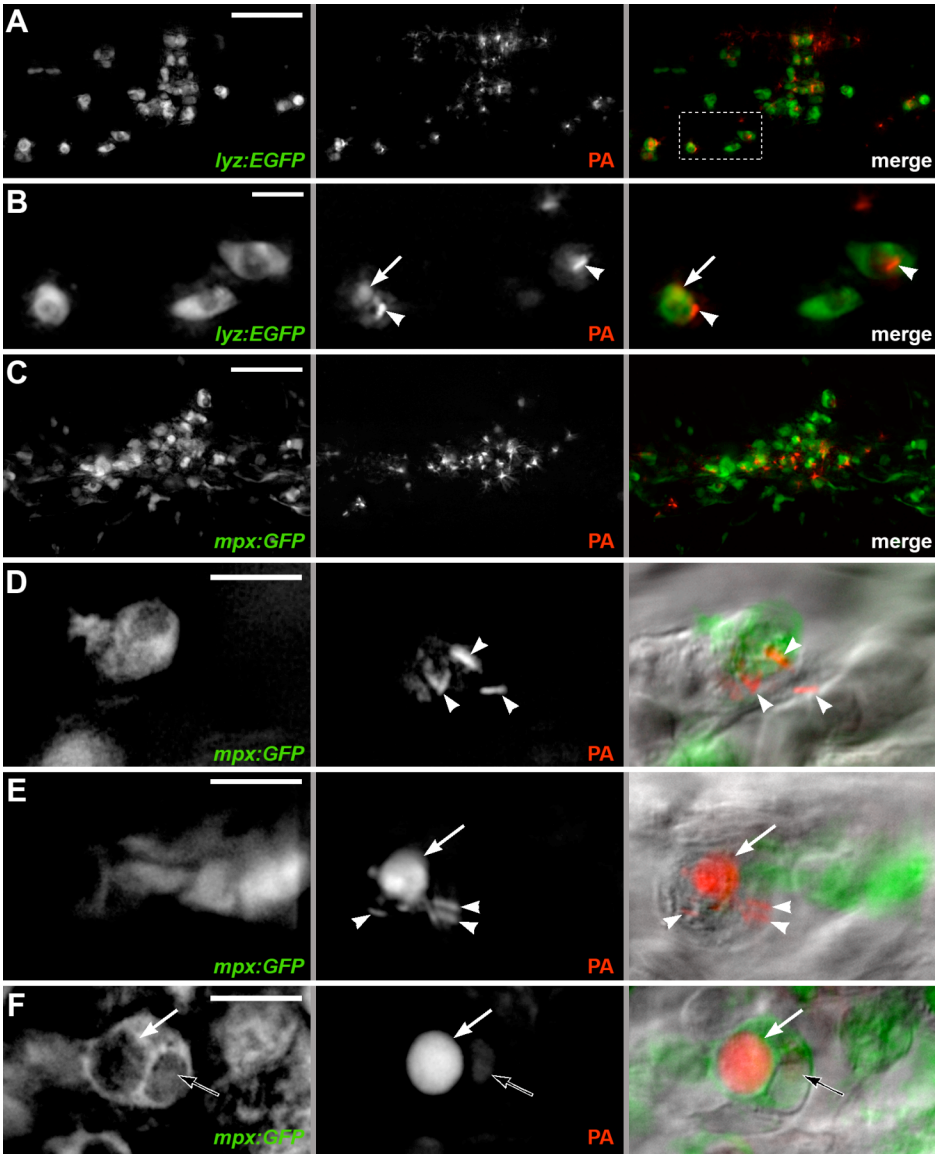

Figure 3.4. PA infection of *Tg(lyz:EGFP)nz117* and *Tg(mpx:GFP)uwm1* lines.

A-B, *Tg(lyz:EGFP)nz117* embryo injected with mCherry-expressing PA. Left, green channel (EGFP), center, red channel (PA), and overlay (right).

A. Typical projected z-series images of a *Tg(lyz:EGFP)nz117* embryo inoculated with ~1400 CFU per embryo of strain PAK, taken at two hpi. Box represents region shown in panel B; scale bar = 50 μm.

B. Close-up of *Tg(lyz:EGFP)*-positive cells that have phagocytosed PA. Arrowheads indicate bacteria in phagocytes. Arrow, digested bacteria. Scale bar

= 10 μm.

C-F, *Tg(mpx:GFP)uwm1* embryos (green channel, left) injected with mCherry-expressing PA (red channel, center), with DIC overlay of merged channels (right).

C. Typical projected z-series images of the ventral tail of an embryo that had been inoculated with ~200 CFU per embryo of mCherry-expressing strain PAK, taken at two hpi. Scale bar, 50μm. See Movie 3.3.

D. *Tg(mpx:GFP)*-expressing cell with intact PA, at two hpi. The embryo had been inoculated with ~600 CFU per embryo of mCherry-expressing strain PAO1. Arrowheads indicate intact bacteria within or adhered to the cell. Scale bar, 10μm.

E. *Tg(mpx:GFP)*-negative cell containing intact and digested PA, at two hpi. The embryo had been inoculated with ~1000 CFU per embryo of mCherry-expressing strain PAK. Arrowheads indicate intact bacteria. Arrow, pool of red fluorescence presumably from mCherry released by killed PA. Scale bar, 10μm.

F. *Tg(mpx:GFP)*-expressing cell with vacuole containing released mCherry as in panel D (white arrow), and second vacuole containing only faint red fluorescence (black arrow), presumably after near-complete digestion of PA, at two hpi. The embryo had been inoculated with ~800 CFU per embryo of mCherry-expressing strain PAK*exsA*::Ω. Scale bar, 10μm.

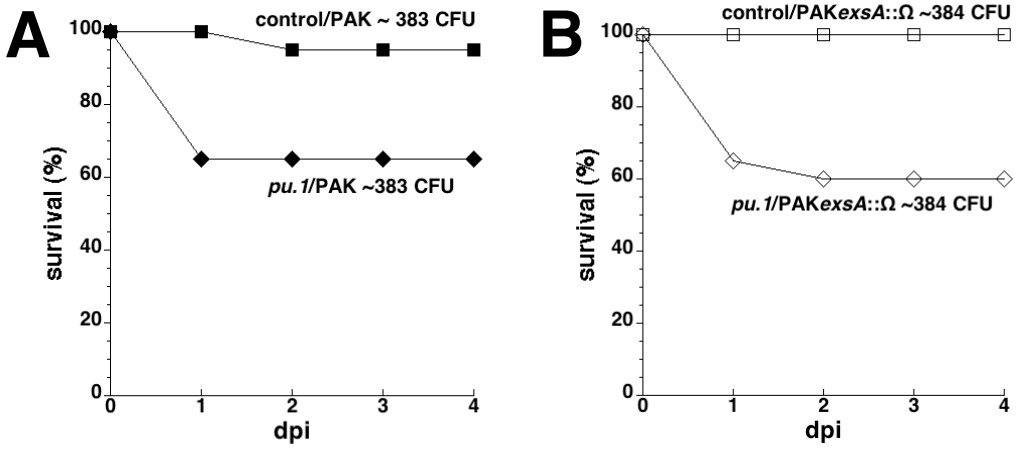

Figure 3.5. Infection of *pu.1* morphant zebrafish embryos with PAK or PAK*exsA*::Ω, a T3SS mutant.

A. *pu.1* morphant embryos are hypersusceptible to infection with the wild-type PAK strain. Groups of *pu.1* morphant (solid diamonds) and control non-morpholino-treated (solid squares) embryos (n = 20 each) were infected with PAK (~400 CFU per embryo) at 52 hpf and monitored for survival over four days. At 1 dpi only 65% of the *pu.1* morphants survived, compared to 100% of the controls. The effect of group on mean survival during the first four days post-infection was significant (p=0.01).

B. The attenuated virulence of the PAK*exsA*::Ω T3SS mutant is restored in *pu.1* morphant embryos. Groups of *pu.1* morphant (open diamonds) and control (open squares) embryos (n = 20 each) were infected with PAK*exsA*::Ω (~400 CFU per embryo) at 52 hpf and monitored for survival over four days. At 1 dpi and 2 dpi, 65% and 60% of the *pu.1* morphant embryos survived, compared to 100% of the infected control group. The effect of group on mean survival during the first four days post-infection was significant (p=0.001).

3.2.6 Supplementary Information

Movie 3.1. Infected macrophage within the clogged caudal artery, corresponding to Fig. 3.3C. A PA-infected macrophage (center) moves within the caudal artery towards an infected cellular aggregate (left) that is clogging the vessel. Scale bar, 20μm.

Movie 3.2. Cellular aggregate within the yolk circulation valley, corresponding to Fig. 3.3D. An aggregation of erythroid cells and occasional macrophages remains in place while blood flow continues adjacent to it. Scale bar, 20μm.

Movie 3.3. Uptake of PA by *Tg(mpx:GFP)*-positive neutrophils shortly after infection, corresponding to Fig. 3.4C. In this three-dimensional perspective, *mpx* expression is shown in green. Extracellular bacteria are rendered in white, bacteria inside GFP-bright cells (neutrophils) are pink, and bacteria inside GFP-dim cells (possible macrophages) are red. Scale grid, 10μm.

3.3 *Leptospira interrogans* stably infects zebrafish embryos, altering phagocyte behavior and homing to specific tissues

3.3.1 Introduction

Though traditionally thought of as a tropical disease, leptospirosis is endemic worldwide, and while many human infections take place without consequence, a subset can cause serious disease or death (Levett, 2001; McBride et al., 2005). Although much has been learned about the biology and transmission of *Leptospira* species, a full account of the mechanisms of their pathogenesis and colonization of hosts is still lacking. Common to both colonization of reservoir hosts and to infection of susceptible animals is dissemination to the kidney (Athanazio et al., 2008; Levett, 2001; Marshall, 1976). From this organ, the bacteria are able to spread through the urine of carriers and victims alike. The precise pathway which leptospires take to the kidney is not clear. In vitro studies show their ability to adhere directly to kidney epithelial cells (Thomas and Higbie, 1990), but at the same time it is apparent that macrophages are capable of phagocytosing these bacteria in the

bloodstream as well (Cinco et al., 1981; Tu et al., 1982). The role of macrophage function in leptospira pathogenesis has been estimated as negligible (Cinco et al., 1981; Tu et al., 1982), to protective (Isogai et al., 1986) to possibly necessary for disease (Alves et al., 1991).

A variety of animal models for leptospirosis have been established, each with unique advantages and drawbacks. Guinea pigs (Faine, 1957a) and hamsters (Haake, 2006; Miller et al., 1974) are the primary models of hosts susceptible to acute disease, while several animals including mice (Marshall, 1976), rats (Athanazio et al., 2008), monkeys (Palmer et al., 1987), dogs (Faine, 1957b) and skunks (Tabel and Karstad, 1967) are not susceptible but variously plausible as models of reservoir hosts. It is not certain to what degree the infection and colonization of these various model hosts are alike.

The zebrafish is increasingly used as a model organism for bacterial pathogenesis, with published studies of adult infection with mycobacteria (Swaim et al., 2006), streptococci (Neely et al., 2002), Edwarsiella (Pressley et al., 2005) and others. The ability to conduct forward genetic screens, along with the economy of infecting large numbers of animals are key advantages to this model (Lesley and Ramakrishnan, 2008; van der Sar et al., 2004). Beyond these, the zebrafish embryo allows unparalleled in vivo microscopy and is amenable to further genetic manipulation. Minute details of the early steps of bacterial pathogenesis have been published using zebrafish embryos infected with *Mycobacterium marinum* (Clay et al., 2007; Davis et al., 2002; Volkman et al.,

2004), *Salmonella enterica* (Davis et al., 2002; van der Sar et al., 2003) and *Pseudomonas aeruginosa* (Brennan et al., In Preparation). By 32 hours post fertilization a zebrafish embryo has a circulatory system and a fully functional innate immune system, along with a variety of distinct tissue types, making it a self-contained 'laboratory' for the study of bacterial infection.

In this work we have investigated the earliest events in leptospiremia by injecting *L. interrogans* sv. Lai into the developing zebrafish. Judging by the first 36 hours of infection, *L. interrogans* may produce chronic or delayed acute infection in the zebrafish embryo, but phagocytes appear to play a central role in the initial host response to infection and in the localization of leptospires to target tissues.

3.3.2 Materials and methods

Animal care and strains

Wild-type AB zebrafish embryos were maintained and infected by injection into the caudal vein or hindbrain ventricle at 24-30 hours post fertilization unless otherwise noted (Cosma et al., 2006a; Davis et al., 2002; Volkman et al., 2004).

Bacterial strains

Leptospira interrogans serovar Copenhageni strain Fiocruz L1-130 was isolated from a patient in Salvador, Brazil (Ko et al, 1999). Virulent leptospires isolated from infected Golden Syrian hamsters were grown in EMJH medium supplemented with 1% rabbit serum and 100 ug/mL 5-fluorouracil at 30°C

(Johnson et al, 1967). Staining was performed in a 1:1000 dilution of SYTO-83 (Invitrogen) for 30 minutes, followed by rinsing with PBS to remove unbound dye. Inoculum was estimated based on fluorescence microscopy after injection.

Microscopy

Widefield microscopy was performed on a Nikon E600 equipped with DIC optics and 100W Mercury lamp. Objectives used included, 10x Plan Fluor, 0.3 NA, 20x Plan Fluor, 0.5 NA, and 60x Water Fluor, 1.0 NA. Widefield fluorescence and DIC images were captured on a CoolSnap CF CCD camera (Photometrics) using MetaMorph 7.1 (Molecular Devices).

Image processing

Dataset analysis and visualization was performed using MetaMorph 7.1 (Molecular Devices). Movies were produced from stacks compiled in MetaMorph. Additional movie compilation and formatting was performed in Adobe Premiere 6.0 and QuickTimePro 7.4 (Apple). Figure processing and assembly performed in Adobe Photoshop CS2.

3.3.3 Results

To determine the effect of *Leptospira interrogans* infection on developing zebrafish, we injected doses of roughly 10 to 100 organisms into 30 hour post fertilization zebrafish by either the caudal vein or hindbrain ventricle. Inoculation

by either route resulted in infection persistent over 48 hours, with no lethality or gross pathology. To determine the fate of leptospira after injection, we stained cultures with SYTO 83 to render them red fluorescent before injection, and visualized infection with DIC and fluorescence microscopy. Within the first two hours post intravenous infection we found many macrophages in the blood contained red fluorescent leptospira (figure 3.6A). Although high magnification DIC microscopy allowed visualization of extracellular bacteria immediately after infection (Figure 3.6B, Movie 3.4), by four hpi we were unable to detect extracellular bacteria. These results suggested that leptospira inoculated into the bloodstream are rapidly taken up by phagocytes, presumably macrophages based upon their morphology.

To examine the capacity for leptospira to attract macrophages, we injected a similar dose into the hindbrain ventricle at 30 hours post infection, a time in development when very few if any macrophages reside in this compartment (Herbomel et al., 2001). Macrophages were rapidly recruited to the ventricle and took up the bacteria within the first four hours (figure 3.6C). This result showed that the uptake of leptospira by macrophages did not require blood flow to bring the two together, but that macrophages actively migrated to the site of infection.

After encountering leptospira in the bloodstream or the hindbrain ventricle, the macrophages took on a distinct morphology. Although the bacteria appeared to be contained within compartments away from the cytoplasm (Figure 3.6A, C), the macrophages generated numerous small vesicles which moved rapidly about

the cytoplasm (Figure 3.6D and Movie 3.5). Occasional membrane blebbing was also visible (Movie 3.6).

By 24 hours post infection, there was no gross pathology although fluorescent bacteria were still plentiful. All fluorescence correlated with intracellular clusters, always found in cells of a similar phenotype as the day before—many subcellular vesicles were present, often moving throughout the cytoplasm (figure 3.7A, Movie 3.7). The affected cells which were found in the brain also contained several larger vesicles which may have been apoptotic bodies (figure 3.7B). Such cells were common in embryos infected via hindbrain, found occasionally in embryos infected intravenously, and not in uninfected controls (data not shown).

The most striking feature of embryos 24 hours after intravenous infection was the localization of fluorescent bacteria. While some fluorescent clusters were present in the caudal vein (Figure 3.7C, arrowheads), the majority were dorsolateral to the dorsal aorta in the trunk (Figure 3.7D-E, Movie 3.8), a location which has been show to play a part in early hematopoiesis (Murayama et al., 2006). Previous experimental infections of zebrafish embryos with other organisms have not demonstrated such localization, suggesting that this accumulation is specific to infection with leptospira. To confirm this suggestion, we compared leptospiral infection to infection with *Pseudomonas aeruginosa* over the same time course. Infection with *P. aeruginosa* produces either overwhelming infection or clearance over the first 36 hours of infection,

depending upon dosage (Brennan et al., In Preparation). At 24 hours post infection with a non-lethal dose of *P. aeruginosa*, we found that the remaining bacteria were similar in number to *Leptospira* remaining at 24 hours. Despite the fact that both bacteria were apparently contained within phagocytes at this time, there was no accumulation of *P. aeruginosa*-infected cells at the developing kidney (Figure 3.7F).

3.3.4 Discussion

We undertook the study of leptospiral infection of zebrafish embryos in order to assess the usefulness of zebrafish in general as a model host for infection, as well as to examine the details of early pathogenesis directly in vivo. At least in embryos and larvae, infection with *L. interrogans* appears to be asymptomatic for the first 48 hours. It is not clear if this trend is inherent to the host-pathogen interaction or perhaps due to the lack of a functional adaptive immune system at this point in zebrafish development (Traver et al., 2003). Also, it is possible that more damaging effects of infection require more than 48 hours to develop. At any rate, the immediate response of zebrafish embryos to *L. interrogans* infection is consistent. Leptospires are taken up by phagocytes within a few hours of injection. The lack of antibody of any kind at this early stage in development demonstrates that it is not required for phagocytosis, as has been suggested (Banfi et al., 1982; McGrath et al., 1984; Tu et al., 1982). The zebrafish complement system appears to be quite functional by this time

(Wang et al., 2008), so it may be that complement-based opsonization is all that is required. Phagocytosis does not appear to rely upon accidental encounters with phagocytes, as injection into the hindbrain, which normally contains very few if any phagocytes (Herbomel et al., 2001), results in active migration of macrophages to the site of infection. Proposed models for leptospiral pathogenesis mostly expect extended periods of leptospiremia, with bare bacteria finding their way into target tissues (Marshall, 1976; Sitprija et al., 1980; Yang, 2007). It is possible that the infecting dose used in our experiments was too low to simulate a pathogenic infection. Barring this, however, our results suggest that leptospires are intracellular from very early in infection.

Observations of zebrafish embryonic macrophages which have ingested leptospires suggests that they are affected by the experience for long after. The appearance of small to medium sized vesicles moving about the cytoplasm takes place within one or two hours of the encounter, and infected cells with this characteristic morphology are still visible 24 hours later. It is not certain if this represents the persistence of the same affected cells, gradually gaining more vesicles, or the death of the initial macrophage followed by re-uptake of bacteria by another cell. Indeed, there has been evidence of apoptotic effects on infected host cells (Merien et al., 1997; Merien et al., 1998; Zhang et al., 2008), and we report here the blebbing appearance of affected cells after hindbrain infection. In our observations this blebbing was relatively rare, and so further observations are required to learn how relevant it is to pathogenesis.

It has been shown that some of the macrophages yolk circulation valley at the advent of circulation actually migrate into the brain, change their gene expression profiles, and become microglia (Herbomel et al., 2001). These cells then collect and dispose of apoptotic bodies of neurons (Herbomel et al., 2001; Peri and Nusslein-Volhard, 2008), although they are also capable of fighting infection (Davis et al., 2002). By 24 hours after injection of *L. interrogans* into the hindbrain ventricle, these cells are often seen as clusters of multiple apoptotic bodies, strikingly similar to microglia made incapable of digesting their cargo by knockdown of v0-ATPase a1 (Peri and Nusslein-Volhard, 2008). To our knowledge, functional impairment of macrophages after leptospiral infection has never been reported, and this infection model, along with the experimental approaches of Peri et al, provide an ideal opportunity to explore this possibility mechanistically.

At 24 hours post infection, leptospira were conspicuously located dorsolateral to the dorsal aorta. This location corresponds to that of early hematopoietic cells populating a tissue analogous to the 'aorta-gonad-mesonephros' (AGM) hematopoietic tissues in developing mammals (Murayama et al., 2006). Blood cell precursors migrate from this area to the caudal hematopoietic tissue (CHT) in the ventral tail, starting around 24 hours post fertilization. While some infected cells were indeed found in the CHT (Figure 3.7C), there were consistently more at or near the AGM. The developmental timing of our observation of infected cells here corresponds with the later times of

AGM to CHT migration (which ends around 72 hours post fertilization) (Murayama et al., 2006), so the trunk tissue could still be acting as a hematopoietic site. The fate of this tissue, after its period as a hematopoietic zone, is unknown, and from our studies it is not clear whether the infection is within cells destined to depart or within other more permanent cells. The strikingly specific appearance of leptospires in this tissue is very intriguing in terms of leptospiral pathogenesis.

3.3.5 Figures

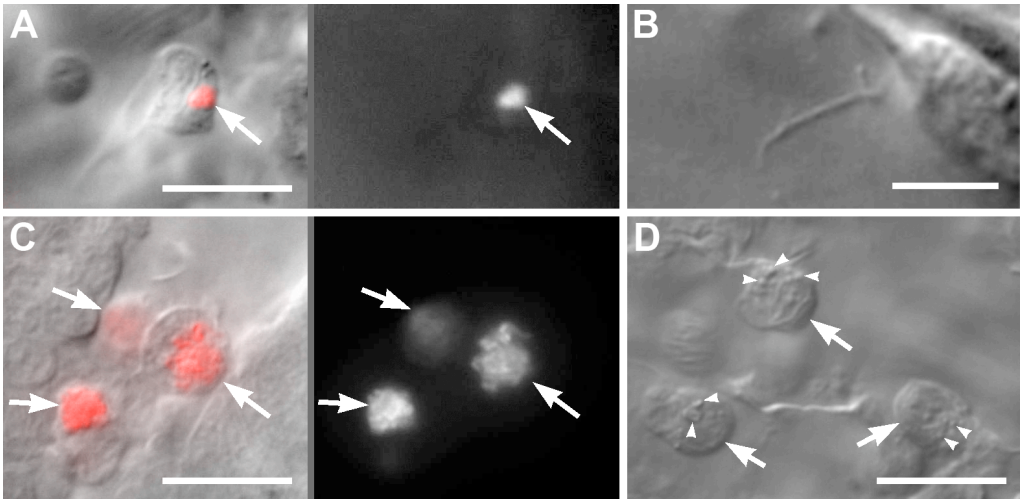

Figure 3.6. Cellular details of early phagocyte-leptospire interactions. A. Phagocyte containing leptrospires within two hours of intravenous infection. Left, DIC overlay; right, SYTO 83 fluorescence. B. Single leptospire visible by DIC microscopy shortly after injection. See also Movie 1. C. Phagocytes containing large numbers of leptospires four hours after injection into hindbrain ventricle. Left, DIC overlay; right, SYTO 83 fluorescence. D. Phagocytes (arrows) containing leptospires also acquired numerous small cytoplasmic vesicles (arrowheads). See Movie 2. All scale bars 20μm.

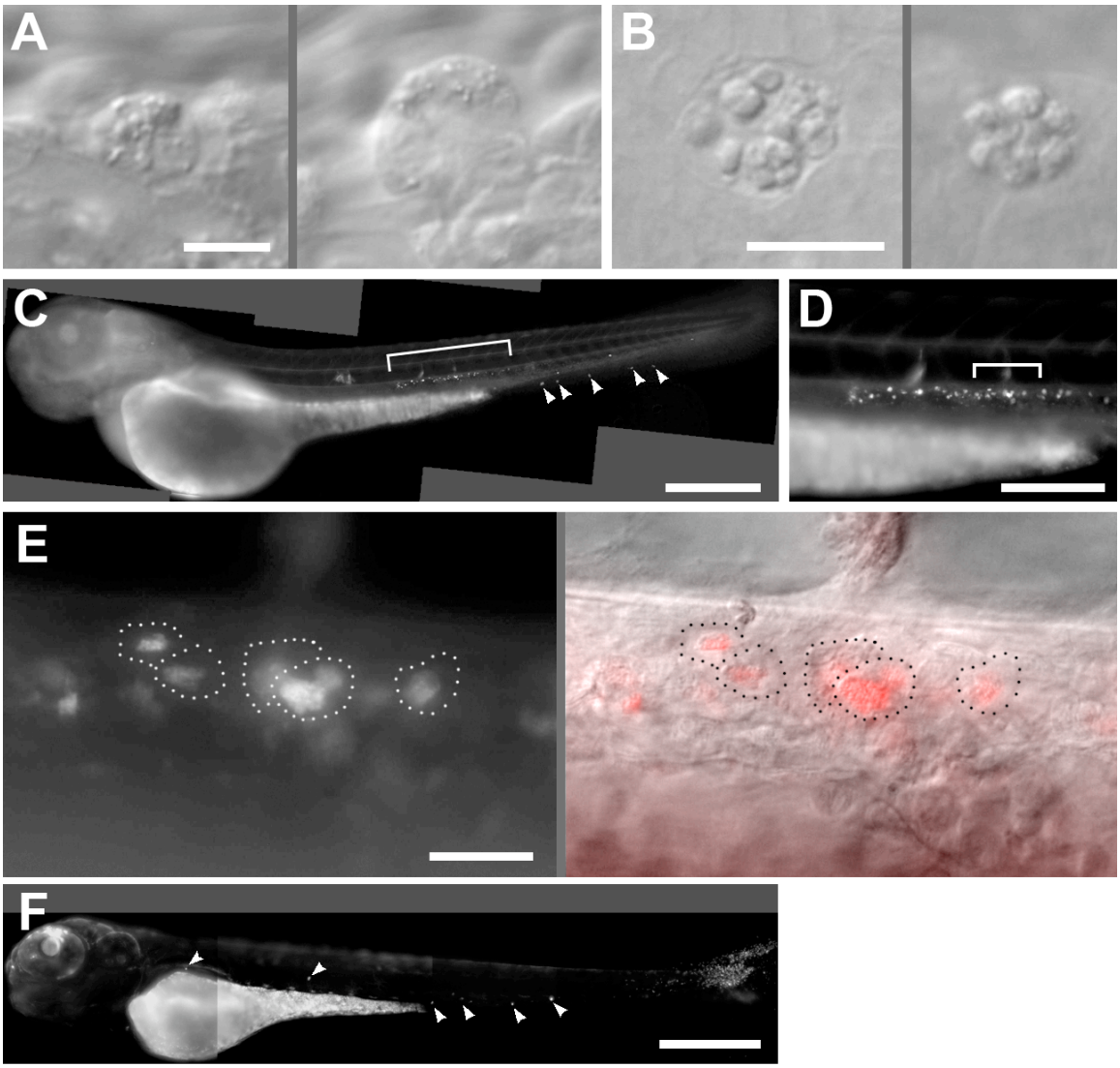

Figure 3.7. Leptospirosis of the zebrafish embryo at 24 hours post infection. A. Two affected cells containing cytoplasmic vesicles, now larger. Scale bar, 10μm. B. Affected cells in the brain, apparently containing clusters of undigested apoptotic bodies. Scale bar, 10μm. C. Fluorescent image of whole embryo infected with SYTO 83-stained leptospira. While some fluorescent leptospires appear around the ventral tail (arrowheads), the majority have localized near the dorsal aorta (bracket). Scale bar, 300μm. D. Higher magnification of the area bracketed in E, showing numerous distinct clusters of stained leptospires lateral to the dorsal aorta, just ventral to the notochord. Scale bar, 100μm. E. Higher magnification of the area bracketed in D, with SYTO 83 fluorescence to the left

and DIC overlay to the right. See Movie 5. Dotted lines indicate the outlines of infected cells. Scale bar 20μm. F. Fluorescence image of embryo 24 hours after infection with green fluorescent *P. aeruginosa*. Infected cells (arrowheads) appear in various places throughout the circulation. Scale bar 300μm.

3.3.6 Supplementary information

Movie 3.4. A single leptospire in the hindbrain ventricle shortly after injection.

Movie 3.5. Phagocytes with intracellular vesicles, shortly after intravenous infection.

Movie 3.6. Infected cells in the hindbrain ventricle. The lowermost cell undergoes blebbing similar to that seen during apoptosis.

Movie 3.7. Phagocytes in the blood flow with large cytoplasmic vesicles at 24 hours post infection.

Movie 3.8. Cells containing leptospires, dorsolateral to the dorsal aorta.

3.4 Summary

In addition to the above mentioned bacterial pathogens, we have observed a few others in the zebrafish embryo at varying levels of detail, and each has followed its own unique pathogenic course, with striking similarities to the corresponding course seen in mammalian infection. Figure 3.8 Illustrates the result of infection with various bacterial pathogens studied. *E. coli* and *B. subtilis* are non-pathogenic to embryos when administered intravenously, both being cleared by embryonic macrophages (Herbomel et al., 1999), although large doses of stationary phase *E. coli* can cause rapid death by mechanism apparently similar to septic shock (Davis and Ramakrishnan, unpublished). As noted in the previous sections, both *P. aeruginosa* and *L. interrogans*, are capable of

surviving in the embryo despite the response of phagocytes. *P. aeruginosa* can additionally be lethal in large enough doses. The outcome of infection with very high numbers of leptospira is not known.

The intracellular pathogens *Salmonella arizonae*, a pathogenic species suited to the lower temperatures of ectotherms, and *M. marinum* differ markedly in pathogenesis both from each other and from the other bacterial species we have observed. Even very small doses of *S. arizonae* prove deadly within hours (Davis et al., 2002). This pathogen appears to thrive both inside and outside of macrophages, eventually overwhelming all phagocytes and growing rapidly in all tissues (see section 5.2 and (Davis et al., 2002)). In contrast, *M. marinum* is taken up by macrophages extremely rapidly, such that intracellular bacteria are not seen after one to two hours post infection. Bacterial replication proceeds gradually but seldom fails to produce a fatal result (Davis et al., 2002).

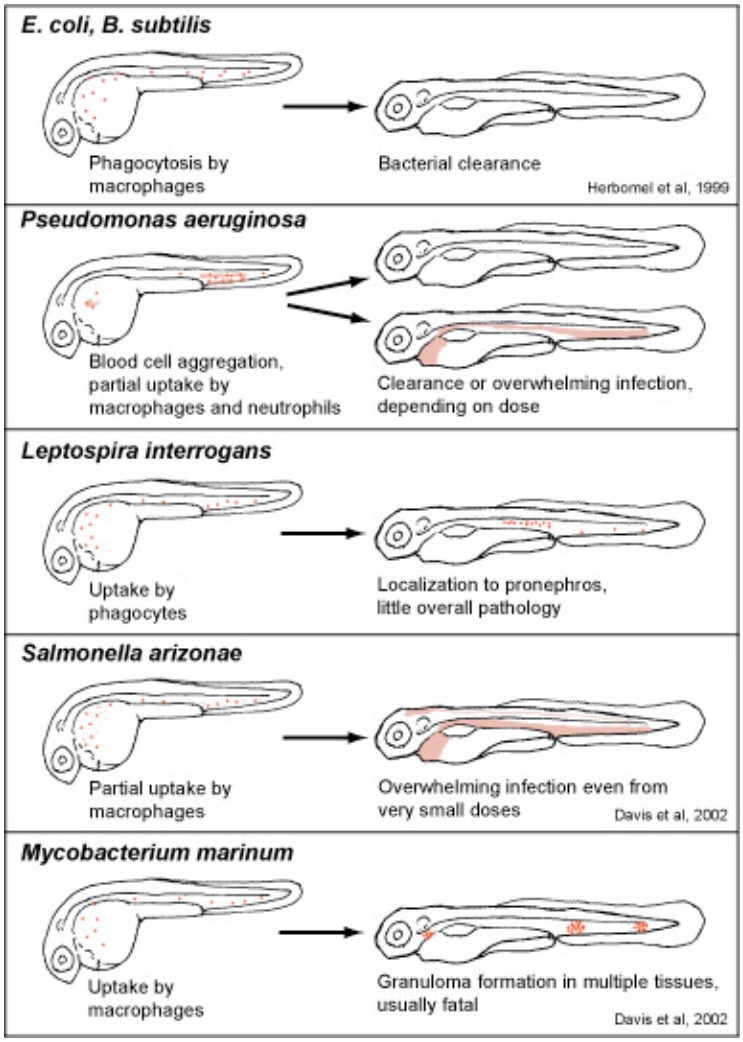

Figure 3.8

On the strength of the detailed observations we and others have made of embryonic zebrafish infections with such a varied series of pathogens, it is safe to conclude that this organism provides a valuable, and specific, tool for understanding bacterial pathogenesis. Because these embryos do not yet possess an adaptive immune system, the cannot recapitulate the full range of host responses present in adult humans. However, the presence of a fully functional phagocyte system, active blood circulation, and a variety of distinct tissue types, makes the embryo an excellent model organism for the study of

innate immunity to infection. With this in mind, the next chapters will illustrate the new understanding of mycobacterial pathogenesis we have been able to acquire using the zebrafish embryonic infection model.

Chapter 4

Dichotomous role of the macrophage in early *Mycobacterium marinum* infection of the zebrafish [1]

[1]This chapter has been published as: Clay, H., **Davis, J. M.**, Beery, D., Huttenlocher, A., Lyons, S. E., and Ramakrishnan, L. (2007). Dichotomous Role of the Macrophage in Early *Mycobacterium marinum* Infection of the Zebrafish. Cell Host and Microbe *2*, 29-39. For my part in this manuscript, I performed microscopical analysis, and participated in experimental design and interpretation. I was directly responsible for data in figure 4.6E and F, and both supplemental movies.

4.1 Introduction

Mycobacteria are facultative intracellular pathogens that infect and survive in host macrophages. Infected macrophages disseminate into the tissue and recruit additional macrophages and lymphocytes to form organized aggregates called granulomas where mycobacterial growth is restricted but not necessarily eradicated (Dannenberg, 1993; Flynn and Chan, 2001b).

While macrophages are known to be key effectors in combating mycobacterial growth after the initiation of adaptive immunity, their role in the early stages of infection is unclear (Flynn and Chan, 2001a; North and Jung, 2004). The ability to grow in cultured macrophages in the absence of stimuli from adaptive immunity is a key distinguishing feature between pathogenic and nonpathogenic mycobacteria (Cosma et al., 2003). In vitro studies have demonstrated that macrophages can significantly restrict pathogenic mycobacterial growth only upon co-incubation with lymphocytes or cytokines such as IFN-γ, suggesting a requirement for adaptive immunity in countering bacterial survival strategies (Flesch and Kaufmann, 1990; Mackaness, 1969; Russell, 1995). Therefore, it is possible that mycobacterial growth is completely unrestricted in macrophages until they become activated by components of the adaptive immune response. In support of this hypothesis, pathogenic mycobacteria can use multiple receptors to gain entry into cultured macrophages (Ernst, 1998) and express factors that facilitate their uptake by macrophages (Mueller-Ortiz et al., 2001; Schorey et al., 1997), suggesting that the bacteria

utilize the host macrophage as a specialized niche that they have evolved to survive in. On the other hand, cultured alveolar macrophages support higher growth of *M. tuberculosis* in the presence of glucocorticoids, suggesting that macrophages do curb bacterial growth using a steroid-sensitive mechanism in the absence of adaptive immune cues (Rook et al., 1987).

Studies in a variety of animal models of tuberculosis have found that mycobacterial numbers increase exponentially during early infection when only innate immunity operates, and plateau co-incident with the development of adaptive immunity (Alsaadi and Smith, 1973; Lazarevic et al., 2005; Lurie et al., 1952; Swaim et al., 2006). *M. tuberculosis*-infected mice depleted of macrophages had decreased bacterial loads and increased survival at five weeks post infection, an effect that was lost when only activated macrophages were depleted (Leemans et al., 2001; Leemans et al., 2005), suggesting that optimal mycobacterial growth is actually dependent on entry into macrophages. In addition, the induction of apoptosis that occurs in infected macrophages has been hypothesized to be a host protective response that deprives the mycobacteria of its ideal environmental niche (Fratazzi et al., 1999). Yet there is also evidence supporting the hypothesis that macrophages can restrict mycobacterial growth from early on. In the mouse model, genetic differences have been identified that influence the rate of mycobacterial replication within macrophages (Pan et al., 2005). However, the role of the macrophage in early tuberculosis when only innate immunity is operant has not been tested directly,

owing to the complexity of the mammalian models that are traditionally used (North and Jung, 2004).

Mycobacterium marinum is a close genetic relative of *M. tuberculosis* and is used as a model to study mycobacterial pathogenesis (http://www.sanger.ac.uk/Projects/M_marinum/). *M. marinum* and *M. tuberculosis* both localize to similar subcellular compartments within infected macrophages (Barker et al., 1997). A subset of *M. marinum* is found in the cytoplasm associated with actin-based motility (Stamm et al., 2003). While actin motility has yet to be demonstrated for *M. tuberculosis*, it has also been found to localize to the cytosol of infected macrophages (McDonough et al., 1993; Myrvik et al., 1984). Therefore it is unresolved whether cytosolic localization represents a difference between the two organisms.

Zebrafish are natural hosts to *M. marinum* and develop organized caseating granulomas that are pathologically similar to those of *M. tuberculosis* (Cosma et al., 2004; Pozos and Ramakrishnan, 2004; Swaim et al., 2006). The zebrafish infection model also mimics mammalian models of tuberculosis in the rapid early increase in bacterial numbers and the dependence upon adaptive immunity for control of infection (Swaim et al., 2006). While the zebrafish has a complex innate and adaptive immune system similar to that of mammals, its embryos and early swimming larvae lack elements of adaptive immunity (Traver et al., 2003). The accessibility of developing zebrafish embryos before the development of adaptive immunity allows study of host-*Mycobacterium* interactions in the sole

context of innate immunity (Davis et al., 2002; Traver et al., 2003; Volkman et al., 2004). The embryo infection model recapitulates the early stages of tuberculosis including granuloma formation, demonstrating the same early rapid increase in bacterial numbers as well as the dependence on the same bacterial virulence determinants seen in the adult zebrafish and mammals (Cosma et al., 2006b; Davis et al., 2002; Volkman et al., 2004).

We have taken advantage of the optical transparency and genetic tractability of the zebrafish embryo to directly dissect the role of the macrophage in early mycobacterial infection by comparing sequential events in embryos that have or lack macrophages. We find that macrophages respond rapidly to infection by migrating to the bacteria and upregulating cytokines. Higher bacterial burdens are rapidly achieved when macrophages are absent, demonstrating that the naïve macrophage curtails bacterial growth considerably. However, we find a critical role for macrophages in tissue dissemination of the mycobacteria, suggesting that these cells have a complex role in determining the outcome of early infection.

4.2 Results

Macrophages, not neutrophils, phagocytose M. marinum early in infection

While macrophages are the main phagocytic cells of mycobacteria (Dannenberg, 1993; Flynn and Chan, 2001a), neutrophils are found to interact with these bacteria in some infection models (Abadie et al., 2005). Zebrafish embryos have

both macrophages and neutrophils (Clay and Ramakrishnan, 2005). By differential interference contrast (DIC) microscopy, the cells containing mycobacteria were morphologically similar to macrophages rather than to neutrophils (Mathias et al., 2006; Renshaw et al., 2006). In order to determine the extent to which neutrophils were phagocytosing mycobacteria, we performed dual fluorescent antibody detection of L-plastin, an actin-bundling protein present in both macrophages and neutrophils, and myeloperoxidase (MPO), an enzyme that is expressed only by neutrophils and not macrophages in the zebrafish (Clay and Ramakrishnan, 2005; Mathias et al., 2006). Embryos injected with *M. marinum* via the caudal vein (Fig. 4.1A) were assessed for uptake of bacteria by MPO-positive cells. The majority of bacteria were found in L-plastin-positive, MPO-negative cells, indicating that while neutrophils are present, they are significantly less likely to phagocytose *M. marinum* (Fig. 4.1B and C). There is still the possibility that neutrophils are impacting infection by altering the activity of macrophages, as has been suggested in other systems (Tan et al., 2006).

Macrophages migrate rapidly and specifically to mycobacteria and upregulate inflammatory cytokines

To examine the earliest interactions between mycobacteria and macrophages we injected mycobacteria or similar-sized fluorescent beads into the hindbrain ventricle at 30 hours post fertilization. The hindbrain ventricle (Fig. 4.1A) is a neuroepithelial-lined structure (Lowery and Sive, 2005) that normally has zero to

two phagocytic cells at this time (Herbomel et al., 1999) and we had previously found that phagocytes are recruited to this cavity upon injection of mycobacteria (Davis et al., 2002). To test the specificity of this migration, we compared the number of cells in the hindbrain ventricle in response to injection of bacteria versus injection of like-sized latex particles or medium alone. Phagocytes arrived at the hindbrain ventricle within six hours in response to mycobacteria, but not in response to inert latex beads or injection medium (Fig. 4.2A). Both live and heat-killed bacteria recruited phagocytes, suggesting that cell wall lipids or heat stable proteins stimulate macrophage migration pathways (Krutzik and Modlin, 2004).

The use of Fluorescent Whole Mount In Situ Hybridization (FISH) (Clay and Ramakrishnan, 2005) indicated that infected cells expressed the macrophage marker *c-fms*, which encodes the receptor for macrophage colony stimulating factor (Fig. 4.2C) (Herbomel et al., 1999). To assess macrophage activation we looked for the induction of inflammatory cytokine expression, specifically Tumor Necrosis Factor-a (TNF) and Interleukin 1b (IL-1b), in infected macrophages. Double FISH revealed that infected macrophages upregulate both TNF and IL-1b specifically in response to infection (Fig. 4.2B, C and data not shown), while neither cytokine was detectable in macrophages of uninfected embryos within 24 hours of *M. marinum* infection (Fig. 4.2C and data not shown). While FISH was unable to detect the expression of these cytokines in uninfected embryos, this does not rule out the possibility that uninfected macrophages in infected embryos upregulate proinflammatory cytokines, as DIC identification of

bacteria following the FISH procedure is not always possible. It is also possible that these cytokines were induced in other cell types below the limit of detection of FISH. However, we were able to confirm TNF and IL-1b induction in whole infected embryos using quantitative real-time PCR (Fig. 4.2D). Taken together, these data show that macrophages respond rapidly and specifically to mycobacteria by migrating to sites of inoculation and upregulating key cytokines.

Mycobacterial growth is increased in the absence of macrophages

To determine the effect of macrophages on the growth of mycobacteria in vivo, we created embryos lacking macrophages by injection of modified anti-sense oligonucleotides (morpholino, or MO) directed against the myeloid transcription factor gene *pu.1*, creating embryos we will refer to as morphants (Rhodes et al., 2005). Consistent with previous results (Rhodes et al., 2005), DIC microscopy (Davis et al., 2002; Herbomel et al., 1999) revealed the lack of macrophages in the *pu.1* morphants but not control embryos and these findings were confirmed by the absence of *c-fms*-positive cells by FISH (data not shown). As noted previously, there were some residual MPO-positive cells in the morphants (Rhodes et al., 2005).

While macrophages are almost completely lost in the first 48 hours, small numbers may reappear over the course of the next several days in some embryos as the MO is diluted by embryonic growth and as a second wave of hematopoiesis is initiated (Murayama et al., 2006; Nasevicius and Ekker, 2000).

To confirm the loss of macrophages over time, we infected control and *pu.1* morphants intravenously with *M. marinum* expressing the red fluorescent protein dsRed under a constitutive promoter and green fluorescent protein (GFP) under a macrophage-activated promoter (Cosma et al., 2004). Within seven hours post infection (hpi) of control embryos, all bacteria were both red and green fluorescent by virtue of being phagocytosed by macrophages (Fig. 4.3A). In contrast, almost none of the red fluorescent bacteria became green fluorescent in the *pu.1* morphants, even at four days post infection (dpi) (Fig. 4.3B). Examination by DIC microscopy suggested that most, if not all, mycobacteria remained extracellular in the absence of macrophages. Notably, no increased uptake of mycobacteria by the small population of residual neutrophils in the *pu.1* morphants was found over the low background levels found in the control fish (Fig. 4.1B, C and data not shown).

To assess *M. marinum* growth in the presence and absence of macrophages, we compared bacterial loads in intravenously infected embryos by fluorescence microscopy and by enumerating bacterial counts. Mycobacterial burdens were higher in the absence of macrophages, reaching a ten-fold difference per embryo at four dpi when injected into the blood stream (Figs. 4.3C and 4.4A and B). Bacterial burdens were also found to be significantly higher in the absence of macrophages when bacteria were injected into the HV (Fig. 4.3C) suggesting that macrophages rapidly curtail mycobacterial growth whether they

first encounter these pathogens in the bloodstream or after traversing epithelial surfaces to the infection site.

Consistent with the mouse *pu.1* mutant phenotype which is embryonic lethal between 17-18 days (Scott et al., 1994), the zebrafish *pu.1* morphants had variable mortality occurring after seven days post fertilization (dpf) depending on the penetrance of the morpholino. The morphants appeared morphologically normal during the course of our experiments and did not display increased susceptibility to the environmental microbes encountered in their conventional (non germfree) rearing conditions, suggesting a specific hypersusceptibility to macrophage pathogens, including mycobacteria. To address further the specificity of their hypersusceptibility to mycobacteria, we infected the *pu.1* morphants with similar numbers of a nonpathogenic *Escherichia coli* strain and found that they cleared the bacteria rapidly in a time frame identical to control embryos (Supplementary Fig. 4.1). Second, the hypersusceptibility phenotype is unlikely to result from nonspecific effects preceding the embryonic lethal phenotype seen at and after seven days pf. The zebrafish earl grey (*egy*) mutant that is embryonic lethal at seven to eight dpf with thymic hypoplasia and other organ-specific defects but normal myeloid and erythroid lineages (Trede et al., 2007) has a normal response to *M. marinum* infection that is indistinguishable from wildtype embryos (Davis et al., 2002). We also examined infection in another embryonic lethal mutant, neurogenin 1 (*ngn1*), which has severe defects in primary neuron development and dies between six and eight dpf (Cornell and

Eisen, 2002; Golling et al., 2002). The *ngn1* mutants have normal macrophages and the course and phenotype of *M. marinum* infection was found to be identical to clutch-matched controls (Supplementary Fig. 4.2).

Taken together these data strongly suggest that the hypersusceptibility of the *pu.1* morphants to mycobacteria results from their lack of macrophages. The considerable restriction of mycobacterial growth by macrophages precedes cues from the adaptive immune system, which has not yet developed in the embryo, as well as granuloma initiation, which occurs after three to five days of infection (Davis et al., 2002).

The lack of macrophages rescues the growth attenuation of the mycobacterial virulence determinant Erp

Virulence determinants such as Erp exert their influence on virulence by enabling mycobacterial growth in macrophages from early on (Berthet et al., 1998; Cosma et al., 2006a; Cosma et al., 2003). To test the specificity of the mode of action of such virulence determinants, we examined the course of infection of an Erp-deficient *M. marinum* strain (Cosma et al., 2006a) in control versus *pu.1* morphants. Due to the enhanced susceptibility of Erp-deficient bacteria to detergents in the embryo lysis buffer, CFU cannot be enumerated (Cosma et al., 2006a) and we could assess bacterial burdens within the embryos only by microscopy. Erp-deficient bacteria showed the expected growth attenuation in control embryos by fluorescent microscopy (Cosma et al., 2006a) (Fig. 4.4A and

C). However, similar to the WT bacteria, the mutant bacteria attained much higher levels in the *pu.1* morphants (Fig. 4.4B and D). This experiment shows that mycobacteria express virulence determinants that specifically allow them to overcome the restrictive growth environment found within macrophages in the context of innate immunity. However, despite the specific macrophage growth enhancement afforded by such determinants, the bacteria can only partially overcome macrophage defenses and fail to attain maximal growth in these cells.

Macrophages are required for early dissemination of mycobacteria into host tissue

In the absence of macrophages, bacteria grew rapidly to fill the compartments in which they were injected in the *pu.1* morphant embryos, be it the vasculature in the case of intravenous injection, or the brain ventricle cavity in the case of hindbrain injections. DIC microscopy showed that these bacteria were growing extracellularly. However, it was unclear whether or not mycobacteria had access to deeper tissue in *pu.1* morphants. Our finding that macrophages can substantially curtail mycobacterial growth even early in infection led us to speculate that the organisms might derive a different benefit from establishing early residence in macrophages, namely gaining dissemination into distant tissues. Macrophages are thought to carry mycobacteria into tissues where they aggregate into granulomas (Dannenberg, 1993). Similarly, our real-time visualization studies in the zebrafish embryo had shown *Mycobacterium*-infected

macrophages traversing epithelial barriers (Davis et al., 2002). However, in vitro studies using transwells have suggested that while macrophages enhance mycobacterial transit across epithelial barriers, they are not required for it (Bermudez et al., 2002). Indeed, the mycobacterial RD1 virulence determinant had been suggested to mediate direct bacterial transit across epithelia, using indirect assessments based on the inability of RD1-deficient bacteria to lyse epithelial cells in culture (Hsu et al., 2003).

We were able to assess directly in vivo the role of macrophages in early mycobacterial dissemination by quantitating dissemination events in the presence and absence of macrophages. We made this assessment at 16 hpi so as to avoid two confounding variables occurring at later time points, namely the increased bacterial burdens that occurred starting around two days pi in the absence of macrophages (Fig 4.3C and data not shown) and the return of macrophages in some *pu.1* morphants at later time points. While isolated macrophages would not substantially limit net bacterial growth, they would be sufficient to account for bacterial dissemination events in this assay.

To establish infection, *M. tuberculosis* is proposed to first cross epithelial barriers and subsequently disseminate hematogenously to other sites within the lungs (Dannenberg, 1993; Harding and Smith, 1977; McMurray, 2003). Therefore, we wished to assess the role of macrophages in mycobacterial traversal of both epithelial and vascular endothelial barriers. First we determined whether bacteria that were injected into the hindbrain ventricle could disseminate

into host tissue in the absence of macrophages (Fig. 4.5A-C). Bacteria disseminated out of the hindbrain ventricle in more than half of the control morphants, whereas none of the *pu.1* morphants displayed any extraventricular bacteria (Table 4.1). All extraventricular bacteria were found to reside within phagocytes as determined by DIC microscopy, suggesting that macrophages are required for bacteria to cross the epithelial barrier of the hindbrain ventricle and gain access to additional host tissues.

To determine if macrophages are required for hematogenous tissue dissemination of mycobacteria, we made use of the *fli1:EGFP* transgenic zebrafish line which expresses GFP throughout the vasculature (Lawson and Weinstein, 2002). Red fluorescent mycobacteria were injected into the bloodstream of control and *pu.1* morphant *fli1:EGFP* embryos. Infected fish were monitored by fluorescent microscopy to determine whether or not bacteria could traverse the vascular endothelium in the absence of macrophages (Fig. 4.6). A significantly higher number of control embryos had extravascular bacteria compared to *pu.1* morphants at 16 hpi (Table 4.1). All bacteria in the control embryos appeared to reside within phagocytes as determined by DIC and confocal microscopy. In the two *pu.1* morphants that did have extravascular bacteria by 16 hpi, the bacteria appeared to be in residual macrophages as judged by DIC microscopy. To confirm our findings that bacteria were not traversing the vascular endothelium without macrophages, we examined the embryos at higher resolution by confocal microscopy. Three dimensional

reconstruction images confirm that several bacteria in embryos with macrophages had traversed the vasculature whereas bacteria in hosts lacking macrophages remain within the vasculature (Fig. 4.6E and F and Supplemental movies 4.1 and 4.2). These data demonstrate that macrophages are required for mycobacterial traversal of both epithelial and endothelial barriers early in infection.

4.3 Discussion

The zebrafish infection model, by allowing genetic manipulation of both host and pathogen, highlights the complex relationship between pathogenic mycobacteria and host phagocytes starting from their earliest encounter. By depleting macrophages in the sole context of innate immunity we have revealed a dual early role in simultaneously curtailing mycobacterial numbers while enabling these pathogens to establish systemic infection by disseminating them to deeper tissues. Our recent finding that *M. marinum* infection of zebrafish is moderated by adaptive immunity akin to *M. tuberculosis* infection of mice and humans (Swaim et al., 2006) suggests that the relative contribution of innate and adaptive immunity to the control of mycobacterial infection is similar in fish and mammals. Moreover, we have observed the same early increase in mycobacterial numbers in both adult and embryonic zebrafish occurs in mammalian models of tuberculosis (Swaim et al., 2006; Volkman et al., 2004). These findings in the zebrafish are consistent with the existing model based on *M. tuberculosis*

infection of mammals including those based on aerosol infection of alveolar macrophages, that higher bacterial burdens are achieved in macrophages prior to the initiation of adaptive immunity. Therefore the results presented in this study that mycobacterial burdens are even higher in the absence of macrophages may also be relevant to mammalian tuberculosis.

The model that macrophages do little to curtail pathogenic mycobacterial growth without cues from adaptive immunity has been supported mainly by the mouse macrophage depletion studies concluding that *M. tuberculosis* numbers are lower in the context of nonselective depletion of host macrophages (Leemans et al., 2001; Leemans et al., 2005). However, these conclusions are problematic. Macrophage depletion resulted in lower lung bacterial counts only at five weeks but not at two weeks post infection, calling into question their conclusion that residence in naïve macrophages promotes mycobacterial growth. Rather these results suggest that macrophage depletion may have altered priming of the adaptive immune response. In support of this alternative interpretation, they found that macrophage depletion was associated with altered T-cell recruitment to the lung as well as dysregulation of both T-cell activating and T-cell produced cytokines (Leemans et al., 2001; Leemans et al., 2005). The failure of these studies to find the early bacterial growth enhancement in the absence of macrophages that we found could be due to differences between the models used. Alternatively, the partial macrophage depletion (~70%) achieved in

prior studies may have decreased the extent of extracellularly growing mycobacteria.

Our findings in *M. marinum* are supported by epidemiological evidence from tuberculosis suggesting an early microbicidal activity of human macrophages against *M. tuberculosis*. First, there is evidence to suggest that innate immunity plays a role in clearing *M. tuberculosis*. Differential rates of PPD skin-test conversion, an indication that adaptive immunity has been invoked, in different populations with the same level of exposure to *M. tuberculosis* suggests genetic differences in the innate ability to clear infection (Stead, 2001). Additionally, epidemiological studies have linked host factors that are thought to operate during innate immunity, including vitamin D receptor, Nramp, and components of the complement and IL-1b pathways (Bellamy et al., 1999; Bellamy et al., 1998; Selvaraj et al., 1999; Wilkinson et al., 1999) to human susceptibility to tuberculosis.

Our dissection of the earliest mycobacterium-macrophage interaction is the first study to directly address the ability of innate macrophages to restrict pathogenic mycobacterial growth. Our data show that these primary host cells for mycobacteria do not provide them with an optimal niche if growth alone is considered. The question, then, is why these exquisitely host-adapted pathogens would reside in a cell that prevents maximal growth. Part of the answer may lie in the enhanced dissemination that is afforded by residence in macrophages. A number of intracellular pathogens utilize dissemination by host

phagocytes to establish infection within specific host tissues. A recent study has demonstrated that *Listeria monocytogenes* requires a specific subpopulation of dendritic cells for efficient dissemination from blood into the spleen (Neuenhahn et al., 2006). Other intracellular pathogens such as salmonella have been shown to directly influence host cell motility in order to promote tissue invasion (Worley et al., 2006). While such a mycobacterial factor driving host cell dissemination has not been identified, the discovery that the mycobacterial virulence locus RD1 promotes macrophage aggregation into granulomas (Volkman et al., 2004) indicates that additional bacterial factors may enhance the ability of infected macrophages to gain entry into deeper tissues. Alternatively, bacterial factors may promote macrophage recruitment to the infection site, as shown in this study, and general mechanisms, inflammatory or homeostatic, may transport the infected macrophages back into the tissues. Whatever the mechanism, it is the ability of pathogenic mycobacteria to substantially evade macrophage effector functions early in infection that allows them to take advantage of these cells to gain access to deeper tissues.

Tissue dissemination may favor mycobacterial survival and growth by providing these organisms with a secluded niche where they can avoid competition from mucosal flora. Furthermore, taken together, our results suggest a model where mycobacteria may reside initially in macrophages and eventually lyse the host cell and grow extracellularly. Infected macrophage necrosis correlates with increased mycobacterial proliferation and virulence (Chen et al.,

2006; Duan et al., 2002; Pan et al., 2005). A similar growth strategy is employed by salmonella, which also induces cell death after gaining entry into tissues via macrophages (Guiney, 2005). Alternatively, while initial tissue dissemination may favor the pathogen, the migration of infected phagocytes could also benefit the host as a mechanism for antigen presenting cells to prime the adaptive immune response. In particular, dendritic cells have been shown to participate in trafficking mycobacteria into the lymph nodes (Humphreys et al., 2006). Dendritic cell marker homologs such as CD11c have been identified in the zebrafish genome (http://www.ensembl.org/Danio_rerio/index.html) and cells resembling dendritic cells have been produced from long-term spleen cultures in other teleost fish (Bols et al., 1995). We do not see cells resembling dendritic cells in the zebrafish embryo, consistent with the finding that they develop later in ontogeny in the mouse (Dakic et al., 2004).

Therefore we cannot rule out the possibility in our experimental model that the dynamics of early bacterial trafficking may be different in the presence of dendritic cells.

Finally, submaximal growth within macrophages may be an evolutionary survival and transmission strategy for mycobacteria as it may prevent quickly overwhelming its host, enabling extensive transmission during chronic cavitary disease. This extensive co-adaptation of mycobacteria to host may have allowed them to be such successful pathogens over evolutionary time despite the lack of classical virulence determinants, such as toxins (Cosma et al., 2003). The new

recognition of the substantial ability of macrophages to curtail pathogenic mycobacterial growth from very early in infection as well as their role in disseminating infection could provide a pharmacological starting point for new tuberculosis eradication strategies.

4.4 Experimental Procedures

Animal care and strains

Wild-type WIK zebrafish embryos were maintained and infected with bacteria as described (Cosma et al., 2006b; Davis et al., 2002). *Fli1:EGFP* transgenic fish were obtained from ZIRC (http://zfin.org/zirc/home/guide.php). Neurogenin mutant fish were donated by David Raible. Infections were performed one day post-fertilization by injecting bacteria into the hindbrain ventricle or caudal vein.

Microscopy

DIC and widefield fluorescence pictures were taken and compiled as described (Davis et al., 2002; Volkman et al., 2004). Confocal images were acquired on an Olympus Fluoview 1000 laser scanning confocal microscope using a 20x air objective, N.A.=0.7. 3D datasets were deconvolved using Autoquant X software (Media Cybernetics, Inc.), starting from a theoretical point spread function and using ten iterations of an adaptive deconvolution algorithm. Maximum intensity reconstructions and movies were also produced on AutoQuant X.

Bacterial CFU enumeration

CFU counts were taken from whole embryos as follows: Pools of four fish were anaesthetized in microcentrifuge tubes with 4mg/mL Tricaine (Sigma A5040), supplemented with 20mg/mL of kanamycin and placed on ice for 30 minutes. Tubes were spun down briefly and the liquid was aspirated. The embryos were dissociated in100mL 0.1% Triton X-100 by smashing with a p-1000 pipette tip, then lysed by adding 100mL of Mycoprep™ reagent (BD BBL 240862) for nine minutes. After vortexing briefly and adding 1.3mL PBS, the homogenates were centrifuged for15 minutes. 1.2 mL of supernatant was removed and the remaining liquid was diluted in PBS supplemented with 0.05mg/mL BSA and 0.05% Tween80. Serial dilutions were plated on bacterial media supplemented with kanamycin. CFU were counted and plotted on a log scale by taking the number of bacteria on each plate dilution and dividing by the number of pooled fish (3 or 4) to calculate the number of CFU per embryo.

Fluorescent whole mount in situ hybridization

Fluorescent in situ hybridization was performed as described previously (Clay and Ramakrishnan, 2005). Zebrafish *tnf* (ZFIN ID: ZDB-GENE-050317-1) was cloned from a moribund adult zebrafish cDNA pool constructed by isolating RNA from homogenized whole fish tissue using the Absolutely RNA™ RT-PCR Miniprep kit (Stratagene 400800) and cDNA was transcribed using the Accuscript

™ HF cDNA Kit (Stratagene 200820) as described by the manufacturer. Cloning primers used for TNF were:

F 5'-GACTGTGCAGGATCCATGAAGCTTGAGAGTC-3' and

R 5' GATCGAGCTCCCGGGTCACAAACCAAACACCC-3', and cloning primers for IL-1b were F 5'-ACGGATCCAGCTACAGATGCGACATGCA-3' and R 5'-ACGAATTCCTTGAGTACGAGATGTGGAGA-3'.

Antibody staining

Embryos were fixed, dehydrated, and prepared as for in situs as described (Clay and Ramakrishnan, 2005). The MPO antibody was made as described previously (Mathias et al., 2006). Polyclonal antibodies to zebrafish L-plastin were generated by injecting rabbits with a GST-L-plastin fusion protein that was purified as described previously (Bennin et al., 2002). The GST-L-plastin plasmid was a gift from Paul Martin. MPO and -L-plastin antibodies were incubated at 1:300 and 1:500, respectively, and visualized using TSA detection as described (Clay and Ramakrishnan, 2005).

Real time PCR

All real time PCR experiments were performed with three biological replicates with the appropriate controls using SYBR® Green PCR Mix (Applied Biosystems 4309155) or Taqman® PCR Mix (Applied Biosystems 430447) on an ABI 7300 Real-Time PCR Machine at a 60°C annealing temperature. Briefly, bactches of

30-50 embryos were used per condition per biological replicate, and each biological replicate was run in triplicate on two separate plates to minimize any variation resulting from plating conditions. The six data points for each condition were averaged to create a single biological replicate data point. Fold increase for infected over mock-injected embryos was calculated using the DC method using b-actin as a reference. Biological replicates were averaged for statistical analysis. SYBR primers for IL-1b are described (Pressley et al., 2005). Taqman primers for *tnf* are:

F 5'- TTCCAAGGCTGCCATCCATTTA-3' and

R 5'- GGTCATCTCTCCAGTCTAAGGTCTT-3', probe used was

5' ACAGGTGGATACAACTCT-3'.

RNA was extracted using TRIzol® Reagent (Invitrogen 15596-026) per manufacturers protocol. cDNA was transcribed as described above.

Morpholinos

Morpholinos were obtained from Genetools. Control MO were either the Pbx-2 mutant control MO described in Waskiewicz et. al. (Waskiewicz et al., 2002) (used for experiments done for Fig. 3) or 1mM of control MO supplied by Genetools (used for experiments done for Figs. 4 and 5). *pu.1* MO oligos were designed to the transcription initiation site:

(CCTCCATTCTGTACGGATGCAGCAT)

and the exon 4-5 boundary:

(GGTCTTTCTCCTTACCATGCTCTCC)

and combined to final concentrations of 0.375mM and 0.025mM respectively. 5 nL of MO mix was injected per embryo into the yolk at the 1-2 cell stage.

Statistics

Statistical analysis was performed by using In-Stat software (Graphpad Software, Inc).

4.5 Figures

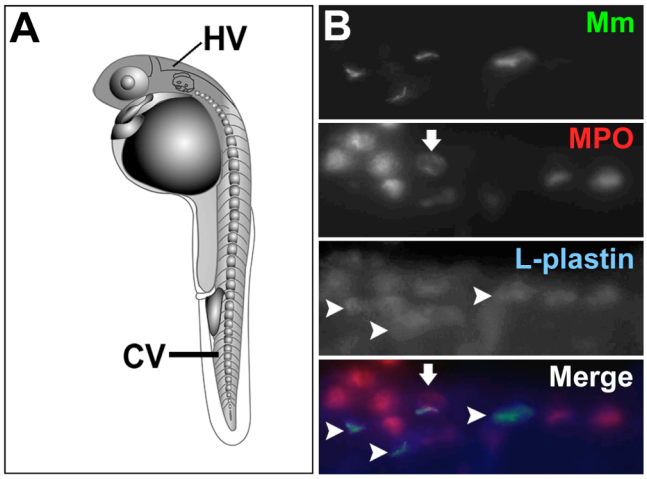

C	MPO+ / MPO-	Average MPO+	Average MPO-	p-value
1 dpi (n=9)	1/34	0.11 ± 0.33	3.89 ± 2.57	<0.001
2 dpi (n=9)	2/59	0.22 ± 0.67	6.56 ± 5.13	<0.001
4 dpi (n=8)	6/59	0.75 ± 0.89	7.38 ± 2.07	<0.001

Fig 4.1. Macrophages are the primary cell to phagocytose *M. marinum*. A) Diagram of one day post fertilization (dpf) zebrafish embryo showing caudal vein (CV) and hindbrain ventricle (HV) injection sites. B) Dual fluorescent labeling of myeloperoxidase (MPO) and L-plastin antibodies in two dpf fish infected with green fluorescent *M. marinum* (Mm). Infected macrophages as indicated by L-

plastin-positive, MPO-negative staining are indicated with arrowheads. An MPO-positive cell that is partially colocalized with GFP expressing bacteria is either adjacent to or possibly phagocytosing a bacterium is indicated with an arrow. Images are taken from the caudal vein. Scale bar, 25 μm. C) Numbers of infected MPO-positive cells versus all infected phagocytes in a low-dose infection (12 ± 3 CFU) analyzed at two, three, and five dpi. Data are presented as total number of infected MPO-positive cells out of total number of infected *M. marinum*-containing cells for all fish, and as average number of MPO-positive and negative cells per fish ± the standard deviation. Statistics were calculated using Student's paired t-test for average numbers of MPO-positive versus MPO-negative cells per fish.

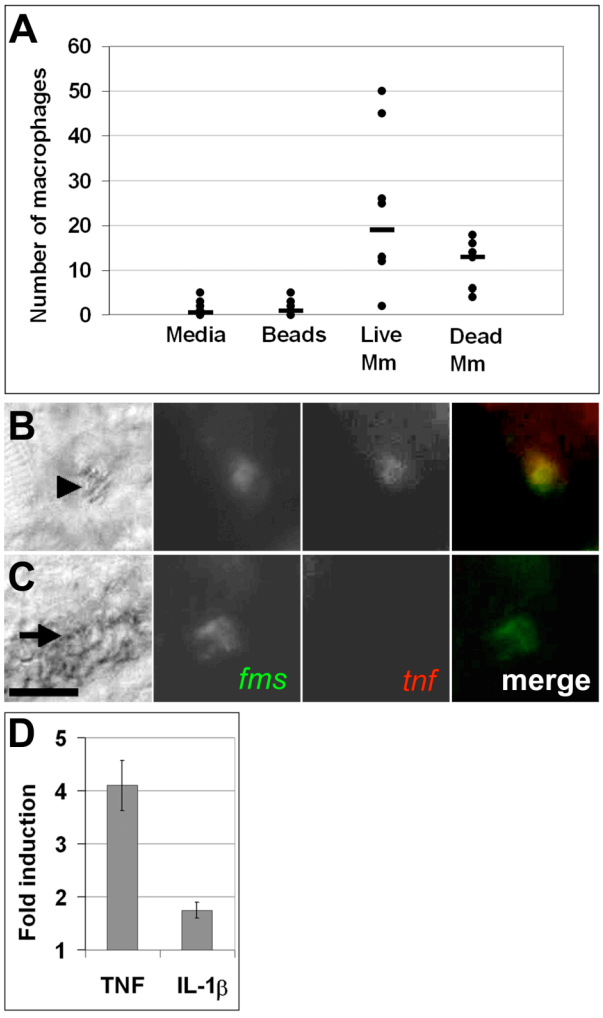

Fig 4.2. Macrophages undergo rapid functional and molecular changes in response to mycobacterial infection. A**)** Graph of number of macrophages recruited six hours after HV injection. Mm is *M. marinum.* Medians are indicated by bars. Data from each condition were compared using a Kruskall-Wallis non-parametric ANOVA ($p<0.0001$). $p<0.01$ for all pair wise comparisons of medium or beads vs. live or dead bacteria. Difference in median number of macrophages recruited by live vs. dead bacteria was not significant. B, C) Differential interference contrast (DIC) (left) and fluorescence images of five dpf infected (B) and uninfected (C) embryos stained using double fluorescence in situ hybridization for *c-fms* (green) and *tnf* (red). Macrophages imaged here were in the caudal vein. Arrowhead in B indicates bacteria within a macrophage visible by DIC microscopy; arrow in C indicates position of uninfected macrophage. Scale bar, 10 μm. D) Quantitative real time PCR values for whole fish one dpi plotted as fold increase over mock injection for TNF at a low dose infection (32 ± 4 CFU, n = 3, $p<0.05$ using a one sample t-test against a hypothetical mean of 1.0) and IL-1β at a high dose infection (205 ± 38 CFU, n = 4, $p<0.05$). Error bars represent standard deviation.

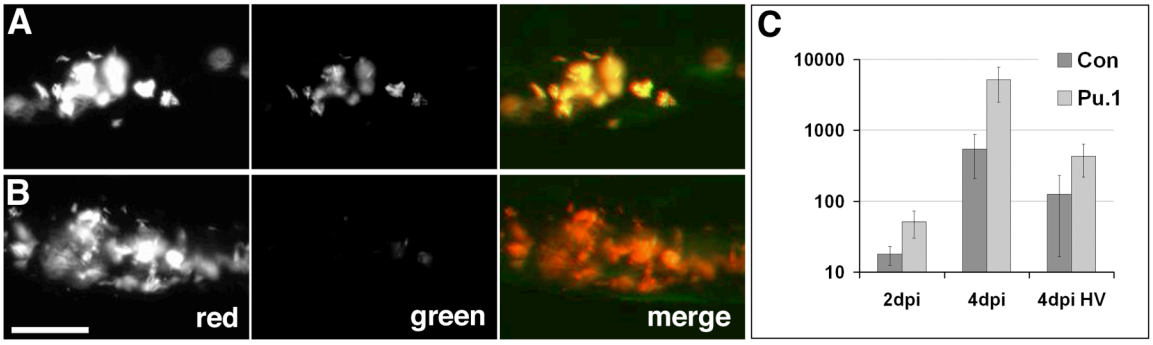

Fig 4.3. Mycobacteria achieve higher burdens in *pu.1* morphant embryos lacking macrophages. Control (A) and *pu.1* morphants (B) infected with *map49::gfp;msp12::dsRed* bacteria that are constitutively red fluorescent and both red and green fluorescent upon macrophage infection, shown here at four dpi. Scale bar, 50 μm. C) Mean bacterial colony forming units (CFUs) per

embryo at two and four dpi. Error bars represent standard deviations. Mean CFUs from in control vs. *pu.1* morphants were significantly different at both time points ($p<0.01$ at two dpi and four dpi, $p<0.05$ at four dpi HV using Student's unpaired t-test). Inoculum for caudal vein infections was 35 ± 8 CFU, n=5 sets of four fish for each data set. Inoculum for hindbrain ventricle (HV) infections was 14 ± 5, n=5 sets of four control and n=4 sets of three *pu.1* morphants.

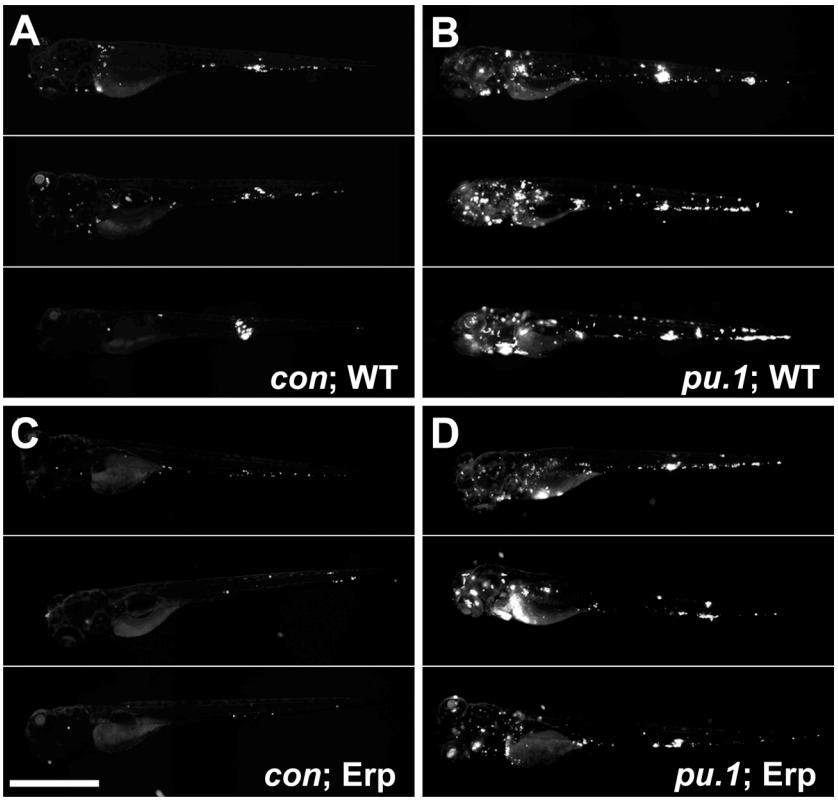

Fig 4.4. The absence of macrophages rescues the growth defect of the *M. marinum* Erp-deficient mutant. For each condition, ten embryos were infected and monitored for four dpi. Images were obtained under the same settings for all embryos and assembled for each condition in descending order of fluorescence (indicating infectivity) as judged visually. Very little difference was noted within embryos in a given condition. The three most infected individual embryos are shown for each condition. Four dpi control (A, C) and *pu.1* morphant (B, D) embryos infected with 50 ± 16 CFU of wild-type (A, B) or 56 ± 6 Erp-deficient *M.*

marinum (C, D). Fluorescence represents infecting bacteria in all panels. Scale bar, 250μm.

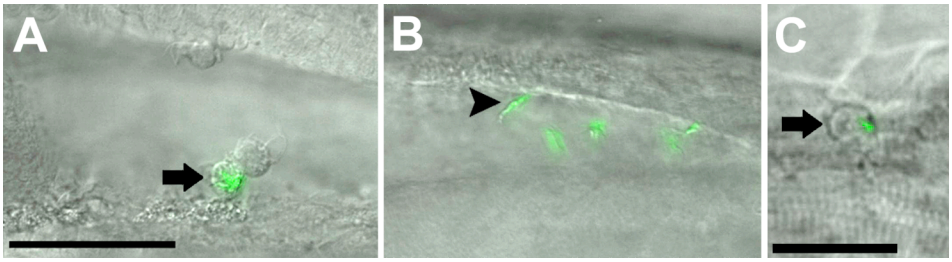

Fig 4.5. Infecting mycobacteria fail to disseminate to tissues in the absence of macrophages. A-C) Control and *pu.1* morphants injected at 22 hpf into the hindbrain ventricle and scored for dissemination out of the ventricle at 16 hpi. Macrophages are visible in the ventricle of a control (A) embryo, an infected macrophage is indicated by an arrow. A *pu.1* morphant (B) has extracellular bacteria (arrowhead) in the hindbrain with no evidence of macrophages in the cavity. Fluorescence is slightly blurred due to Brownian motion of unanchored bacteria in the cavity. C) An infected control macrophage has disseminated out of the hindbrain ventricle and is shown here in the trunk of the tail. Scale bars, 50 μm (A, B), 25 μm (C).

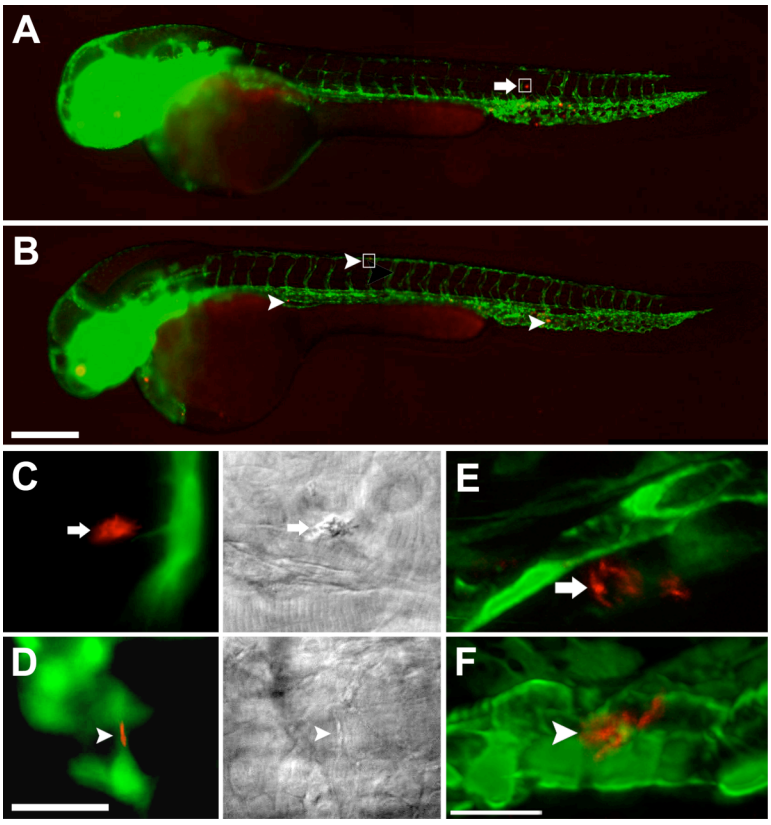

Fig 4.6. Infecting mycobacteria remain in the vasculature in the absence of macrophages. *fli1:EGFP* transgenic embryos infected with 161 ± 10 red fluorescent bacteria imaged 16 hpi by widefield (A-D) or confocal microscopy (E, F). Whole fish overlays of green fluorescent vasculature and red fluorescent injected bacteria for control (A) and *pu.1* morphants (B). Yolk and yolk extension appear red due to autofluorescence. Boxes in (A) and (B) are the areas shown magnified in (C) and (D), respectively. Arrows in control embryos show bacteria that do not colocalize with green fluorescent vasculature indicating they have migrated into tissue (A, C, E). DIC imaging in the right half of panel f shows that bacteria are within a macrophage. Arrowheads in *pu.1* morphant shows a bacterium colocalizing with the vasculature indicating it has not migrated into tissues (B, D, F). DIC imaging in the right half of panel (D) shows that the bacterium is not in a macrophage. Three dimensional reconstruction images (maximum intensity) of 48 hpi control (E) and *pu.1* morphant embryos (F). Movies of rotational views of these images are provided in supplemental movies

1 and 2 to show in greater detail the spatial relationship of the bacteria to the vasculature. Scale bars, 250 μm (A, B), 25μm (C, D), 15μm (E, F).

	con	*pu.1*	p-value
Ventricle Dissemination	6/10	0/10	0.011
Vascular Dissemination	9/11	2/10	0.003

Table 4.1. Macrophages are required for early dissemination of mycobacteria. Dissemination at 16hpi was assessed for bacteria injected into the hindbrain ventricle or into the caudal vein of *fli1:egfp* transgenic embryos. Embryos were scored for dissemination events and statistics were calculated using a contingency table and Fisher's exact t-test.

4.6 Supplemental information

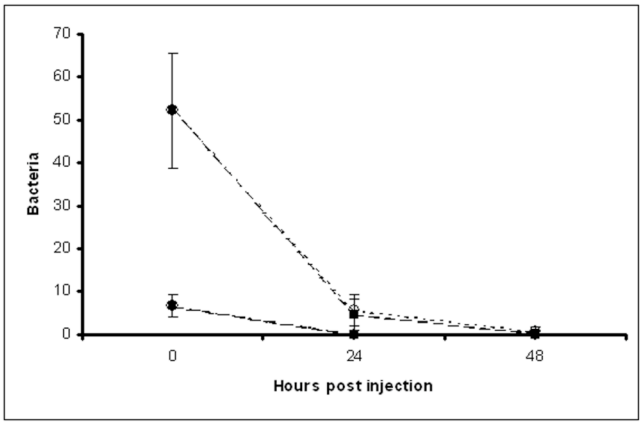

Supplemental Figure 4.1. Control (black squares) and *pu.1* morphant embryos (open circles) clear nonpathogenic *Escherichia coli* at the same rate. Data are almost completely overlapping at individual time points. Injection with dsRed-expressing *E. coli* leads to dose-dependant clearance of bacteria within 48 hours post injection. Time zero indicates inoculation dose and bacteria were

enumerated in the fish by visual inspection for numbers of fluorescent bacteria. Error bars represent standard deviation from the mean.

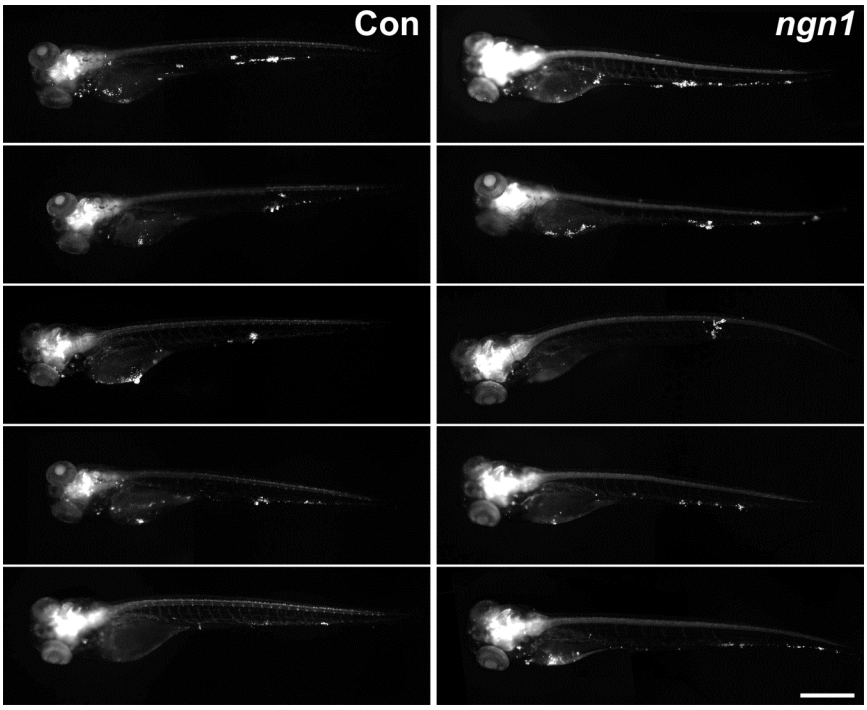

Supplemental Figure 4.2. Increased host mortality due to developmental defects does not recapitulate the *pu.1* morphant phenotype. *M. marinum*-infected neurogenin 1 mutant and clutch-matched control embryos were imaged at four dpi. Embryos express EGFP in some neural cells leading to increased fluorescence in head and along developing spine. Bacterial fluorescence is visible in the trunk and over the yolk.

Movie 4.1

Three dimensional reconstruction images (maximum intensity) of 48 hours post injection control embryo reveals the presence of red fluorescent *Mycobacterium marinum* bacteria outside of the green fluorescent vasculature of transgenic embryos.

Movie 4.2

Three dimensional reconstruction reveals red fluorescent *M. marinum* bacteria only within the vasculature of *pu.1* morphant embryos.

Chapter 5

The role of the granuloma in expansion and dissemination of early tuberculous infection[1]

[1]This chapter has been published as: Davis, J. M. and Ramakrishnan, L. (2009). The role of the granuloma in expansion and dissemination of early tuberculous infection. Cell *136*(1):37-49. I was directly responsible for all data, and participated in all experimental design, interpretation and writing.

5.1 Introduction

At the outset of human pulmonary tuberculosis, inhaled *Mycobacterium tuberculosis* (Mtb) is taken up by phagocytic cells and transported across the alveolar epithelium into the lung. There, infected macrophages recruit additional macrophages and other immune cells to form organized structures called granulomas, pathological hallmarks of tuberculosis (Cosma et al., 2003; Dannenberg, 1993). Granulomas are believed to benefit the host by containing and restricting mycobacteria (Ulrichs and Kaufmann, 2006). One reason for this belief is that granulomas were thought to form only after initiation of adaptive immunity (Saunders and Cooper, 2000), and in animal models of tuberculosis, bacterial growth is rapid for the first two weeks of infection and plateaus co-incident with the development of adaptive immunity (North and Jung, 2004; Swaim et al., 2006). Hence, according to the classical model, granuloma formation requires adaptive immunity and is critical for restricting bacterial expansion (Andersen, 1997; Saunders and Cooper, 2000).

Studies in transparent zebrafish embryos infected with *Mycobacterium marinum* (Mm), a system which recapitulates the earliest stages of tuberculosis, (Clay et al., 2008; Dannenberg, 1993; Lesley and Ramakrishnan, 2008; Stamm and Brown, 2004; Tobin and Ramakrishnan, 2008) refute the classical model of granuloma initiation as a host-protective event in fundamental ways. First, epithelioid granulomas are found to form within days of infection, well before adaptive immunity is present (Davis et al., 2002). Second, granuloma formation

coincides with the accelerated bacterial expansion widely thought to precede it (Volkman et al., 2004). Finally, Mm lacking the ESX-1/RD1 secretion system locus (ΔRD1 Mm) produces attenuated infection (DiGiuseppe Champion and Cox, 2007; Ernst et al., 2007) with poor granuloma formation (Volkman et al., 2004). Together, these findings suggest that granuloma formation actually works as a bacterial tool for expanding infection.

In this study, we sought to determine the mechanisms by which mycobacteria might take advantage of such a widely used host protective response as granuloma formation (Adams, 1976). The unique visual access to cellular events afforded by the zebrafish embryo has allowed us to present the first account of the mechanisms and consequences of tuberculous granuloma formation at the whole animal level. We devised quantitative assays using long-term three dimensional (3D) differential interference contrast (DIC) and fluorescence in vivo microscopy to isolate the steps of granuloma formation. By comparing virulent and ΔRD1 Mm infection in these assays, we determined the impact of RD1 on each step of pathogenesis. Virulent mycobacteria used RD1 to enhance both macrophage recruitment to, and infection within, nascent granulomas. This RD1-enhanced infection rate of the arriving macrophages was closely coupled to their continued rapid motility throughout the structure. Thus multiple newly arriving cells found and phagocytosed single infected dead macrophages, creating new bacterial growth niches. Furthermore, we found that

the primary granuloma promotes early dissemination of infection via egress of infected macrophages to establish secondary granulomas distally.

5.2 Results

Macrophages infected with virulent mycobacteria promote chemotactic recruitment of uninfected macrophages in an RD1-dependent fashion

We ensured that granuloma formation in the zebrafish embryo model occurred via recruitment of uninfected macrophages to single infected ones, as is likely in human tuberculosis (Dannenberg, 1993). We infected embryos with wildtype (WT) Mm into the hindbrain ventricle (Supplementary Figure 5.1) and monitored daily the fate of individual macrophages after they had migrated back into deeper brain tissues (Clay et al., 2007; Davis et al., 2002) (Figure 5.1A, B). Infection expanded quickly into multiple macrophages (Figure 5.1A). These granulomas did not form by aggregation of infected macrophages (Supplementary Figure 5.2), suggesting that uninfected macrophages were recruited, then infected. Expansion to new cells did not occur when the inciting macrophage was infected with ΔRD1 Mm (Figure 5.1B).

To determine the contributions of macrophage recruitment and retention in RD1-mediated granuloma formation, we developed the Hoechst recruitment assay for macrophage arrival at granulomas; we induced brain granulomas by hindbrain ventricle infection then injected the nuclear dye Hoechst 33342 into the circulation via the caudal vein (Supplementary Figure 5.3A). This dye does not

penetrate the blood-brain barrier (data not shown) so that any Hoechst-positive cells in brain granulomas represent migrant phagocytes from the circulation. 24 hours after dye injection, Hoechst-positive cells were rarely found in the brains of uninfected embryos (data not shown) whereas they were numerous in the brains of WT Mm-infected embryos (22.6±4.9, n=8 granulomas in 6 embryos), but only in granulomas (Figure 5.1C, Supplementary Figure 5.3B). Similar-sized ΔRD1 Mm granulomas (induced by infecting with five-fold more bacteria) attracted seven-fold fewer macrophages than WT (3.2±1.6, n=10 granulomas in 9 embryos) (Figure 5.1D, E). Again, Hoechst-positive cells were not detected elsewhere in the brain, suggesting that their reduced number in the granulomas was not due to normal recruitment with impaired retention.

The Hoechst recruitment assay quantitates blood macrophage recruitment, a multistep process involving diapedesis across the vascular endothelium, followed by tissue migration to the granuloma (Algood et al., 2003; Imhof and Aurrand-Lions, 2004). To dissect the contributions of macrophage extravasation and tissue migration to recruitment, we assayed recruitment of resident macrophages of the optic tectum of the brain to nearby infected macrophages (Davis et al., 2002; Herbomel et al., 2001). Using neutral red to identify resident macrophages (Davis et al., 2002; Herbomel et al., 2001), we found them reduced in WT infection by 72.1% (±10.4%) from uninfected levels, but no significant reduction in ΔRD1-infected embryos (n=5 WT embryos and 4 each ΔRD1 and uninfected embryos), by five days post brain infection (Figure

5.1F-I). Therefore, individual infected macrophages promote extravasation and tissue migration of uninfected macrophages to form granulomas in an RD1-dependent fashion.

Macrophages arriving at nascent granulomas become infected more rapidly if the inciting macrophages are infected with RD1-competent bacteria

Macrophages arriving at granulomas appeared to become infected rapidly (Figure 5.1A). To determine the kinetics of their infection, we adapted the Hoechst recruitment assay to monitor fates of arriving macrophages over 24 hours (Supplementary Figure 5.3C). Combining 3D DIC and fluorescence timelapse microscopy, we could distinguish infected and uninfected cells amongst the new arrivals (Figure 5.2A and B). Most arrivals at WT Mm granulomas had become infected (89.1% ±3.1%, n=6 granulomas in six embryos). We compared infection rates in WT and ΔRD1 granulomas first normalizing for macrophage recruitment by examining subsets of WT and ΔRD1 granulomas with similar numbers of new arrivals (Supplementary Figure 5.3C). Only 53.6% (±10.0%) of arrivals to ΔRD1 granulomas had become infected within 24 hours (n=4 granulomas in four embryos), a 40% reduction versus WT (Figure 5.2C). Thus, RD1-competent infection substantially increases the rate of macrophage infection in addition to recruitment itself.

RD1-competent infection of inciting macrophages in the nascent granuloma is associated with a chemotactic morphology and rapid motility of newly arriving macrophages

We next sought to define the mechanism of intercellular bacterial spread in granulomas by examining the appearance and interactions of infected and uninfected cells in WT and ΔRD1 Mm granulomas. Cells attracted to WT granulomas moved rapidly (averaging 4.5±1.0 μm/min., n=10) and had elongated nuclei with extended lamellipodia and prominent uropods, morphological features of leukocytes undergoing chemotaxis (Figure 5.2D, left panel; Movie 5.1) (Sanchez-Madrid and del Pozo, 1999). Some rapidly moving cells were more rounded with extremely prominent cytoplasmic vesicles in their lamellipodia (Figure 5.2D, right panel; Movie 5.1). In contrast, uninfected cells in ΔRD1 granulomas moved slowly (averaging 0.6±0.1 μm/min, n=12), had rounded shapes and nuclei, and fewer cytoplasmic vesicles (Figure 5.2E-F, Movie 5.2), suggesting that they do not experience the same chemotactic signal as cells at WT granulomas. The speeds and distances covered by uninfected cells in WT granulomas were greater (eight and nine times, respectively) than their counterparts at ΔRD1 granulomas (Figure 5.2G-I). In summary, the RD1-mediated chemotactic motility of cells arriving at granulomas was tightly linked to their higher infection rate.

Macrophage motility in the context of extracellular bacteria at the initial site of infection is not RD1-dependent

Macrophage migration occurs at multiple steps in tuberculous infection, first to the initial site of bacterial infection (Clay et al., 2007; Dannenberg, 1993). Previous work has suggested no difference in cell recruitment to WT or ΔRD1 infection sites (Volkman et al., 2004). We examined cells recruited to the hindbrain ventricle one hour after injection of WT or ΔRD1 Mm. In both cases, recruited cells had the chemotactic morphology of those arriving at WT granulomas and in sharp contrast to those at ΔRD1 granulomas (data not shown). Their displacements (Figure 5.2J, K) and speeds (Figure 5.2G) were also similar to uninfected cells at WT granulomas. Thus, RD1 is dispensable for macrophage chemotaxis to extracellular bacteria at the initial infection site, yet required for intracellular bacteria to induce macrophage chemotaxis for granuloma initiation and expansion.

Newly arriving macrophages become infected by phagocytosis of infected macrophages which have recently undergone apoptosis

Next, to determine how the rapid movement of uninfected cells at WT Mm-induced granulomas might lead to their higher infection rates, we studied their movements in the context of infected granuloma macrophages (Figure 5.3A). We were struck by the frequent death of these infected cells, which appeared to be apoptotic based upon morphological hallmarks, i.e. rapid nuclear collapse and fragmentation resulting in spherical remnants (Darzynkiewicz et al., 1997; Tone et al., 2007) (Figure 5.3B, C, Movie 5.3). The dying cells did not lyse; their membranes appeared intact with the bacteria remaining encased within. In

contrast, *Salmonella arizonae* infection of the embryos featured dying macrophages that developed similar apoptotic nuclear morphology but underwent rapid swelling with bacterial release (Davis et al., 2002; Fink and Cookson, 2005) (Movie 5.4).

The DIC appearance of the nuclear spheres of the mycobacterium-infected dead cells corresponded to distinctive compact fluorescent bodies in cells labelled with Hoechst prior to their death, in contrast to diffuse nuclear staining of living cells (Darzynkiewicz et al., 1997) (Figure 5.3D). This feature allowed quantitation of the infected immigrant cells that had died over 24 hours using the Hoechst recruitment assay (Supplementary Figure 5.3C). Most infected arrivals to WT Mm granulomas had died (74.9±4.8%; n=6 granulomas) (Figure 5.3E). That their death was apoptotic was confirmed by staining with acridine orange and Annexin V (Peri and Nusslein-Volhard, 2008) (Figures 5.3F-I).

Strikingly, their death was followed shortly by phagocytosis of their remains, including the bacteria (Figure 5.3C, Movie 5.5). Uninfected cells moved rapidly past living infected cells (Figure 5.3A), engaging in phagocytosis only upon encountering a dead cell (Figure 5.3C). The bacteria from a single heavily infected dead macrophage could be phagocytosed by multiple cells, (Figure 5.3J, Movie 5.6) accounting for the increase in the number of infected macrophages (Figure 5.1B).

Dying ΔRD1 Mm-infected macrophages are not phagocytosed rapidly

RD1 has been reported to increase death of infected macrophages in culture (Gao et al., 2004; Guinn et al., 2004) and in zebrafish embryo granulomas (Clay et al., 2008; Volkman et al., 2004). Our analysis of WT Mm granulomas suggested that infection of new macrophages was dependent on death of infected macrophages as well as chemotactic motility of, and phagocytosis by, new macrophages. We sought to determine the contribution of RD1 to each of these. Using the Hoechst recruitment assay and analyzing WT and ΔRD1 granulomas with similar numbers of newly arrived cells (Supplementary Figure 5.3C), we found a 40% reduction from WT in dead infected arrivals over 24 hours (n=6 granulomas) (Figure 5.3E). This is consistent with previous findings of fewer TUNEL positive cells in ΔRD1 than WT Mm granulomas (Clay et al., 2008; Volkman et al., 2004). Though fewer, the dead cells in ΔRD1 Mm granulomas showed that the same morphology and kinetics of nuclear collapse as in WT granulomas (Movie 5.7). Yet their death did not evoke chemotactic morphology or motility even in nearby uninfected macrophages (data not shown).

Phagocytosis of bacteria from dying cells by multiple arriving cells is likely a major mechanism for granuloma expansion

These data suggested that granuloma expansion is driven by the arrival of new cells which phagocytose resident dying cells at a multiplicity of greater than one. First, to test the prediction that granuloma expansion requires new macrophages for niche expansion, we compared the increase in bacterial burden (as judged by an interval increase in fluorescence area of the granuloma) to the arrival of new

macrophages during a 24-hour period in eight granulomas from seven embryos. We found a tight correlation (Figure 5.4A).

Bacterial expansion by intercellular spread could then occur by rephagocytosis of dead infected macrophages, as predicted by our findings, or by bacterial transfer between live cells as previously reported (Davis et al., 2002; Stamm et al., 2003). To assess the likelihood that death and rephagocytosis is a major mechanism for bacterial expansion in granulomas, we constructed a simple mathematical model of granuloma expansion. The model is expressed as:

$$N_{24} = N_0\left[fm + (1 - f)\right] \quad (1)$$

where N_0 and N_{24} are the number of infected macrophages at time zero and 24 hours, respectively, f is the fraction of infected macrophages dying in the 24 hour period, and m is the number of new infected cells resulting from phagocytosis of a single dying infected cell. Rearranged to express proportional growth of the granuloma in terms of infected cells ($N_{24}/N_0 = G$), this becomes:

$$G = f(m - 1) + 1 \quad (2)$$

This model and its assumptions are detailed further in Section 5.6, Supplemental Information.

To test this model, we followed five granulomas, in five separate embryos, assessing fluorescence area as a measure of bacterial burdens, and counting the numbers of infected macrophages and of apoptotic bodies at 0 and 24 hours

(Figure 5.4B; Supplementary Table 5.2). First, we found a 3.0 (±0.6) fold increase in fluorescence area, similar to the 2.8 (±0.3) fold increase in the number of infected macrophages (Figure 5.4C-E; Supplementary Table 5.3). Second, based on these data, we found $f = 0.8$ (±0.1) and $m = 2.3$ (±0.6) (Supplementary Table 5.3). These values are in accordance with our previous finding that death of infected macrophages is rapid (Figure 5.3E) and our observational expectation of multiplicity based on imaging (data not shown). These calculated values for *f* and *m* predicted average proportional growth of 2.0 ±0.5 which was 71.5% (±4.4%) of the observed growth as measured by increase in the number of infected cells (Figure 5.4E; Supplementary Table 5.3) and 75.0% (±25.2%) of growth estimated by increase in fluorescence area. The closeness of these values suggests that the mechanism of continual death and phagocytosis can account for most, if not all of granuloma expansion.

Some newly infected macrophages egress the primary granuloma

Tracking with 3D DIC microscopy, combined with bacterial volume measurements from fluorescence microscopy revealed that the motility of infected granuloma macrophages decreased inversely to their bacterial load (Figure 5.5A, Movies 5.8-10). This was confirmed by analysis of long-term 3D confocal microscopy of granulomas where fluorescent bacteria within individual macrophages could be identified as distinct clusters. Following their motion over 18 hours, we discovered that five infected macrophages left the granuloma altogether (Figure 5.5B, Movie 5.11). Consistent with our previous observations,

these bacterial clusters were among the smallest in volume (Figure 5.5C). We confirmed that the departing bacteria were intracellular by DIC visualization (Movie 5.12).

To track departing bacteria, we created MD2, an Mm strain constitutively expressing the Kaede photoactivatable protein (Ando et al., 2002), which switches stably from green to red fluorescence on exposure to ultraviolet light, without damage to the bacteria or their infected cells (Supplementary Figure 5.4 and data not shown). Selective photoactivation of single granulomas frequently revealed departure of infected macrophages after 24 hours (Figure 5.5D-F). The intracellular MD2 were both red and green fluorescent (Figure 5.5E), suggesting that they were synthesizing new Kaede protein and thus metabolically active. In addition to departure via tissue migration (Figures 5.5D-F), we observed departed infected macrophages lodged in the distant vasculature (Figure 5.5G-I and Movie 5.13). Monitoring 33 granulomas for 24 hours after photoactivation, we recorded one to four departed macrophages in 18 (54.4%) of them and calculated the mean rate of departure at 1.4(±0.3) per granuloma.

Macrophages exiting the primary granuloma seed distal granulomas to disseminate infection

We extended our monitoring to two days post photoactivation and found 18 granulomas with evidence of departed macrophages at day one. In six cases (33%) the departed bacteria were found in new granulomas (Figure 5.6A-C). The

bacteria in all departed macrophages remained both red and green fluorescent, showing their prolonged viability after departure and potential to initiate new granulomas.

Mammalian tuberculosis is thought to arise from a single primary lesion (Balasubramanian et al., 1994; Rich, 1946). To determine if egress of infected macrophages could account for this dissemination, we monitored embryos infected with 10-50 CFU of green or red fluorescent bacteria for three days and selected ones forming a single granuloma with no other infection foci (Figure 5.6D). Daily monitoring from the day of granuloma formation (t=0) showed that primary granulomas were capable of disseminating infection throughout the body by departure of infected macrophages (Figure 5.6D). All ten embryos monitored had evidence of newly departed infected macrophages by day two (Figure 5.6E), and of secondary granuloma formation by four days (Figure 5.6E). In every case, the appearance of a primary granuloma macrophage preceded secondary granuloma formation, which invariably occurred at the site the departed macrophage was first observed (Figure 5.6D and E). Over three days, the mean rate of macrophage arrival at distal sites was 1.6 (±0.4) per day, similar to the departure rates obtained before. The rate of departure remained relatively constant over the three days of observation, with means of 1.4, 2.2 and 1.3 on days one, two and three post primary granuloma formation (t=0) respectively. The rate of new granuloma formation was 0.30(±0.07) per day, so 19% of newly departed macrophages initiated granuloma formation per day. Together, these

data show that infected macrophages frequently depart primary granulomas and migrate both hematogenously and through tissues. The kinetics of departure and secondary granuloma formation suggest that granuloma macrophages constitute the major if not sole mechanism for dissemination.

5.3 Discussion

Our results suggest that mycobacterial expansion in early granulomas is driven by a continual cycle of death of infected macrophages and their phagocytosis by multiple newly recruited macrophages (Figure 5.7). This model is supported by a direct comparison of the kinetics of these events in the presence and absence of the RD1 virulence determinant and their correlation to infection outcome (Figure 5.7). Furthermore, a simple mathematical model derived from our observed logistics of WT granuloma inception suggests that this mechanism can account for at least 71% and possibly all of granuloma expansion. The small remainder, if any, may be attributable to other mechanisms that may or may not be RD1-dependent. One possible mechanism is direct spread via membrane tethers between individual macrophages as observed in the blood stream (Davis et al., 2002). However, we have not discerned this phenomenon in granulomas during extensive video microscopy. Another possible means of intercellular spread is via actin-based bacterial motility (Stamm et al., 2003; Tobin and Ramakrishnan, 2008). Both Mtb and Mm are reported to escape the phagocytic vacuole into the

cytosol in an RD1-dependent fashion (Stamm et al., 2003; van der Wel et al., 2007), and Mtb has also been shown to require RD1 for intercellular spread in vitro (Guinn et al., 2004). In the case of Mm, once cytoplasmic, ~20% of bacteria become motile in cultured macrophage monolayers via host actin polymerization, and can spread to adjacent cells (Gao et al., 2004; Stamm et al., 2003; Stamm et al., 2005). This motility has not been reported for Mtb and has been proposed to be used for Mm-specific interspecies transmission strategies, rather than the granuloma formation common to Mm and Mtb (Stamm and Brown, 2004; Tobin and Ramakrishnan, 2008). This hypothesis is consistent with our finding that a mechanism distinct from actin-based motility is the major contributor to bacterial expansion in granulomas.

The mechanics and dynamics of granuloma formation we observe in response to RD1-deficient infection of zebrafish embryos mirror those found in BCG-induced granulomas in rabbits (Figure 5.7) (Dannenberg, 2003). BCG produces attenuated infection, similar to ΔRD1 Mm the zebrafish embryo (Volkman et al., 2004), strongly suggesting that without the faster kinetics of granuloma formation induced by RD1, mycobacteria lose the growth advantage they enjoy specifically in nascent granulomas. Extrapolation of observations from attenuated BCG infection (Dannenberg, 2003) to infections with fully virulent organisms may have led to an incorrect conclusion about the consequence of granuloma formation in response to virulent mycobacteria.

We note that the greatly reduced speeds and displacements of macrophages we observed at ΔRD1 granulomas are in accord with recent work visualizing mouse granulomas formed by the RD1-deficient strain BCG, in which the macrophages are reported to be relatively static (Egen et al., 2008). In this study, in the two to three weeks after infection, macrophages were recruited to granulomas, consistent with our observations with ΔRD1 Mm granulomas in zebrafish; however relative macrophage recruitment rates in response to RD1-proficient and -deficient strains were not assessed, precluding a comparison with our findings of the impact of this locus on macrophage recruitment. Strikingly, in that study, while macrophages were recruited to BCG granulomas, once inside they had limited motility in contrast to the highly motile T cells (Egen et al., 2008). This lack of macrophage motility is very possibly due to the lack of RD1 in the inciting bacteria. It is also possible that, independent of RD1, granulomas have distinct macrophage dynamics at this later stage from the very early granulomas we have monitored. While analysis of the effect of RD1 on macrophage dynamics in mature granulomas awaits comparison of isogenic strains in adult animals, there is evidence suggesting that this locus continues to influence granuloma structure after adaptive immunity has been invoked. Adult zebrafish and mice with RD1-deficient Mm and Mtb, respectively, have loose, poorly structured granulomas (Sherman et al., 2004; Swaim et al., 2006). Moreover, ΔRD1 Mm-infected zebrafish embryos continue to have loose noncaseating granulomas even as adults (Volkman et al., 2004). Regardless of its exact role in mature

granuloma dynamics, the role of RD1 in nascent granulomas revealed by this study is likely a critical factor in the irrevocable early bacterial expansion that establishes infection (Andersen, 1997; Kaufmann and Ladel, 1994; Saunders and Cooper, 2000).

RD1 has been thought to promote mycobacterial infection by dampening the innate immune response in order to evade its bactericidal mechanisms (Pathak et al., 2007; Stanley et al., 2003), although more recent evidence suggests that RD1 enhances inflammation (Koo et al., 2008). Our findings suggest that at least in the nascent granuloma, bacteria expressing RD1 actually accelerate aspects of the innate immune response, especially macrophage recruitment, motility, and apoptosis (see below). Accelerated granuloma formation in response to Mtb (as compared to BCG) (Adams, 1975) has been assumed to represent the host's attempt to thwart a more virulent pathogen (Adams, 1975). Our direct observations in vivo suggest that this acceleration is driven by a mycobacterial virulence factor and actually aids bacterial growth.

Our results also shed light on the role of RD1 in granuloma formation (Volkman et al., 2004) and clarify the contributions to this process of the distinct infection phenotypes associated with this virulence locus (DiGiuseppe Champion and Cox, 2007; Ernst et al., 2007). First we show that the presence of intracellular RD1-competent Mm results in enhanced recruitment of uninfected macrophages hematogenously and through tissues to form granulomas. RD1 has been associated with increased death of infected cells in cultured macrophage

monolayers. The increased intercellular spread of RD1-competent bacteria that has been observed is thought to result from bacteria being released into the culture medium and becoming accessible for phagocytosis (Gao et al., 2004; Guinn et al., 2004). However, this mechanism seems unlikely within the tight structural restraints of the granuloma. Indeed, our data reveal that while RD1 is associated with increased cell death, this increase alone seems unlikely to account for the increased infection rate. Rather, the motility of uninfected macrophages and their attraction to dead infected cells, both apparently mediated by RD1, appear to be required for intercellular spread. The lack of even a local chemotactic response to cell death in ΔRD1 granulomas suggests that reduced death in these lesions is not the root cause of the overall reduced macrophage motility and spread of bacteria. Alternatively, RD1-competent and -deficient cell death may be molecularly different despite their similar morphology and kinetics, with only the former producing signals that induce macrophage motility. In either case, reduced overall motility of macrophages appears to be responsible for the slower phagocytosis of dead macrophages in ΔRD1 Mm granulomas. This reduced phagocytosis should account substantially for the lower rate of infection of new arrivals, in combination with the decreased death rate itself.

The constant rapid motility of uninfected cells throughout the granuloma is the most profound difference between granulomas with and without RD1. While chemokines have been implicated in cell migration to form granulomas (Algood et

al., 2003), this is the first evidence of continued chemotactic migration of macrophages after reaching the granuloma, that in turn correlates with their increased infection. Rapid and continuous migration seems to allow these new arrivals access to the few dying infected cells present at a given moment. These logistics are reminiscent of those described for B and T lymphocytes in lymph nodes as they seek out cognate antigen on other lymphocytes, a process also governed by chemotactic signals (Castellino et al., 2006; Okada et al., 2005)—a comparison made yet more intriguing by reports that the mature tuberculous granuloma has structural and functional similarities to secondary lymph nodes (Kahnert et al., 2007; Ulrichs et al., 2004). The rapidly moving uninfected macrophages in WT granulomas display the classic appearance of leukocytes in the presence of a chemotactic signal (Sanchez-Madrid and del Pozo, 1999). Indeed, their speed (average 4.5 μm/min) is comparable to that reported for mouse macrophages responding to a human recombinant M-CSF-receptor gradient (Webb et al., 1996), as well as those of lymphocytes moving in mouse tuberculous granulomas (Egen et al., 2008) and in lymph nodes (Stoll et al., 2002). While the macrophages we observed at WT granulomas were in constant motion, within a single lesion their movements were not in a unified direction, suggesting that the signal guiding them is uniformly distributed. However, in the midst of this apparently random movement, dying cells are rapidly found and phagocytosed, a sequence that would seem to require specifically directed motion towards newly dead cells. Notably, the macrophages approaching and

phagocytosing dead cells have a distinct morphology and more directed motion. To account for this combination of random and directed motion, we propose that a gradientless signal, emanating from infected macrophages throughout the granuloma, induces new cell recruitment and random movement, but a second signal, generated by dying cells, directs nearby macrophages to them for phagocytosis. Both of these movements appear necessary for efficient phagocytosis in nascent granulomas.

The chemokines involved in granuloma formation, and the pathways by which they are induced by bacterial RD1 are not yet understood and are likely to be complex (Algood et al., 2003; Peters and Ernst, 2003). Notably, TNF, a key protective cytokine in tuberculosis, was thought to mediate protection by promoting cell migration and granuloma formation, at least in part by modulating the expression of key chemokines and their receptors (Algood et al., 2003; Flynn and Chan, 2001a). However we have recently found that TNF signalling is not required for granuloma formation, at least in the innate stages of infection detailed in this study (Clay et al., 2008). Rather its primary role in early protection appears to be to restrict mycobacterial growth within macrophages. Indeed, lack of TNF signalling results in accelerated granuloma formation, presumably because of an increased proportional increase in RD1 within the inciting infected macrophages (Clay et al., 2008; Miller and Ernst, 2008). Infection with ΔRD1 Mm results in attenuated infection with poor granuloma formation even in the absence

of TNF signalling, further confirming the lack of involvement of this prime candidate in RD1-mediated granuloma formation.

A striking finding of our study is a very high rate of apoptotic death of infected macrophages, enhanced by RD1 that appears to be a driving factor in granuloma expansion. This finding brings into question our understanding of the role of apoptosis in mycobacterial infection. Macrophage apoptosis has been noted in human tuberculosis granulomas (Cree et al., 1987; Keane et al., 1997) and based on some in vitro studies, has been regarded as detrimental to the infecting mycobacteria, in contrast to necrosis, which favors bacterial growth (Fratazzi et al., 1997; Gan et al., 2008; Keane et al., 2002; Oddo et al., 1998). However, many of these in vitro studies used additional agents to induce death of the infected macrophages (Fratazzi et al., 1997; Gan et al., 2008; Molloy et al., 1994; Oddo et al., 1998), inducing specific death pathways which may have overridden mycobacterium-induced ones. This point is important for the interpretation of these data given that different molecular inducers of apoptotic death (e.g. Fas Ligand versus ATP) have been found to have opposite effects on the viability of the mycobacteria within the dying cell (Lammas et al., 1997). Furthermore, RD1 has been shown to promote death of cultured macrophages infected with Mtb or Mm, and this death shown to be apoptotic in the case of Mm (Gao et al., 2004; Guinn et al., 2004). RD1 is required for intercellular spread in Mtb-infected cultured macrophage monolayers (Guinn et al., 2004; Lesley and Ramakrishnan, 2008) consistent with our in vivo data that apoptotic cell death

can play a role in bacterial expansion. In summary, our findings suggest either that apoptotic cell death in vivo is not actually harmful to mycobacteria—perhaps because bacterium-sparing pathways are invoked—or that the rapid phagocytosis after macrophage death, also an RD1-dependent phenomenon, nullifies any bactericidal effects.

Finally, our results shed light on the role of the primary granuloma in the dissemination of tuberculosis. By serial visualization of infection at the whole organism level from the very earliest events, we have shown how dissemination occurs soon after establishment of the first lesion. Human tuberculosis is increasingly appreciated to be a disseminated infection (Hernandez-Pando et al., 2000) and has been inferred to disseminate hematogenously from the primary granuloma early in infection (Balasubramanian et al., 1994; Chackerian et al., 2002). Our direct imaging of the primary granuloma confirms this model and provides kinetics and a cellular mechanism for this central feature of early pathogenesis. We find that hematogenous dissemination occurs within macrophages that depart established, enlarging granulomas. Macrophages and dendritic cells are required for the initial transport of infection to deeper tissues for establishment of infection (Clay et al., 2007; Dannenberg, 1993). Our work reveals that macrophages repeat their role as bacterial transporters by disseminating infection from the primary granuloma.

In summary, we propose that the pathway of granuloma formation and subsequent bacterial dissemination is based upon macrophage responses

(recruitment, phagocytosis, apoptosis) that are of themselves generally protective (Adams, 1976; Dannenberg, 2003), and that work reasonably well against less virulent (i.e. RD1-deficient) infection. Rather than block these host responses, RD1-competent mycobacteria appear to accelerate them to turn the granuloma response into an effective tool for pathogenesis. The initiation of the adaptive immune response then may halt bacterial expansion not by forming granulomas as suggested by the classical model (Andersen, 1997; Saunders and Cooper, 2000), but by altering the early granuloma into a form of stalemate between host and pathogen.

5.4 Experimental procedures

Animal care and strains

Wild-type AB zebrafish embryos were maintained and infected by injection into the caudal vein or hindbrain ventricle at 24-30 hours post fertilization unless otherwise noted (Cosma et al., 2006a; Davis et al., 2002; Volkman et al., 2004).

Bacterial strains

Fluorescent wild-type Mm M (ATCC #BAA-535) ΔRD1 mutant strains were used. (Volkman et al., 2004). MD2 was derived by transformation with plasmid pMD2 expressing a transcriptional *msp12::kaede* fusion (Chan et al., 2002). See Section 5.6, Supplementary Information for details.

Vital dye staining of embryos

Embryos were injected with 200μg/ml Hoechst 33342 (Invitrogen) via caudal vein, 1/10 dilution Annexin V-AlexaFluor 488 (Invitrogen) via hindbrain ventricle, or soaked in 2μg/ml acridine orange (Sigma-Aldrich) in fish water for 10 minutes. Neutral red staining was performed as described (Davis et al., 2002).

Microscopy

Widefield microscopy was performed on a Nikon E600 equipped with DIC optics, a Nikon D-FL-E fluorescence unit with 100W Mercury lamp and MFC-1000 z-step controller (Applied Scientific Instrumentation). Objectives used included 4x Plan Fluor, 0.13 NA, 10x Plan Fluor, 0.3 NA, 20x Plan Fluor, 0.5 NA, 60x Water Fluor, 1.0 NA and 60x Oil Plan Apo, 1.4 NA. Widefield fluorescence and DIC images were captured on a CoolSnap HQ or CoolSnap CF CCD camera (Photometrics) using MetaMorph 7.1 (Molecular Devices). '3D DIC Microscopy' refers to capturing z-stacks of DIC images, for one or multiple timepoints, and exploring these datasets manually using programs described below. Confocal microscopy was performed on an Olympus Fluoview FV1000 laser scanning confocal microscope equipped with lasers capable of 405nm, 637nm, 488nm, and 561nm excitation. Objectives used were 10x UplanApo air, 0.4 NA and 20x UplanApo air, 0.75 NA.

Image processing

Where indicated, z-stacks were deconvolved using AutoDeblur Gold CWF, Version X1.4.1 (Media Cybernetics), with default settings for blind deconvolution.

Additional dataset analysis and visualization was performed using Imaris x64 6.0 (Bitplane) and MetaMorph 7.1 (Molecular Devices). Movies were produced either directly from Imaris or from stacks compiled in MetaMorph. Additional movie compilation and formatting was performed in Adobe Premiere 6.0 and QuickTimePro 7.4 (Apple). Figure processing and assembly performed in Adobe Photoshop CS2.

Statistics

Student's unpaired t-tests and power trendline calculations were performed using Excel 11.4 (Microsoft Corp.). All other statistical tests were performed using Prism 5.0a (GraphPad Software, Inc.).

5.5 Figures

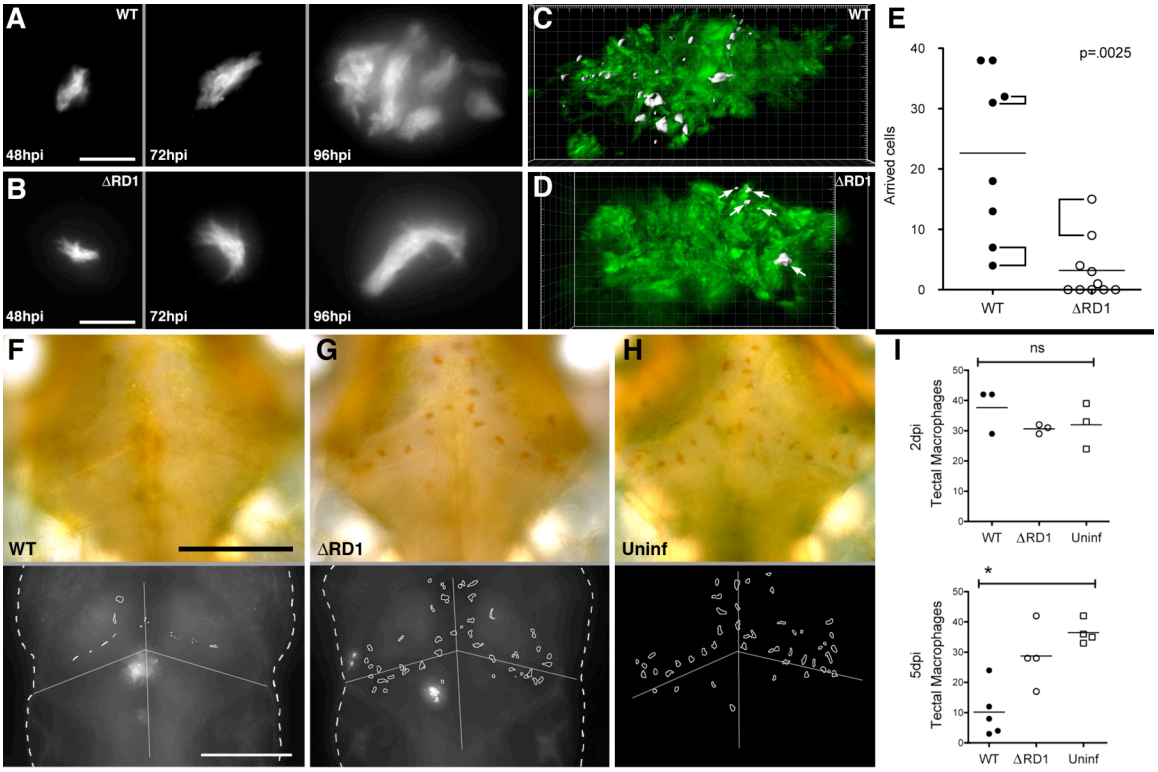

Figure 5.1. The early granuloma enhances bacterial replication by RD1-dependent recruitment and infection of new cells. (A-B) Fluorescent images of WT (**A**) and ΔRD1 (**B**) infected lesions at 48, 72, and 96 hours post infection (hpi). Scale bars, 10μm. (C-D) 3D reconstructions of granulomas in WT (**C**) and ΔRD1 (**D**) infection, showing Hoechst-positive nuclei rendered white (indicated by white arrows in (D)) accumulated over 24 hours. Scale grid, 5μm per square. (**E**) Comparison of numbers of Hoechst-positive arrivals in WT and ΔRD1 lesions after 24 hours. Brackets indicate granulomas in the same embryo. Horizontal lines represent means. *P* value from Mann Whitney test. (F-H) Neutral red-stained optic tectum macrophages at five days post hindbrain injection with WT Mm (**F**), ΔRD1 Mm (**G**), or no infection (**H**). Macrophages detected using neutral red dye (upper panels) and their outlines overlayed on images of the fluorescent bacteria present (lower panels—no fluorescent image collected for uninfected embryos). Scale bars, 100μm. (**I**) Numbers of optic tectum macrophages at 2dpi and 5dpi. $P = 0.47$ (2dpi) and 0.01 (5dpi) (Kruskal-Wallis test, $P<0.05$).

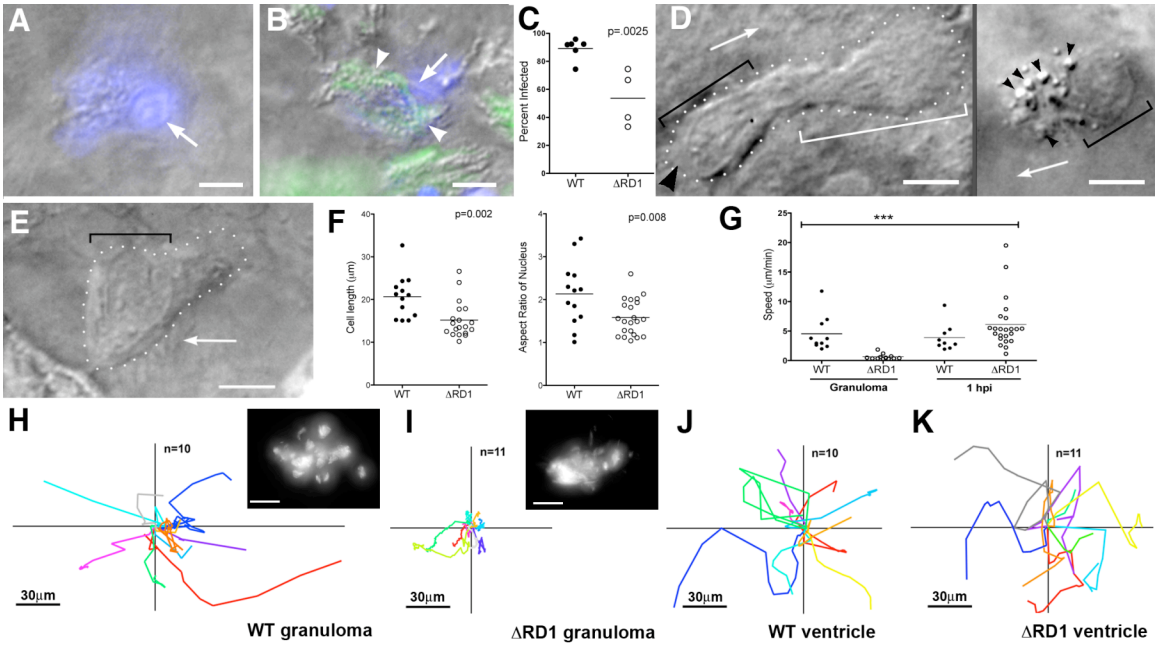

Figure 5.2. Uninfected cells at WT granulomas show distinct morphology, and rapid motility and infection. (A-C) Hoechst-positive nuclei (blue) are distinguishable as uninfected (**A**) or infected (**B**). White arrows, Hoechst-positive nuclei; arrowheads, bacteria (green). (**C**) Infected Hoechst-positive cells in WT vs. ΔRD1 lesions over 24 hours. *P* from Mann Whitney test. (D-E) Distinct morphologies of uninfected cells at WT (**D**) and ΔRD1 (**E**) lesions. (D) Left: highly motile cell at WT granuloma with lamellipodium (white bracket), elongated nucleus (black bracket) and uropod (large black arrowhead). Arrow indicates direction of travel. Right: distinct appearance in WT granulomas of highly vesicular macrophage shortly before phagocytosis. Small black arrowheads, vesicles. Scale bars, 5μm. (E) Less motile cell at ΔRD1 granuloma with no lamellipodium and rounded nucleus (black bracket). Scale bar, 5μm. (**F**) Comparison of overall cell length, left, and nuclear aspect ratio, right, of uninfected cells at WT and ΔRD1 granulomas. *P* by unpaired Student's t test. (**G**) Speeds of uninfected cells at WT or ΔRD1 granulomas, or at the site of injection one hour post infection in the hindbrain ventricle. Bracket above indicates results of 1 way ANOVA (Kruskal-Wallis test)—uninfected cells at ΔRD1 granulomas

(***) differed significantly from all others (P<0.005), other differences not significant. (H-K) Tracks of uninfected cells in (G). (**H**, **I**) cells at WT and ΔRD1 granulomas—all cells tracked for each strain from one granuloma. Insets, fluorescence view of whole granuloma. Inset scale bar, 30μm. (**J**, **K**) cells at one hour post injection. 1 hpi tracks from two WT-infected embryos and three ΔRD1-infected embryos. Scale bars 5μm unless noted otherwise.

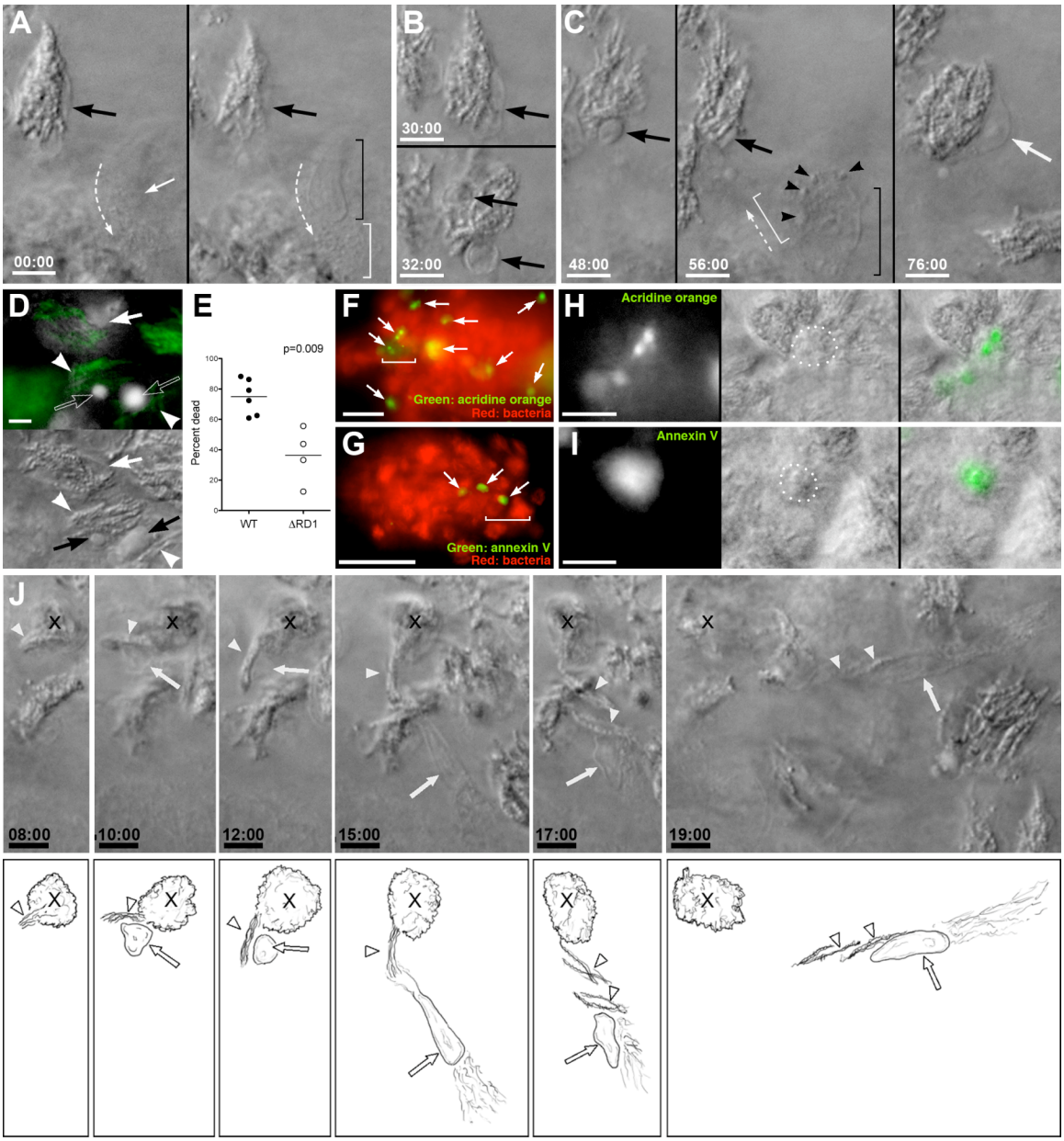

Figure 5.3. Death and phagocytosis of infected macrophages. (A-C) DIC timelapse of death and phagocytosis of infected macrophage. (**A**) two focal planes at time zero showing bacteria in cell with healthy nucleus (large black arrow), with uninfected cell (small white arrow and brackets as in Figure 5.2D) passing by. Dashed arrow, direction of travel. (**B**) Same infected cell as in (A), before (top) and after (bottom) nuclear collapse. (**C**) Same cell after further nuclear collapse into apoptotic sphere, and later timepoints showing complete phagocytosis by new macrophage (black and white brackets and white arrow). Small black arrowheads, vesicles in approaching macrophage. (**D**) Hoechst (white) and bacterial GFP (green) overlay above, with matching DIC below, showing compact Hoechst-positive apoptotic nuclei (black arrows) associated with bacteria (white arrowheads), compared to diffuse Hoechst-staining of live nuclei (white arrow). (**E**) Infected Hoechst-positive apoptotic cells per granuloma in WT and ΔRD1 lesions over 24 hours. *P* from Mann Whitney test. (F-I) Apoptotic cells in WT granulomas detected by acridine orange (F, H) or annexin V (G, I). (**F**) Granuloma of red fluorescent Mm with acridine orange-positive cells (white arrows). Bracket indicates area shown in (H). (**G**) Granuloma of red fluorescent Mm with annexin V-positive cells (white arrows). Bracket indicates area shown in (I). (**H**) Acridine orange signal (left) corresponds with DIC appearance of apoptotic bodies (dotted circle, middle). Overlay, right. Scale bar, 10μm. (**I**) Annexin V signal (left) corresponds with DIC appearance of apoptotic bodies (dotted circle, middle). Overlay, right. Scale bar, 10μm. (**J**) DIC timelapse images of single macrophage (nucleus indicated by white arrow) pulling a small group of bacteria (white arrowheads) from a larger cluster (X). Below, sketches derived from these panels with additional details from other planes at same timepoint. Scale bars 5μm.

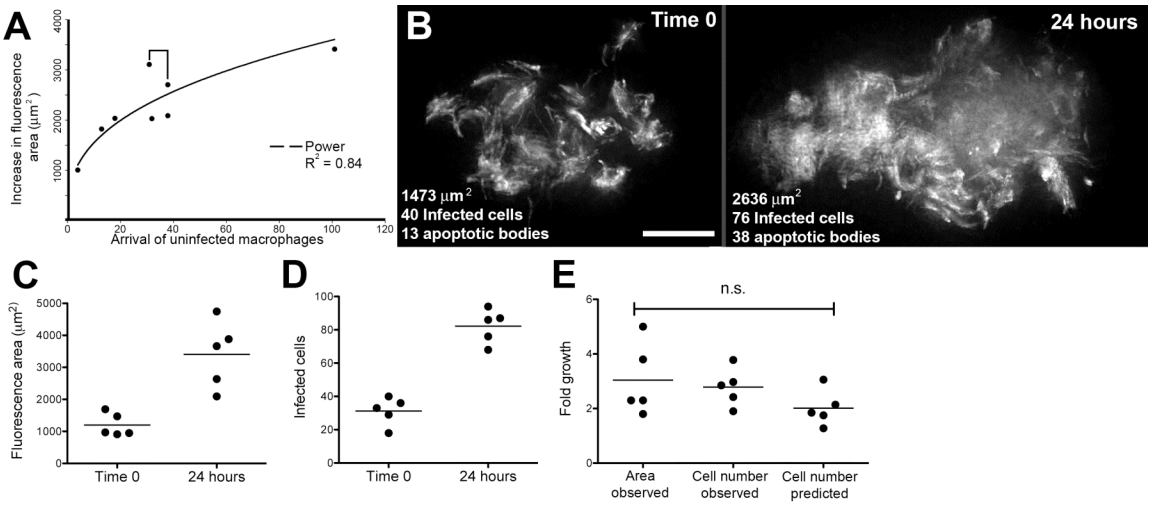

Figure 5.4. Bacterial expansion in early granulomas as a function of macrophage arrival, infection, death and rephagocytosis. (**A**) Correlation of bacterial growth in granulomas, measured by fluorescence area with arrival of new macrophages. Data from 8 granulomas in 7 embryos. Bracket indicates pair of granulomas imaged in the same embryo. (**B**) Deconvolved fluorescence images of granuloma at time 0 (above) and 24 hours (below). Scale bar, 20μm. (C-D) Bacterial expansion in five granulomas over 24 hours as measured by (**C**) fluorescence area, and (**D**) number of infected cells. (**E**) Fold growth as measured in panels (C-D) as compared to predicted fold growth based on mathematical modeling. Differences not significant (ANOVA).

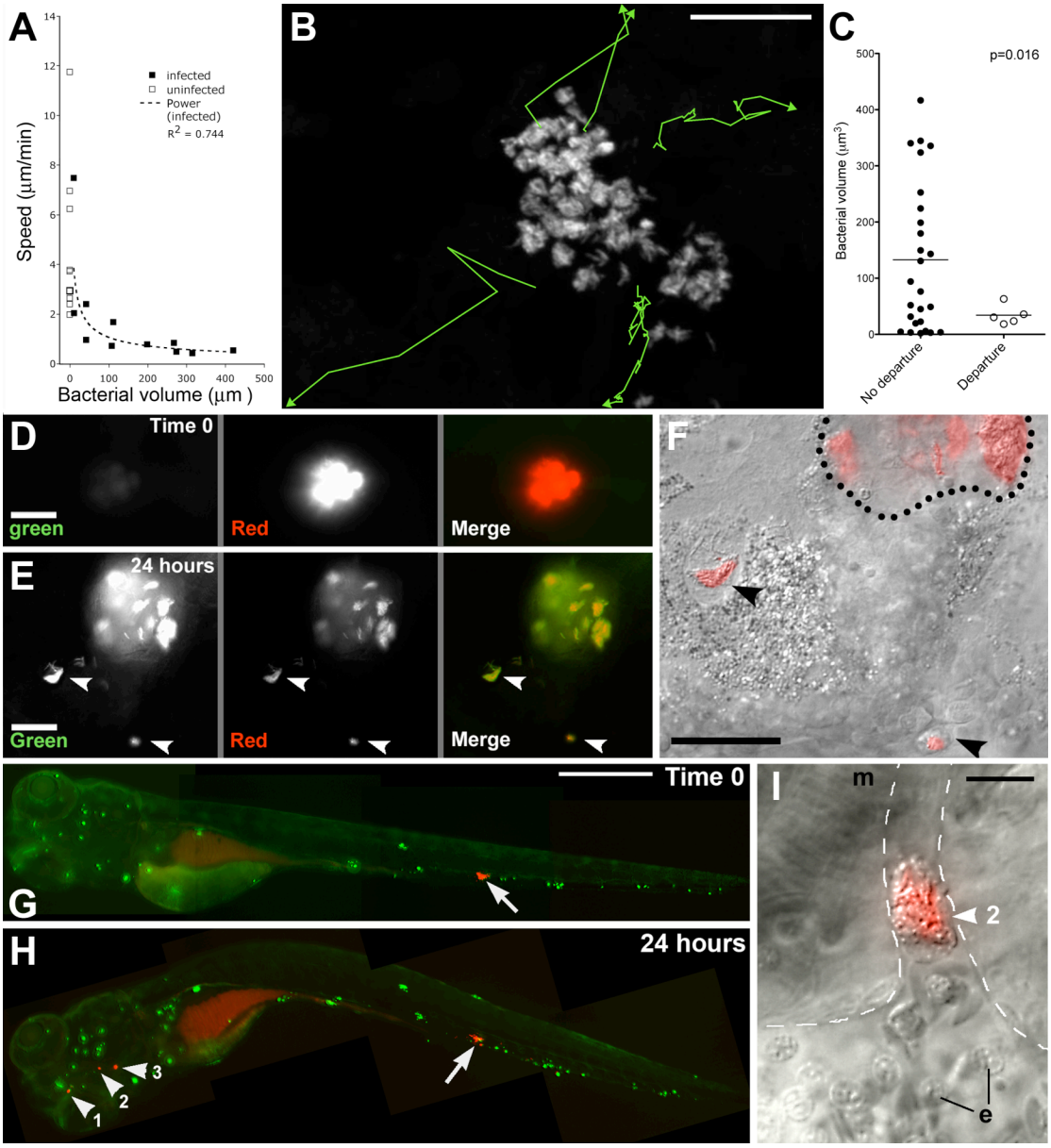

Figure 5.5. Motility and departure of infected granuloma macrophages. (**A**) Average speeds of infected and uninfected cells vs. their bacterial volumes. (**B**) Tracks of departing infected macrophages from Movie 5.11. Scale bar, 50μm. (**C**) Bacterial volumes and average speeds of departing macrophages in (B), compared to those that did not depart. *P* by Student's t test. (D-F) Departure of infected macrophages from brain granuloma. (**D**) Granuloma immediately after photoactivation (red) and (**E**) 24 hours later, demonstrating granuloma growth, and departure of infected macrophages (arrowheads). (**F**) DIC/red fluorescence

overlay of departing macrophages (arrowheads). Dotted line represents granuloma edge. Scale bars in (D-F) 20μm. (G-I) Hematogenous dissemination from tail granuloma. (**G**) a single granuloma (arrow) photoactivated at 3dpi. Scale bar, 300μm. (**H**) At 4dpi, photoactivated bacteria (arrowheads) seen in gill vasculature. (**I**) DIC image of cluster #2 from panel H. Dashed line: limits of vasculature, e: erythrocyte, m: muscle. Scale bar 10μm.

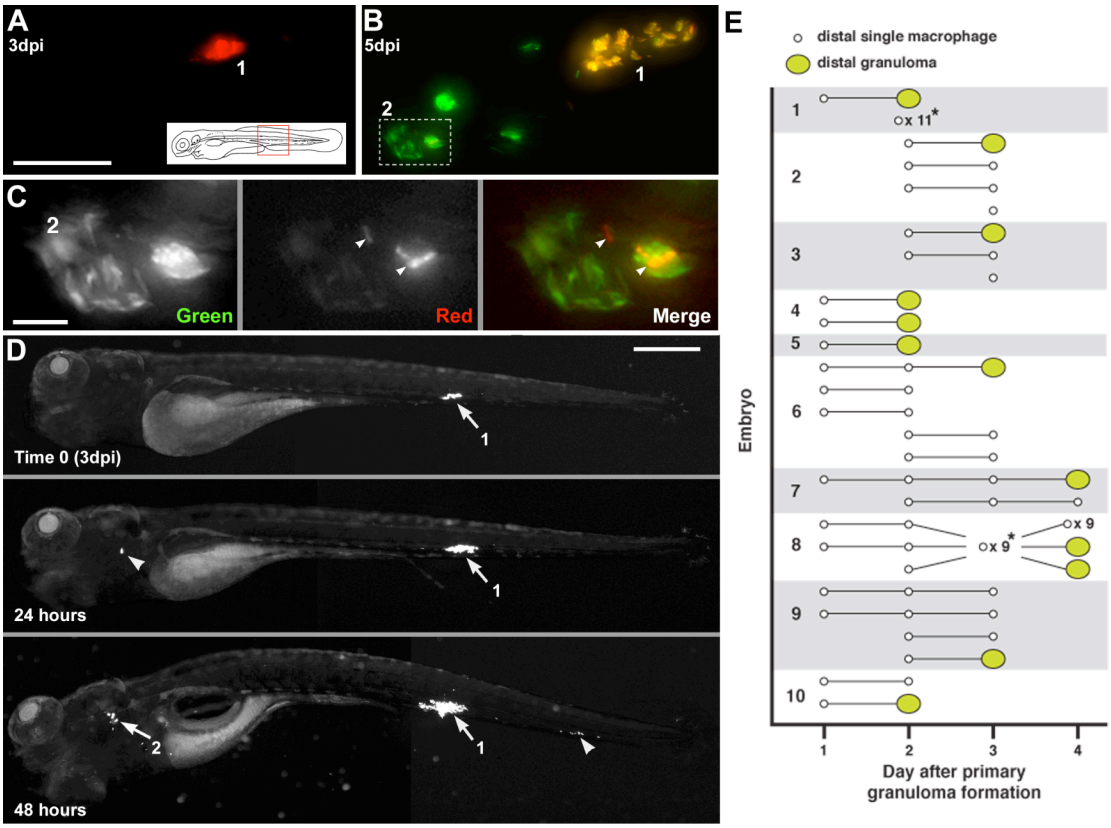

Figure 5.6. Departing bacteria form secondary granulomas. A-C. Bacteria from one granuloma spread to another. (**A**) Primary granuloma immediately after photoactivation at 3 dpi. (**B**) At 5dpi, the original granuloma (1) persists and a new one (2) has appeared nearby. Dashed box, area shown in panel C. (**C**) photoactivated bacteria from granuloma 1 spreading in granuloma 2. (**D**) single granuloma at 3dpi (white arrow, 1) with departure of bacteria to new location 24 hours later (white arrowhead). By 48 hours, the original granuloma (1) continues

to grow, the new locus is forming a granuloma (2) and a third locus of infection has appeared (arrowhead). Scale bar, 300μm. (**E**) Dissemination from single primary granulomas in 10 embryos. Horizontal lines indicate fate of departing macrophages (remain single or form granuloma) on successive days. *Indicates dissemination of multiple macrophages which could not be tracked definitively between days, or which appeared on the last day of tracking. The embryo from (D) is shown as 1.

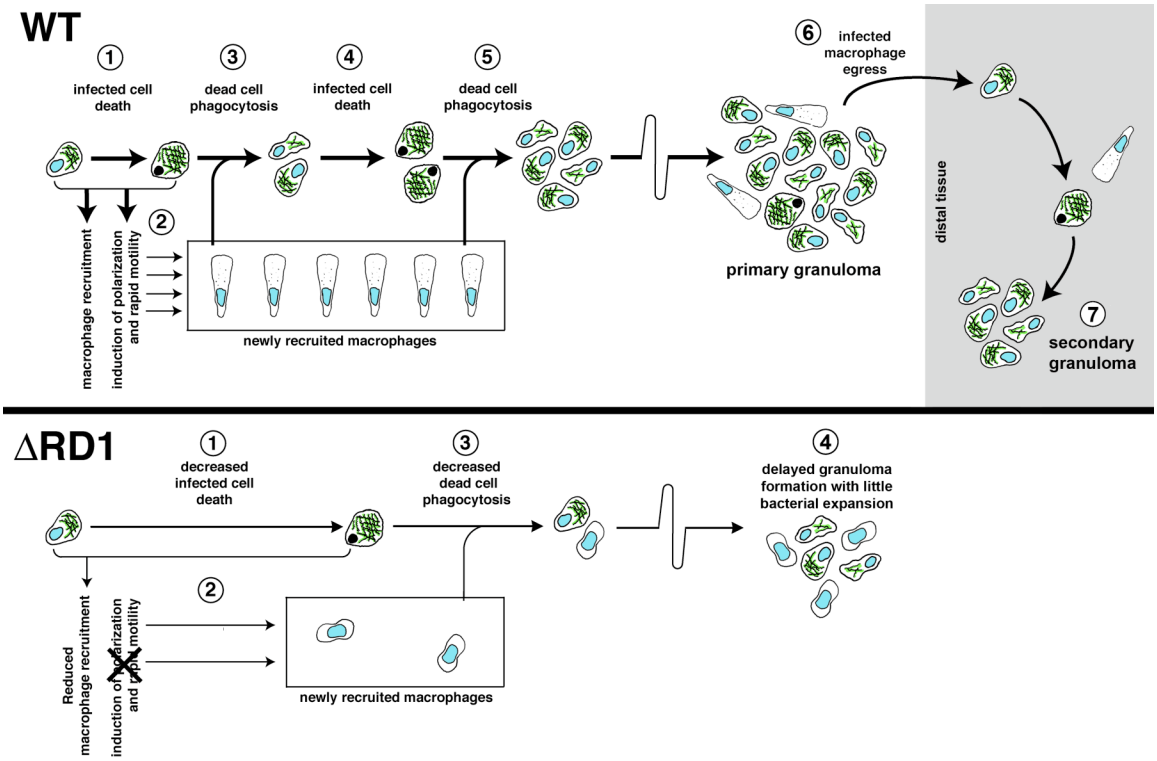

Figure 5.7. Mechanisms and consequences of early granuloma formation and the impact of RD1. Top: WT pathogenesis. An infected cell (1) recruits new macrophages and induces their rapid motility (2). Upon its death, it is phagocytosed by the recruited cells (3). After more bacterial growth, these infected cells also die (4) and are phagocytosed by more recruited macrophages (5). Infected cells egress the primary granuloma (6), to initiate secondary granulomas (7). Bottom: the same events altered by the absence of RD1. An

infected cell allows intracellular bacterial growth similar to WT. The death of this cell is delayed compared to WT (1), and the recruited macrophages are fewer in number and lack the rapid motility seen in WT (2). Slower infected macrophage death and rephagocytosis of dead cells (3) combine to produce small, delayed granulomas with better containment of infection (4).

5.6 Supplementary information

Supplementary Figures

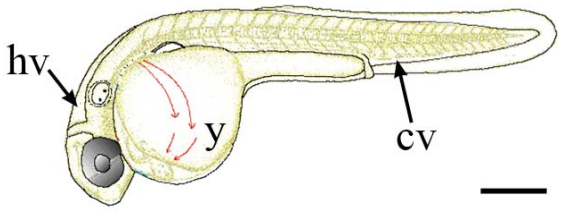

Supplementary Figure 5.1

Overview of zebrafish embryo anatomy. cv: caudal vein, hv, hindbrain ventricle, y, yolk. Scale bar, 300μm.

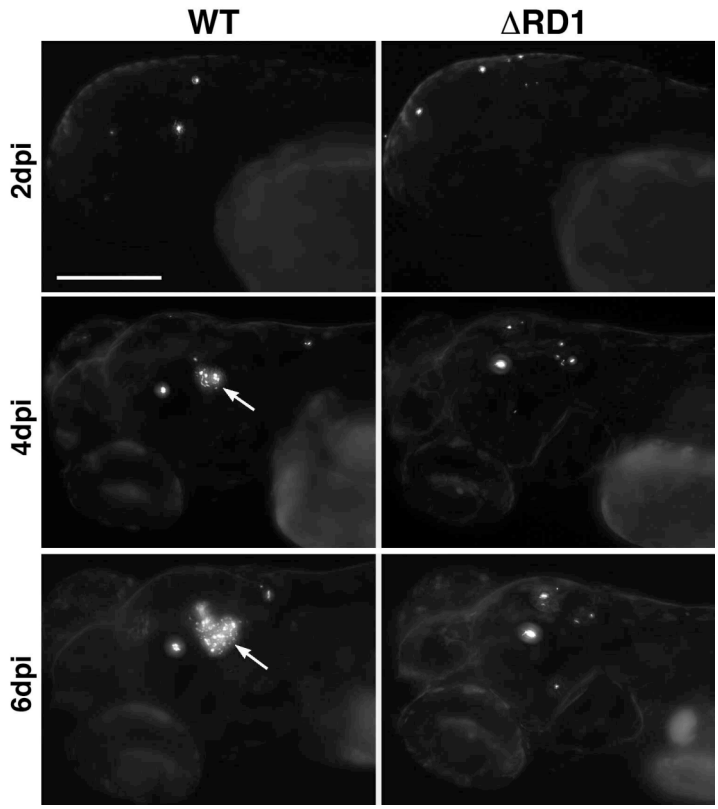

Supplementary Figure 5.2

Overall progression of infection after hindbrain ventricle injection of 50-100 CFU of WT (left) or ΔRD1 (right) Mm. Though the burden of bacteria at 2dpi appears similar, the advent of a granuloma (arrows) in WT by 4dpi results in dramatically greater bacterial numbers by 6dpi. All bacteria present in these animals were only found in the head (data not shown), thus granuloma formation does not proceed from recruitment of infected cells. Scale bar, 200μm.

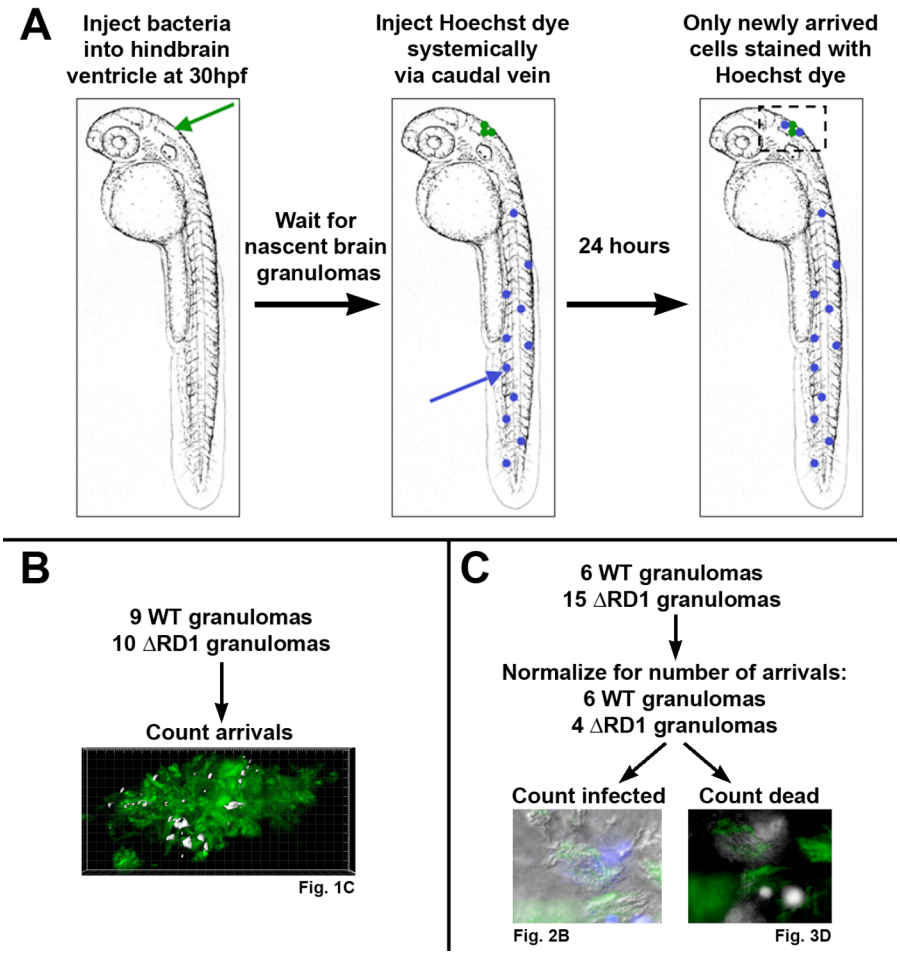

Supplementary Figure 5.3

Experiment to enumerate and characterize macrophages newly arrived to a granuloma within 24 hours. (**A**) Outline of injections. Bacteria are injected into the hindbrain ventricle at 30 hours post fertilization (hpf). In order to form infected lesions large enough to compare with WT bacteria, ~5x the dose of ΔRD1 was used (50-100 in WT vs 250-500 in ΔRD1). Nascent brain granulomas usually appear two to three days post infection (dpi). At this point embryos with nascent granulomas are injected via tail vein with Hoechst 33342 nuclear dye, which stains the nuclei of cells in the blood and many tissues, but not the brain (data not shown). (B-C) Outline of counting and analysis. (**B**) At 24 hours after the Hoechst injection, the granulomas are imaged to quantitate the number of cells recruited. See Figure 1C-E. (**C**) To study the fates of arrived macrophages, a second set of granulomas was analyzed. Embryos were

injected as before, but a subset of granulomas with no significant difference in arrival number were analyzed. (WT: 39.3+/- 13.6, ΔRD1: 30.0 +/- 12.99, p=0.312). (Analysis of this subset or of all granulomas yielded the same results). 3D DIC timelapse was used in addition to widefield fluorescence to allow positive identification of infected state. See Figure 2A-C. Collapsed nuclei have a distinct fluorescent appearance, but were cross-checked with DIC footage as well. See Figure 3D-E.

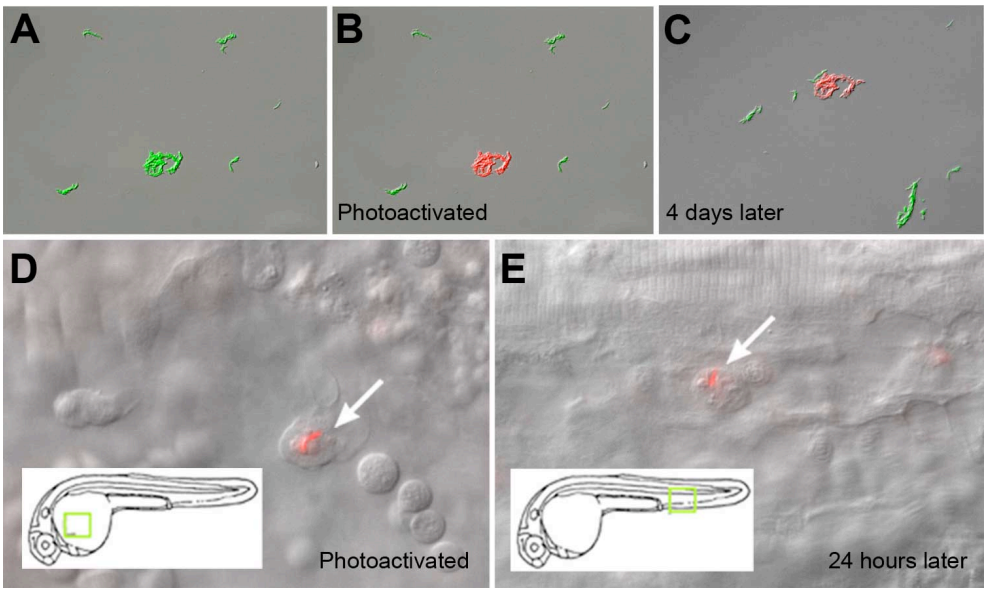

Supplementary Figure 5.4

M. marinum expressing Kaede photoactivatable protein to mark and track infected macrophages in vivo. (**A**-**B**) Merged image of photoactivated (red) and non-photoactivated (green) bacteria in medium immediately before (A) and after (B) photoactivation. (**C**) Same bacteria still detectable four days later. (**D**) Single macrophage containing photoactivated *M. marinum* (red channel only) in yolk circulation valley of embryo, immediately after photoactivation. (**E**) The same bacteria detected 24 hours later in caudal vein. Insets show location in embryo.

Supplementary Information

Mathematical modeling of the role of macrophage death in granuloma growth.

To establish a simple model for granuloma expansion, we started with a series of assumptions, supported by our experimental results. The most important are: 1) granuloma growth can be measured by an increase in the number of infected macrophages (Figure 5.4 B, D), 2) apoptotic bodies are stable for at least 24 hours and are left behind by all infected macrophage deaths, and 3) the live bacterial contents of dead macrophages may be phagocytosed either whole or in part by either infected or uninfected macrophages. We reasoned that the number of infected macrophages present at 24 hours (N_{24}) must be a function of the number present at time 0 (N_0). Some fraction (*f*) of N_0 will die during the 24-hour period, and their bacterial contents will be taken up by a number (*m*, for multiplicity) of new macrophages. Therefore the dying macrophages will result in a new number of infected macrophages which equals $N_0(fm)$. This number, plus the number of infected macrophages not dying ($N_0(1-f)$) will total the number of infected macrophages present at 24 hours, as shown in equation 1.

$$N_{24} = N_0\left[fm + (1-f)\right] \qquad (1)$$

Rearranged to express proportional growth of the granuloma in terms of infected cells ($N_{24}/N_0 = G$), this becomes:

$$G = f(m-1) + 1 \qquad (2)$$

We propose that the major mechanism for cell-to-cell bacterial spread in nascent granulomas is the apoptotic death of infected macrophages followed by the phagocytosis of these cells and their bacterial cargo by one or more other macrophages. In order to estimate the relative importance of this mechanism to the increase in the number of infected cells in a growing granuloma, we formed single brain granulomas in five different embryos and imaged each at time 0 (when the granulomas were still relatively small) and 24 hours later. Because

granulomas near the hindbrain ventricle tend to be planar in shape, we first used a simple measure of bacterial fluorescence area in a flattened image to estimate granuloma size and growth. Next, the fluorescence datasets were deconvolved and analyzed in three dimensions in order to estimate the number of infected macrophages (discrete clusters of bacteria) present at both timepoints. Finally, high resolution DIC stacks taken at the same timepoints allowed the detection and enumeration of apoptotic bodies, which serve as effective markers of previous apoptosis events (Figure 5.3F-I). In cases of fragmentation of apoptotic bodies (as in Figure 5.3B), we counted clustered fragments as a single apoptotic event. The results of these measurements are summarized in Supplementary Table 5.2.

We reasoned that if the proposed mechanism was the only one responsible for expansion in the number of infected cells, the change in cell number over 24 hours could be predicted based upon the number of infected macrophages present at time zero, provided the fraction of cells that die per unit time (*f*) and the multiplicity of infection (*m*) are known (see text). The assumptions we made in designing the model, and the rationale for each, are displayed in Supplementary Table 5.1.

Given Equation 2 and the data from before and after a 24 hour period of granuloma expansion (Supplementary Table 5.2), we had the data necessary to calculate values for *f*, *m*, and G as well as the opportunity to use calculated values of f and m to derive a predicted value for G. We reasoned that comparing this predicted G to the measured G would provide an estimation of the percentage of actual granuloma expansion that could be explained by the proposed mechanism operating according to the proposed model.

<u>Estimation of *f*, the fraction of infected cells present at time 0 which die by 24 hours:</u>

For each embryo, the number of new apoptotic bodies formed would be equal to the number of original infected macrophages which had died. Therefore *f* could be calculated by:

$$f = \frac{A_{24} - A_0}{N_0} \quad (3)$$

Where:

A_0 = apoptotic bodies present at time 0

A_{24} = apoptotic bodies present at 24 hours

N_0 = infected cells present at time 0

Calculating *f* for all five fish resulted in a mean of 0.77 (+/- 0.12).

Estimation of *m*, the number of new infected macrophages resulting from a single apoptotic event:

Based on our assumptions and the observations we had made of single or multiple macrophages engulfing the remains and bacteria from infected macrophages, we expected this number to be greater than one and perhaps as high as three or four. We used the following formula to derive a measured *m* from the infection data:

$$m = \frac{N_{24} - N_0}{A_{24} - A_0} \quad (4)$$

Where N_{24} = infected cells present at 24 hours.

The value for G is defined as I_{24}/I_0.

The resulting actual and predicted values for G for each embryo are listed in Supplementary Table 5.3. As mentioned in the text, the results suggest that this mechanism accounts for a large majority of granuloma expansion. Our model does not account for possible positive feedback in the system, which would mean the entire effect of the process is amplified as time goes by, since more infected

cells are present over time. This effect may well account for the rest of the observed granuloma expansion, but since we do not have a good estimate of the magnitude of this effect, we have chosen the conservative stance of leaving it out. Given the extreme simplicity of our model, this analysis only vouches for the plausibility of our proposed mechanism being the major factor in granuloma expansion. The results leave room for additional mechanisms, but can also account for our proposed mechanism being the only one.

Supplementary Methods

Bacterial Strain Production

Kaede-expressing Mm was prepared as follows: The Kaede ORF was PCR amplified from the –pKaede-MC1 plasmid (MBL Int. Corp.) using the primers KaedeProkF (5'-CCCGGTACCAGATCTTTAAATCTAGATTTAGAAGGAGATATACATATGGTGAGTCTGATT-3') and KaedeProkR (5'-GATCGCTAGCAGTTACTTGACGTTG-3'). The product was then cleaved with KpnI and NheI and cloned into pMSP12::gfp (Chan et al., 2002), which was similarly digested to remove the gene encoding Green Fluorescent Protein (gfp). This resulting plasmid, bearing Kaede driven by msp12, was named pMSP12-Kaede. Mm transformed with p-msp12-Kaede was named MD2.

Mounting of Embryos for Timelapse Microscopy

Embryos imaged for two hours or less were immobilized in 1.5% low melting point agarose on glass cover slips and covered in fish water with tricaine (as per (Cosma et al., 2006b; Davis et al., 2002). For long-term timelapse (up to 18 hours) embryos were similarly mounted in a chamber based on that described by Kamei et al (Kamei et al., 2004; Kamei and Weinstein, 2005) but modified for use with an inverted confocal microscope, with ~30ml of tricaine/fish water and no recirculation.

Image Analysis

Tracking of cells in DIC was performed in Imaris by visualizing DIC planes in Ortho Slice mode and creating spots at the estimated centroid of the nucleus at each time point. Bacterial volumes were estimated in Imaris either by calculation of fluorescence volume or by calculation of surfaces traced manually over DIC images. Area measures of granuloma fluorescence were performed in MetaMorph by collapsing fluorescence z-stacks using maximum intensity projection to produce a 2D image. The image was the thresholded to exclude background light intensities and the total area above threshold measured.

Supplementary Tables

Supplementary Table 5.1

Assumptions used for mathematical modeling of granuloma expansion

Assumption	Rationale
Granuloma growth can be measured by increase in the number of infected macrophages. The supply of new cells is provided by constantly arriving uninfected macrophages.	Figure 5.1B shows the typical expansion mode, with distinct additional clusters of bacteria rather than the expansion of a monolithic cluster. Figure 5.4A shows the evidence that rapid recruitment of new cells correlates with expanding WT granulomas. Infected cells have been shown to be incapable of dividing in granulomas (Dannenberg, 2003).
All infected macrophage deaths are rapid and apoptotic, always leaving behind apoptotic bodies which are stable for at least 24 hours.	The rapid course of nuclear collapse and apoptotic body formation is illustrated in Figure 5.2B and Movie 5.3. Figure 5.3D-I details the accumulation of apoptotic bodies over 24 hours and the correlation of the DIC appearance of apoptotic bodies with molecular markers of apoptosis.
Dead infected macrophages may be engulfed either whole or in part by either infected or uninfected macrophages.	Figure 5.3C and Movie 5.5 show the engulfment of a whole dead macrophage by a single cell, and Figure 5.3J and Movie 5.6 show an example of the partial engulfment of the bacteria of an infected cell while the rest is engulfed by another. We have also collected video evidence of up to four macrophages sharing the bacteria of a single dead cell (data not shown).
When an apoptotic body is engulfed, it is taken up entirely by one macrophage, while the bacterial contents of the cell may be shared among multiple macrophages.	The events of Figure 5.3J and Movie 5.6 support this phenomenon, and other data not presented suggest that phagocytosis by multiple cells generally involves one major but incomplete phagocytosis, with smaller portions of the contents rapidly taken up by other nearby cells.
All observed apoptotic bodies are within macrophages.	Figure 5.3B and C picture the same cell undergoing death and engulfment over the course of 46 minutes. Timelapse of these events is shown in Movies 5.4 and 5.5. Based on this and similar observations not shown, we surmise that a dead cell spends very little time before being phagocytosed.
Infected macrophages depart rarely.	Instances and frequency of infected cell departure are addressed in Figure 5.5. In the context of a large number of infected macrophages in a growing granuloma, we find the impact of these departures on overall growth to be negligible.

Supplementary Table 5.2

Measurements of expansion and apoptosis in a granuloma over 24 hours.

Embryo*	Area of bacterial fluorescence (μm^2), time 0	Area of bacterial fluorescence (μm^2), 24 hours	Infected cells, time 0	Infected cells, 24 hours	Apoptotic bodies, time 0	Apoptotic bodies, 24 hours
1	1473	2636	40	76	13	38
2	1693	3883	33	94	24	57
4	950	4746	36	87	24	48
5	969	3665	29	86	15	39
8	912	2095	18	68	13	26

*Embryo numbers are discontinuous--starting from nine embryos, some were lost to handling or were excluded when DIC imaging proved too poor to enumerate apoptotic bodies.

Supplementary Table 5.3

Observed and calculated growth, death fraction, and multiplicity of infection in 24 hour granulomas.

Embryo	Observed G from fluorescence area	Observed G from infected cell counts	Predicted G	Calculated *f*	Calculated *m*
1	1.8	1.9	1.3	0.6	1.4
2	2.3	2.8	1.8	1.0	1.8
4	5.0	2.4	1.7	0.7	2.1
5	3.8	3.0	2.1	0.8	2.4
8	2.3	3.8	3.1	0.7	3.8
Average	**3.0**	**2.8**	**2.0**	**0.8**	**2.3**
SEM	0.6	0.3	0.5	0.1	0.6

Supplementary Movie Legends

Movie 5.1

Highly motile uninfected phagocytes at WT granuloma. Left: single DIC focus-through of a phagocyte (white arrow) with prominent leading lamellipodium and uniformly fine cytoplasmic granules. Right, phagocyte (white arrow), also with prominent lamellipodium, but with cytoplasmic vesicles of varying sizes. Scale bar, 10μm.

Movie 5.2

Uninfected macrophage at ΔRD1 granuloma. Repeated focusthroughs of an uninfected cell (white arrow) at a ΔRD1 lesion similar in size to that in Movie 5.1. Note the drastically reduced motility and lack of distinct lamellipodium. See figure 5.2E. Time scale: minutes and seconds. Scale bar: 10μm.

Movie 5.3

Death of an infected macrophage in a WT granuloma. Two DIC focusthrough views separated by two minutes, showing the nucleus of an infected macrophage (black arrow) immediately before and immediately after nuclear collapse and fragmentation (black arrows). See figure 5.3B. Time scale: hours, minutes, and seconds counting from time zero shown in figure 5.3A. Scale bar: 10μm.

Movie 5.4

Death of a macrophage infected with *S. arizonae*. In vivo DIC timelapse of pyroptosis of *Salmonella arizonae* infected zebrafish macrophage. The macrophage nucleus (black arrow) undergoes collapse morphologically very similar to that seen in mycobacterial granulomas (Fig. 5.3B and Movie 5.3), but in this case the cell swells and appears very near lysing. Black arrowheads, bacteria. Time scale: hours, minutes, and seconds. Scale bar: 10μm.

Movie 5.5

Phagocytosis of a dead infected macrophage in a WT granuloma. Repeated DIC focusthrough views separated by ~two minutes each, showing the remnants of the macrophage nucleus seen collapsing in figure 5.3B and Movie 5.3 (black arrow) remaining clustered with associated bacteria. The entire carcass is rephagocytosed by a new uninfected macrophage (white arrow). See figure 5.3C. Small white arrows indicate other uninfected cells moving nearby. Time scale: hours and minutes counting from time zero shown in figure 5.3A. Scale bar: 10μm.

Movie 5.6

Dead infected macrophage phagocytosed by multiple new cells. Repeated DIC focusthrough views separated by ~two minutes each, showing partial rephagocytosis of the bacteria from a dead macrophage (X) by a previously uninfected macrophage, as shown in figure 5.3J. The bacteria being taken are indicated by white arrowheads. The nucleus of the macrophage taking the bacteria, when visible, is indicated by a white arrow. The nucleus of the other macrophage (not indicated), which is phagocytosing the rest of the bacteria, is sometimes visible at the lower right-hand edge of the cluster. Time scale: hours and minutes. Scale bar: 10μm.

Movie 5.7

Death of an infected macrophage in a ΔRD1 granuloma. Three successive DIC focusthrough views each separated by two minutes, showing nuclear collapse in a ΔRD1-infected macrophage inside a granuloma. Compare to nuclear collapse in WT, Fig. 5.3B and Movie 5.3. Time scale: hours, minutes and seconds. Scale bar, 5μm.

Movie 5.8

High motility of a lightly infected cell. Repeated DIC focusthrough views separated by two minutes each, showing a lightly infected cell (white arrow) moving rapidly (averaging 7.5μm/minute). Time scale: minutes and seconds, counting from time zero in Movie 5.6. Scale bar: 10μm.

Movie 5.9

Motility of a moderately infected cell. Repeated DIC focusthrough views separated by ~two minutes each, showing a moderately infected cell (white arrow) in the same granuloma pictured in Movie 5.8. Morphology is similar, but speed is reduced (averaging 2.4μm/minute). Time scale: hours and minutes. Scale bar: 10μm.

Movie 5.10

Low motility and membrane ruffling of a heavily infected cell. Repeated DIC focusthrough views separated by two minutes each, showing an extremely infected macrophage still alive but with very little motility (average speed 0.54μm/minute). The white arrow indicates a portion of the cell nucleus. Active cellular protrusions in all directions suggest this cell is alive and active. Note the appearance of several dead cell fragments, remnants of macrophages which previously had contained these bacteria. Time scale: hours and minutes. Scale bar: 5μm.

Movie 5.11

Clusters of fluorescent Mm departing a granuloma. Long-term timelapse confocal microscopy of a brain granuloma with fluorescent bacteria pictured in figure 5.5B. Only the bacteria are visible, but their movements are as expected from views of infected macrophages by DIC microscopy. Clusters marked with green dots depart from the lesion and out of frame. Time scale: hours and minutes (ten minutes per timepoint). Scale bar: 10μm.

Movie 5.12

Infected macrophages departing a granuloma. Visualization of macrophage efflux from a granuloma by DIC microscopy. In the first frame, dashed black lines and numbers indicate three different infected macrophages present inside the granuloma (outlined in white). All three infected macrophages depart toward the left of the frame, in numerical order. Time scale: minutes and seconds. Scale bar: 25μm.

Movie 5.13

Infected macrophages lodged in the vasculature after departure from a granuloma. DIC timelapse of infected macrophages 1 and 2 pictured in 5.5H and I. Both cells carry photoactivated bacteria originating from a tail granuloma, and are lodged in the gill vasculature, partially blocking it. Erythrocytes are seen nearby in the bloodstream. Scale bar, 20μm.

Chapter 6

Discussion

In this work, I have first demonstrated the broad applicability of the embryonic zebrafish infection model to study bacterial pathogenesis, and the specificity it shows in response to distinct pathogens. Beyond this, I have used this model specifically to detail events in early tuberculosis pathogenesis inaccessible with other models. Finally, I have used the quantitative analyses of in vivo observations of infection, along with a specific bacterial mutant, to dissect the process of tuberculous granuloma formation into distinct cellular components.

Broad applicability of the embryonic zebrafish infection model

In work published soon after entering medical school, we developed the zebrafish embryo model and demonstrated that infection of zebrafish embryos with *Mycobacterium marinum,* a close genetic relative of *Mycobacterium tuberculosis,* produced bone fide epithelioid granulomas in the absence of adaptive immunity. This phenotype was mycobacterium-specific; infection with *Salmonella arizonae* produced an utterly different phenotype at cellular and subcellular levels (Davis et al., 2002). Here I have presented detailed analyses of embryonic infection with *Pseudomonas aeruginosa* and *Leptospira interrogans*, which not only underscore the distinct host responses to different pathogens, but also go far toward establishing new infection models for these pathogens. Thus, the zebrafish embryo is a versatile and reliable model host for bacterial pathogenesis that allows a cellular dissection of the host-pathogen interface not accessible in traditional animal models.

New details of mycobacterial pathogenesis detailed using embryonic zebrafish infection

A major advantage of the zebrafish embryo is the excellent visual access it provides for microscopy. The number of fluorescent probes and fluorescent transgenic markers for zebrafish is constantly expanding, but in addition to these tools is simple Differential Interference Contrast microscopy. This mode allows the collection of myriad cellular and subcellular details all at once, without the need for specific probes. I have enhanced this mode through the addition of three-dimensional dataset acquisition (see Chapter 5) in timelapse.

This highly effective observational tool has made it possible to observe both previously suggested and completely unexpected details of mycobacterial pathogenesis, such as recruitment of macrophages to the infection site, phagocytosis of bacteria, and transport of bacteria to distant tissues, in real time. Among other observations, we have found (see Chapter 4) that although mycobacteria make no effort at all to avoid phagocytosis in vivo, they actually grow better outside of phagocytes than inside. However, in return for less effective replication, the bacteria receive transport to new tissues, in effect 'diversifying their holdings' and raising their chances of gaining a foothold.

Experimental dissection of the mechanisms and consequences of early granuloma formation

Previous findings in the zebrafish model have shown that the bacterial virulence determinant RD1 specifically encourages the establishment of granulomas (Volkman et al., 2004). The earliest steps of granuloma formation have been somewhat mysterious, since these events are sparse and difficult to visualize in mammalian model organisms. The combination of a bacterial mutant with a defect in this very process, and a model host which is visually accessible, small (so that finding and tracking early events is relatively easy), and lacking in adaptive immune components, made dissection of this crucial process possible. We therefore proceeded with the series of experiments detailed in Chapter 5. The results suggest that, while the classically regarded granuloma (present during the adaptive immune response) may represent a rough stalemate between host and pathogen, the earliest stages of the granuloma actually aid mycobacterial expansion and dissemination, and are induced by bacterial virulence determinants.

Future challenges of the zebrafish model of infection

In this work I feel we have taken good advantage of the present capabilities of the zebrafish infection model, particularly in visualization and genetic manipulation. As touched on in Chapter 2, the possibilities for genetic manipulation of zebrafish are growing, fueled by research both within and outside the field of infectious diseases. The zebrafish genome has been nearly complete and annotated for some years now, and no doubt a full and satisfactory version

of that resource will expand the possibilities greatly. The greatest challenge for work in the zebrafish as an infection model remains the relative lack of immunologic reagents. Although serious commercial efforts are ongoing, the reliable production of antibodies to native zebrafish proteins is still only a hope. Several antibodies raised against human and mouse proteins have proven useful in the zebrafish, but the heavy glycosylation of fish proteins has meant that species-specific antibodies are very difficult to produce conventionally.

The expanding use of small molecule screens in zebrafish embryos may offer a viable alternative to antibodies for biochemical manipulation. Because embryos can absorb many small molecules directly, screening at a very large scale is feasible in this model. Several known chemical inhibitors of human enzymes (such as to matrix metalloproteinases) (Volkman et al, in preparation), have been shown to be effective in zebrafish embryos. Therefore, some of the need for specific reagents might be met in this way. Still, the direct, specific, protein level interaction of antibodies will be needed for the zebrafish.

As mentioned in Chapter 2, in depth analysis of the zebrafish adaptive immune system is still only beginning. In the present work, we have circumvented or even taken advantage of the immunologic realities of the zebrafish to focus exclusively on innate immunity. This approach is quite valid for the understanding of early events in infection or in studying infection of extremely young or immunocompromised patients. Still, more will need to be known about

the other arm of zebrafish immunity in order for the model to realize its full potential.

Further questions in tuberculous granuloma formation

Using this zebrafish model, we have made significant discoveries about the biology of early tuberculosis. Aspects of granuloma biology are at work far earlier than anyone had suspected. This early granuloma appears to be detrimental to the host's self-protection. At another level, the macrophage itself appears to aid infection by doing many of the things that usually help defend the host, whether by phagocytosing mycobacteria initially (only to provide a free ride to other tissues) or by showing up in force to devour dead cells in early granulomas (only to aid expansion and, ultimately, dissemination). It is a frustrating aspect of studying early infection to know how difficult it would be to alter these stages of disease clinically. And yet, alterations in these earliest steps may provide our best hope to lighten the burden of disease. As detailed in Chapter 1, there is some evidence that the innate immune system is sometimes capable of eradicating (early) infection. On the other hand, thus far, the adaptive immune response has not been demonstrated to eradicate infection—only to limit it.

One category of further questions centers around the limitations of the zebrafish embryo. In an adult animal, what types of cells are present at the initial granuloma? The zebrafish offers a reductionist view of infection in living tissue. What role, if any, do dendritic cells (or other immune cells not present in the

zebrafish embryo) (Traver et al., 2003) play at this phase? Do neutrophils (present and observable in zebrafish embryos) (Le Guyader et al., 2008; Mathias et al., 2006) also have a role? How do the kinetics of growth compare between early human and early zebrafish TB? The model pays for its exquisite access to cellular events with difficult questions about applicability to human disease. We have attempted throughout to place our findings in the context of infections of mammalian models, and when available humans.

Finally, many molecular details remain to be filled in to the outline of early granuloma biology provided here. As mentioned in Chapter 5, the complex downstream events which require the bacterial RD1 locus to produce early granuloma expansion are not known. The separate steps of phagocyte recruitment, motility, infection and death, all requiring RD1, must be teased apart in their distinct details. How are they interrelated? Which, if any, can be intercepted without detriment to the host? As for dissemination through departure, is the signal inducing motility to and within granulomas the same as the one leading to departure? Are particular tissues preferred targets for departing infected macrophages? Continued work is needed within the model, and with other model organisms, to answer these questions. But, continued development and expansion of the zebrafish model itself will also be necessary.

References

Abadie, V., Badell, E., Douillard, P., Ensergueix, D., Leenen, P. J., Tanguy, M., Fiette, L., Saeland, S., Gicquel, B., and Winter, N. (2005). Neutrophils rapidly migrate via lymphatics after Mycobacterium bovis BCG intradermal vaccination and shuttle live bacilli to the draining lymph nodes. Blood *106*, 1843-1850.

Adams, D. O. (1975). The structure of mononuclear phagocytes differentiating in vivo. II. The effect of Mycobacterium tuberculosis. Am J Pathol *80*, 101-116.

Adams, D. O. (1976). The granulomatous inflammatory response. A review. Am J Pathol *84*, 164-191.

Aderem, A., and Underhill, D. M. (1999). Mechanisms of phagocytosis in macrophages. Annu Rev Immunol *17*, 593-623.

Agius, C., and Roberts, R. J. (2003). Melano-macrophage centres and their role in fish pathology. J Fish Dis *26*, 499-509.

Algood, H. M., Chan, J., and Flynn, J. L. (2003). Chemokines and tuberculosis. Cytokine Growth Factor Rev *14*, 467-477.

Algood, H. M., and Flynn, J. L. (2004). CCR5-deficient mice control Mycobacterium tuberculosis infection despite increased pulmonary lymphocytic infiltration. J Immunol *173*, 3287-3296.

Alliot, F., Lecain, E., Grima, B., and Pessac, B. (1991). Microglial progenitors with a high proliferative potential in the embryonic and adult mouse brain. Proc Natl Acad Sci U S A *88*, 1541-1545.

Alper, S., McBride, S. J., Lackford, B., Freedman, J. H., and Schwartz, D. A. (2007). Specificity and complexity of the Caenorhabditis elegans innate immune response. Mol Cell Biol *27*, 5544-5553.

Alsaadi, A. I., and Smith, D. W. (1973). The fate of virulent and attenuated Mycobacteria in guinea pigs infected by the respiratory route. Am Rev Respir Dis *107*, 1041-1046.

Alves, V. A., Gayotto, L. C., Yasuda, P. H., Wakamatsu, A., Kanamura, C. T., and De Brito, T. (1991). Leptospiral antigens (L. interrogans serogroup ictero-haemorrhagiae) in the kidney of experimentally infected guinea pigs and their relation to the pathogenesis of the renal injury. Exp Pathol *42*, 81-93.

Amores, A., Force, A., Yan, Y. L., Joly, L., Amemiya, C., Fritz, A., Ho, R. K., Langeland, J., Prince, V., Wang, Y. L.*, et al.* (1998). Zebrafish hox clusters and vertebrate genome evolution. Science *282*, 1711-1714.

Andersen, P. (1997). Host responses and antigens involved in protective immunity to Mycobacterium tuberculosis. Scand J Immunol *45*, 115-131.

Ando, R., Hama, H., Yamamoto-Hino, M., Mizuno, H., and Miyawaki, A. (2002). An optical marker based on the UV-induced green-to-red photoconversion of a fluorescent protein. Proc Natl Acad Sci U S A *99*, 12651-12656.

Armstrong, J. A., and Hart, P. D. (1975). Phagosome-lysosome interactions in cultured macrophages infected with virulent tubercle bacilli. Reversal of the

usual nonfusion pattern and observations on bacterial survival. J Exp Med *142*, 1-16.

Astarie-Dequeker, C., N'Diaye, E. N., Le Cabec, V., Rittig, M. G., Prandi, J., and Maridonneau-Parini, I. (1999). The mannose receptor mediates uptake of pathogenic and nonpathogenic mycobacteria and bypasses bactericidal responses in human macrophages. Infect Immun *67*, 469-477.

Athanazio, D. A., Silva, E. F., Santos, C. S., Rocha, G. M., Vannier-Santos, M. A., McBride, A. J., Ko, A. I., and Reis, M. G. (2008). Rattus norvegicus as a model for persistent renal colonization by pathogenic Leptospira interrogans. Acta Trop *105*, 176-180.

Avet-Rochex, A., Bergeret, E., Attree, I., Meister, M., and Fauvarque, M. O. (2005). Suppression of Drosophila cellular immunity by directed expression of the ExoS toxin GAP domain of Pseudomonas aeruginosa. Cell Microbiol *7*, 799-810.

Bafica, A., Scanga, C. A., Feng, C. G., Leifer, C., Cheever, A., and Sher, A. (2005). TLR9 regulates Th1 responses and cooperates with TLR2 in mediating optimal resistance to Mycobacterium tuberculosis. J Exp Med *202*, 1715-1724.

Bajenoff, M., and Germain, R. N. (2007). Seeing is believing: a focus on the contribution of microscopic imaging to our understanding of immune system function. Eur J Immunol *37 Suppl 1*, S18-33.

Balasubramanian, V., Wiegeshaus, E. H., Taylor, B. T., and Smith, D. W. (1994). Pathogenesis of tuberculosis: pathway to apical localization. Tuber Lung Dis *75*, 168-178.

Banfi, E., Cinco, M., Bellini, M., and Soranzo, M. R. (1982). The role of antibodies and serum complement in the interaction between macrophages and leptospires. J Gen Microbiol *128*, 813-816.

Barker, L. P., George, K. M., Falkow, S., and Small, P. L. (1997). Differential trafficking of live and dead Mycobacterium marinum organisms in macrophages. Infect Immun *65*, 1497-1504.

Barreda, D. R., Neumann, N. F., and Belosevic, M. (2000). Flow cytometric analysis of PKH26-labeled goldfish kidney-derived macrophages. Dev Comp Immunol *24*, 395-406.

Barton, G. M., and Medzhitov, R. (2002). Toll-like receptors and their ligands. Curr Top Microbiol Immunol *270*, 81-92.

Bates, C. S., Toukoki, C., Neely, M. N., and Eichenbaum, Z. (2005). Characterization of MtsR, a new metal regulator in group A streptococcus, involved in iron acquisition and virulence. Infect Immun *73*, 5743-5753.

Bates, J. M., Mittge, E., Kuhlman, J., Baden, K. N., Cheesman, S. E., and Guillemin, K. (2006). Distinct signals from the microbiota promote different aspects of zebrafish gut differentiation. Dev Biol *297*, 374-386.

Beatty, W. L., Rhoades, E. R., Ullrich, H. J., Chatterjee, D., Heuser, J. E., and Russell, D. G. (2000). Trafficking and release of mycobacterial lipids from infected macrophages. Traffic *1*, 235-247.

Beatty, W. L., and Russell, D. G. (2000). Identification of mycobacterial surface proteins released into subcellular compartments of infected macrophages. Infect Immun *68*, 6997-7002.

Beatty, W. L., Ullrich, H. J., and Russell, D. G. (2001). Mycobacterial surface moieties are released from infected macrophages by a constitutive exocytic event. Eur J Cell Biol *80*, 31-40.

Belcourt, D. R., Lazure, C., and Bennett, H. P. (1993). Isolation and primary structure of the three major forms of granulin-like peptides from hematopoietic tissues of a teleost fish (Cyprinus carpio). J Biol Chem *268*, 9230-9237.

Bellamy, R., Ruwende, C., Corrah, T., McAdam, K. P., Thursz, M., Whittle, H. C., and Hill, A. V. (1999). Tuberculosis and chronic hepatitis B virus infection in Africans and variation in the vitamin D receptor gene. J Infect Dis *179*, 721-724.

Bellamy, R., Ruwende, C., Corrah, T., McAdam, K. P., Whittle, H. C., and Hill, A. V. (1998). Variations in the NRAMP1 gene and susceptibility to tuberculosis in West Africans. N Engl J Med *338*, 640-644.

Bennett, C. M., Kanki, J. P., Rhodes, J., Liu, T. X., Paw, B. H., Kieran, M. W., Langenau, D. M., Delahaye-Brown, A., Zon, L. I., Fleming, M. D., and Look, A. T. (2001). Myelopoiesis in the zebrafish, Danio rerio. Blood *98*, 643-651.

Bennin, D. A., Don, A. S., Brake, T., McKenzie, J. L., Rosenbaum, H., Ortiz, L., DePaoli-Roach, A. A., and Horne, M. C. (2002). Cyclin G2 associates with protein phosphatase 2A catalytic and regulatory B' subunits in active complexes and induces nuclear aberrations and a G1/S phase cell cycle arrest. J Biol Chem *277*, 27449-27467.

Bermudez, L. E., Sangari, F. J., Kolonoski, P., Petrofsky, M., and Goodman, J. (2002). The efficiency of the translocation of Mycobacterium tuberculosis across a bilayer of epithelial and endothelial cells as a model of the alveolar wall is a consequence of transport within mononuclear phagocytes and invasion of alveolar epithelial cells. Infect Immun *70*, 140-146.

Berthet, F. X., Lagranderie, M., Gounon, P., Laurent-Winter, C., Ensergueix, D., Chavarot, P., Thouron, F., Maranghi, E., Pelicic, V., Portnoi, D.*, et al.* (1998). Attenuation of virulence by disruption of the Mycobacterium tuberculosis erp gene. Science *282*, 759-762.

Black, R. A., Rauch, C. T., Kozlosky, C. J., Peschon, J. J., Slack, J. L., Wolfson, M. F., Castner, B. J., Stocking, K. L., Reddy, P., Srinivasan, S.*, et al.* (1997). A metalloproteinase disintegrin that releases tumour-necrosis factor-alpha from cells. Nature *385*, 729-733.

Blaser, H., Reichman-Fried, M., Castanon, I., Dumstrei, K., Marlow, F. L., Kawakami, K., Solnica-Krezel, L., Heisenberg, C. P., and Raz, E. (2006). Migration of zebrafish primordial germ cells: a role for myosin contraction and cytoplasmic flow. Dev Cell *11*, 613-627.

Bols, N. C., Yang, B. Y., Lee, L. E., and Chen, T. T. (1995). Development of a rainbow trout pituitary cell line that expresses growth hormone, prolactin, and somatolactin. Mol Mar Biol Biotechnol *4*, 154-163.

Brennan, M. K., Davis, J. M., Mathias, J. R., Hall, C. J., Emerson, J. C., Crosier, P. S., Huttenlocher, A., Ramakrishnan, L., and Moskowitz, M. (2009) *Pseudomonas aeruginosa* Type III secretion system interacts with phagocytes to modulate systemic infection of zebrafish embryos. Cell Micro (in press).

Brenot, A., King, K. Y., Janowiak, B., Griffith, O., and Caparon, M. G. (2004). Contribution of glutathione peroxidase to the virulence of Streptococcus pyogenes. Infect Immun *72*, 408-413.

Broussard, G. W., and Ennis, D. G. (2007). Mycobacterium marinum produces long-term chronic infections in medaka: a new animal model for studying human tuberculosis. Comp Biochem Physiol C Toxicol Pharmacol *145*, 45-54.

Brown, S. B., Tucker, C. S., Ford, C., Lee, Y., Dunbar, D. R., and Mullins, J. J. (2007). Class III antiarrhythmic methanesulfonanilides inhibit leukocyte recruitment in zebrafish. J Leukoc Biol *82*, 79-84.

Cadieux, B., Chitramuthu, B. P., Baranowski, D., and Bennett, H. P. (2005). The zebrafish progranulin gene family and antisense transcripts. BMC Genomics *6*, 156.

Caron, E., and Hall, A. (1998). Identification of two distinct mechanisms of phagocytosis controlled by different Rho GTPases. Science *282*, 1717-1721.

Casanova, J. L., and Abel, L. (2002). Genetic dissection of immunity to mycobacteria: the human model. Annu Rev Immunol *20*, 581-620.

Castellino, F., Huang, A. Y., Altan-Bonnet, G., Stoll, S., Scheinecker, C., and Germain, R. N. (2006). Chemokines enhance immunity by guiding naive CD8+ T cells to sites of CD4+ T cell-dendritic cell interaction. Nature *440*, 890-895.

Chackerian, A. A., Alt, J. M., Perera, T. V., Dascher, C. C., and Behar, S. M. (2002). Dissemination of Mycobacterium tuberculosis is influenced by host factors and precedes the initiation of T-cell immunity. Infect Immun *70*, 4501-4509.

Chan, K., Knaak, T., Satkamp, L., Humbert, O., Falkow, S., and Ramakrishnan, L. (2002). Complex pattern of Mycobacterium marinum gene expression during long-term granulomatous infection. Proc Natl Acad Sci U S A *99*, 3920-3925.

Chen, M., Gan, H., and Remold, H. G. (2006). A mechanism of virulence: virulent Mycobacterium tuberculosis strain H37Rv, but not attenuated H37Ra, causes significant mitochondrial inner membrane disruption in macrophages leading to necrosis. J Immunol *176*, 3707-3716.

Chen, S. C., Adams, A., Thompson, K. D., and Richards, R. H. (1998). Electron microscope studies of the in vitro phagocytosis of Mycobacterium spp. by rainbow trout Oncorhynchus mykiss head kidney macrophages. Dis Aquat Organ *32*, 99-110.

Cheung, D. O., Halsey, K., and Speert, D. P. (2000). Role of pulmonary alveolar macrophages in defense of the lung against Pseudomonas aeruginosa. Infect Immun *68*, 4585-4592.

Chiang, C. Y., and Riley, L. W. (2005). Exogenous reinfection in tuberculosis. Lancet Infect Dis *5*, 629-636.

Chong, S. W., Nguyet, L. M., Jiang, Y. J., and Korzh, V. (2007). The chemokine, Sdf-1, and its receptor, Cxcr4, are required for formation of muscle in zebrafish. BMC Dev Biol *7*, 54.

Cinco, M., Banfi, E., and Soranzo, M. R. (1981). Studies on the interaction between macrophages and leptospires. J Gen Microbiol *124*, 409-413.

Clark, H. F., and Shepard, C. C. (1963). Effect of Environmental Temperatures on Infection with Mycobacterium Marinum (Balnei) of Mice and a Number of Poikilothermic Species. J Bacteriol *86*, 1057-1069.

Clay, H., Davis, J. M., Beery, D., Huttenlocher, A., Lyons, S. E., and Ramakrishnan, L. (2007). Dichotomous Role of the Macrophage in Early *Mycobacterium marinum* Infection of the Zebrafish. Cell Host and Microbe *2*, 29-39.

Clay, H., and Ramakrishnan, L. (2005). Multiplex Fluorescent *In Situ* Hybridization in Zebrafish Embryos Using Tyramide Signal Amplification. Zebrafish *2*, 105-111.

Clay, H., Volkman, H. E., and Ramakrishnan, L. (2008). Tumor necrosis factor signaling mediates resistance to mycobacteria by inhibiting bacterial growth and macrophage death. Immunity *29*, 283-294.

Coburn, J., and Frank, D. W. (1999). Macrophages and epithelial cells respond differently to the Pseudomonas aeruginosa type III secretion system. Infect Immun *67*, 3151-3154.

Cooper, A. M., Dalton, D. K., Stewart, T. A., Griffin, J. P., Russell, D. G., and Orme, I. M. (1993). Disseminated tuberculosis in interferon gamma gene-disrupted mice. J Exp Med *178*, 2243-2247.

Cooper, M. S., Szeto, D. P., Sommers-Herivel, G., Topczewski, J., Solnica-Krezel, L., Kang, H. C., Johnson, I., and Kimelman, D. (2005). Visualizing morphogenesis in transgenic zebrafish embryos using BODIPY TR methyl ester dye as a vital counterstain for GFP. Dev Dyn *232*, 359-368.

Corbett, E. L., Watt, C. J., Walker, N., Maher, D., Williams, B. G., Raviglione, M. C., and Dye, C. (2003). The growing burden of tuberculosis: global trends and interactions with the HIV epidemic. Arch Intern Med *163*, 1009-1021.

Cornell, R. A., and Eisen, J. S. (2002). Delta/Notch signaling promotes formation of zebrafish neural crest by repressing Neurogenin 1 function. Development *129*, 2639-2648.

Cosma, C. L., Davis, J. M., Swaim, L. E., Volkman, H., and Ramakrishnan, L. (2006a). Animal Models of Mycobacterium marinum infection. In Current Protocols in Microbiology, C. K. Coico et al, eds. (John Wiley & Sons, Inc.).

Cosma, C. L., Humbert, O., and Ramakrishnan, L. (2004). Superinfecting mycobacteria home to established tuberculous granulomas. Nat Immunol *5*, 828-835.

Cosma, C. L., Humbert, O., Sherman, D. R., and Ramakrishnan, L. (2008). Trafficking of Superinfecting Mycobacterium Organisms into Established

Granulomas Occurs in Mammals and Is Independent of the Erp and ESX-1 Mycobacterial Virulence Loci. J Infect Dis *198*, 1851-1855.

Cosma, C. L., Klein, K., Kim, R., Beery, D., and Ramakrishnan, L. (2006b). Mycobacterium marinum Erp Is a Virulence Determinant Required for Cell Wall Integrity and Intracellular Survival. Infect Immun *74*, 3125-3133.

Cosma, C. L., Sherman, D. R., and Ramakrishnan, L. (2003). The secret lives of the pathogenic mycobacteria. Annu Rev Microbiol *57*, 641-676.

Coutinho, I. R., Berk, R. S., and Mammen, E. (1988). Platelet aggregation by a phospholipase C from Pseudomonas aeruginosa. Thromb Res *51*, 495-505.

Cree, I. A., Nurbhai, S., Milne, G., and Beck, J. S. (1987). Cell death in granulomata: the role of apoptosis. J Clin Pathol *40*, 1314-1319.

Crosnier, C., Vargesson, N., Gschmeissner, S., Ariza-McNaughton, L., Morrison, A., and Lewis, J. (2005). Delta-Notch signalling controls commitment to a secretory fate in the zebrafish intestine. Development *132*, 1093-1104.

Cywes, C., Hoppe, H. C., Daffe, M., and Ehlers, M. R. (1997). Nonopsonic binding of Mycobacterium tuberculosis to complement receptor type 3 is mediated by capsular polysaccharides and is strain dependent. Infect Immun *65*, 4258-4266.

D'Argenio, D. A., Gallagher, L. A., Berg, C. A., and Manoil, C. (2001). Drosophila as a model host for Pseudomonas aeruginosa infection. J Bacteriol *183*, 1466-1471.

Da Silva, R. P., Hall, B. F., Joiner, K. A., and Sacks, D. L. (1989). CR1, the C3b receptor, mediates binding of infective Leishmania major metacyclic promastigotes to human macrophages. J Immunol *143*, 617-622.

Dacheux, D., Toussaint, B., Richard, M., Brochier, G., Croize, J., and Attree, I. (2000). Pseudomonas aeruginosa cystic fibrosis isolates induce rapid, type III secretion-dependent, but ExoU-independent, oncosis of macrophages and polymorphonuclear neutrophils. Infect Immun *68*, 2916-2924.

Dai, X. M., Ryan, G. R., Hapel, A. J., Dominguez, M. G., Russell, R. G., Kapp, S., Sylvestre, V., and Stanley, E. R. (2002). Targeted disruption of the mouse colony-stimulating factor 1 receptor gene results in osteopetrosis, mononuclear phagocyte deficiency, increased primitive progenitor cell frequencies, and reproductive defects. Blood *99*, 111-120.

Dakic, A., Shao, Q. X., D'Amico, A., O'Keeffe, M., Chen, W. F., Shortman, K., and Wu, L. (2004). Development of the dendritic cell system during mouse ontogeny. J Immunol *172*, 1018-1027.

Dambly-Chaudiere, C., Cubedo, N., and Ghysen, A. (2007). Control of cell migration in the development of the posterior lateral line: antagonistic interactions between the chemokine receptors CXCR4 and CXCR7/RDC1. BMC Dev Biol *7*, 23.

Danilova, N., Bussmann, J., Jekosch, K., and Steiner, L. A. (2005). The immunoglobulin heavy-chain locus in zebrafish: identification and expression of a previously unknown isotype, immunoglobulin Z. Nat Immunol *6*, 295-302.

Dannenberg, A. M., Jr. (1993). Immunopathogenesis of pulmonary tuberculosis. Hosp Pract *28*, 51-58.

Dannenberg, A. M., Jr. (2003). Macrophage turnover, division and activation within developing, peak and "healed" tuberculous lesions produced in rabbits by BCG. Tuberculosis (Edinb) *83*, 251-260.

Darby, C., Cosma, C. L., Thomas, J. H., and Manoil, C. (1999). Lethal paralysis of Caenorhabditis elegans by Pseudomonas aeruginosa. Proc Natl Acad Sci U S A *96*, 15202-15207.

Darzynkiewicz, Z., Juan, G., Li, X., Gorczyca, W., Murakami, T., and Traganos, F. (1997). Cytometry in cell necrobiology: analysis of apoptosis and accidental cell death (necrosis). Cytometry *27*, 1-20.

Davis, J. M., Clay, H., Lewis, J. L., Ghori, N., Herbomel, P., and Ramakrishnan, L. (2002). Real-time visualization of Mycobacterium-macrophage interactions leading to initiation of granuloma formation in zebrafish embryos. Immunity *17*, 693-702.

DesJardin, L. E., Kaufman, T. M., Potts, B., Kutzbach, B., Yi, H., and Schlesinger, L. S. (2002). Mycobacterium tuberculosis-infected human macrophages exhibit enhanced cellular adhesion with increased expression of LFA-1 and ICAM-1 and reduced expression and/or function of complement receptors, FcgammaRII and the mannose receptor. Microbiology *148*, 3161-3171.

DiGiuseppe Champion, P. A., and Cox, J. S. (2007). Protein secretion systems in Mycobacteria. Cell Microbiol *9*, 1376-1384.

Drennan, M. B., Nicolle, D., Quesniaux, V. J., Jacobs, M., Allie, N., Mpagi, J., Fremond, C., Wagner, H., Kirschning, C., and Ryffel, B. (2004). Toll-like receptor 2-deficient mice succumb to Mycobacterium tuberculosis infection. Am J Pathol *164*, 49-57.

Duan, L., Gan, H., Golan, D. E., and Remold, H. G. (2002). Critical role of mitochondrial damage in determining outcome of macrophage infection with Mycobacterium tuberculosis. J Immunol *169*, 5181-5187.

Egen, J. G., Rothfuchs, A. G., Feng, C. G., Winter, N., Sher, A., and Germain, R. N. (2008). Macrophage and T cell dynamics during the development and disintegration of mycobacterial granulomas. Immunity *28*, 271-284.

Ellis, A. E., and De Sousa, M. (1974). Phylogeny of the lymphoid system. I. A study of the fate of circulating lymphocytes in plaice. Eur J Immunol *4*, 338-343.

Ellis, A. E., Munro, A. L. S., and Roberts, R. J. (1976). Defence mechanisms in fish: fate of intraperitoneally introduced carbon in the plaice *(Pleuronectes platessa)*. Journal of Fish Biology *8*, 67-78.

Epstein, W. L., and Fukuyama, K. (1989). Mechanisms of granulomatous inflammation. Immunol Ser *46*, 687-721.

Ernst, J. D. (1998). Macrophage receptors for Mycobacterium tuberculosis. Infect Immun *66*, 1277-1281.

Ernst, J. D., Trevejo-Nunez, G., and Banaiee, N. (2007). Genomics and the evolution, pathogenesis, and diagnosis of tuberculosis. J Clin Invest *117*, 1738-1745.

Espinal, M. A. (2003). The global situation of MDR-TB. Tuberculosis (Edinb) *83*, 44-51.

Faine, S. (1957a). Virulence in Leptospira. I. Reactions of guinea-pigs to experimental infection with Leptospira icterohaemorrhagiae. Br J Exp Pathol *38*, 1-7.

Faine, S. (1957b). Virulence in leptospira. II. The growth in vivo of virulent Leptospira icterohaemorrhagiae. Br J Exp Pathol *38*, 8-14.

Fauvarque, M. O., Bergeret, E., Chabert, J., Dacheux, D., Satre, M., and Attree, I. (2002). Role and activation of type III secretion system genes in Pseudomonas aeruginosa-induced Drosophila killing. Microb Pathog *32*, 287-295.

Fenton, M. J., and Golenbock, D. T. (1998). LPS-binding proteins and receptors. J Leukoc Biol *64*, 25-32.

Finck-Barbancon, V., Goranson, J., Zhu, L., Sawa, T., Wiener-Kronish, J. P., Fleiszig, S. M., Wu, C., Mende-Mueller, L., and Frank, D. W. (1997). ExoU expression by Pseudomonas aeruginosa correlates with acute cytotoxicity and epithelial injury. Mol Microbiol *25*, 547-557.

Fine, P. E. (1995). Bacille Calmette-Guerin vaccines: a rough guide. Clin Infect Dis *20*, 11-14.

Fink, S. L., and Cookson, B. T. (2005). Apoptosis, pyroptosis, and necrosis: mechanistic description of dead and dying eukaryotic cells. Infect Immun *73*, 1907-1916.

Flesch, I. E., and Kaufmann, S. H. (1990). Activation of tuberculostatic macrophage functions by gamma interferon, interleukin-4, and tumor necrosis factor. Infect Immun *58*, 2675-2677.

Flynn, J. L. (2006). Lessons from experimental Mycobacterium tuberculosis infections. Microbes Infect *8*, 1179-1188.

Flynn, J. L., and Chan, J. (2001a). Immunology of tuberculosis. Annu Rev Immunol *19*, 93-129.

Flynn, J. L., and Chan, J. (2001b). Tuberculosis: latency and reactivation. Infect Immun *69*, 4195-4201.

Flynn, J. L., and Chan, J. (2003). Immune evasion by Mycobacterium tuberculosis: living with the enemy. Curr Opin Immunol *15*, 450-455.

Flynn, J. L., Cooper, A. M., and Bishai, W. (2005). Animal Models of Tuberculosis. In Tuberculosis and the Tubercle Bacillus, S. T. Cole, K. D. Eisenach, D. N. McMurray, and W. R. Jacobs, Jr., eds. (Washington, D.C., ASM Press).

Flynn, J. L., Goldstein, M. M., Chan, J., Triebold, K. J., Pfeffer, K., Lowenstein, C. J., Schreiber, R., Mak, T. W., and Bloom, B. R. (1995). Tumor necrosis factor-alpha is required in the protective immune response against Mycobacterium tuberculosis in mice. Immunity *2*, 561-572.

Frank, D. W., Nair, G., and Schweizer, H. P. (1994). Construction and characterization of chromosomal insertional mutations of the Pseudomonas aeruginosa exoenzyme S trans-regulatory locus. Infect Immun *62*, 554-563.

Fratazzi, C., Arbeit, R. D., Carini, C., Balcewicz-Sablinska, M. K., Keane, J., Kornfeld, H., and Remold, H. G. (1999). Macrophage apoptosis in mycobacterial infections. J Leukoc Biol *66*, 763-764.

Fratazzi, C., Arbeit, R. D., Carini, C., and Remold, H. G. (1997). Programmed cell death of Mycobacterium avium serovar 4-infected human macrophages prevents the mycobacteria from spreading and induces mycobacterial growth inhibition by freshly added, uninfected macrophages. J Immunol *158*, 4320-4327.

Fremond, C. M., Yeremeev, V., Nicolle, D. M., Jacobs, M., Quesniaux, V. F., and Ryffel, B. (2004). Fatal Mycobacterium tuberculosis infection despite adaptive immune response in the absence of MyD88. J Clin Invest *114*, 1790-1799.

Gan, H., Lee, J., Ren, F., Chen, M., Kornfeld, H., and Remold, H. G. (2008). Mycobacterium tuberculosis blocks crosslinking of annexin-1 and apoptotic envelope formation on infected macrophages to maintain virulence. Nat Immunol *9*, 1189-1197.

Gao, L. Y., Guo, S., McLaughlin, B., Morisaki, H., Engel, J. N., and Brown, E. J. (2004). A mycobacterial virulence gene cluster extending RD1 is required for cytolysis, bacterial spreading and ESAT-6 secretion. Mol Microbiol *53*, 1677-1693.

Garrity-Ryan, L., Kazmierczak, B., Kowal, R., Comolli, J., Hauser, A., and Engel, J. N. (2000). The arginine finger domain of ExoT contributes to actin cytoskeleton disruption and inhibition of internalization of Pseudomonas aeruginosa by epithelial cells and macrophages. Infect Immun *68*, 7100-7113.

Gearing, A. J., Beckett, P., Christodoulou, M., Churchill, M., Clements, J., Davidson, A. H., Drummond, A. H., Galloway, W. A., Gilbert, R., Gordon, J. L., and et al. (1994). Processing of tumour necrosis factor-alpha precursor by metalloproteinases. Nature *370*, 555-557.

Glickman, M. S., and Jacobs, W. R., Jr. (2001). Microbial pathogenesis of Mycobacterium tuberculosis: dawn of a discipline. Cell *104*, 477-485.

Goehring, U. M., Schmidt, G., Pederson, K. J., Aktories, K., and Barbieri, J. T. (1999). The N-terminal domain of Pseudomonas aeruginosa exoenzyme S is a GTPase-activating protein for Rho GTPases. J Biol Chem *274*, 36369-36372.

Golling, G., Amsterdam, A., Sun, Z., Antonelli, M., Maldonado, E., Chen, W., Burgess, S., Haldi, M., Artzt, K., Farrington, S*., et al.* (2002). Insertional mutagenesis in zebrafish rapidly identifies genes essential for early vertebrate development. Nat Genet *31*, 135-140.

Griffin, J. P., and Orme, I. M. (1994). Evolution of CD4 T-cell subsets following infection of naive and memory immune mice with Mycobacterium tuberculosis. Infect Immun *62*, 1683-1690.

Guiney, D. G. (2005). The role of host cell death in Salmonella infections. Curr Top Microbiol Immunol *289*, 131-150.

Guinn, K. M., Hickey, M. J., Mathur, S. K., Zakel, K. L., Grotzke, J. E., Lewinsohn, D. M., Smith, S., and Sherman, D. R. (2004). Individual RD1-region genes are required for export of ESAT-6/CFP-10 and for virulence of Mycobacterium tuberculosis. Mol Microbiol *51*, 359-370.

Gupta, A. K., Shashi, S., Mohan, M., Lamba, I. M., and Gupta, R. (1993). Epidemiology of Pseudomonas aeruginosa infections in a neonatal intensive care unit. J Trop Pediatr *39*, 32-36.

Haake, D. A. (2006). Hamster model of leptospirosis. Curr Protoc Microbiol *Chapter 12*, Unit 12E 12.

Hall, C., Flores, M. V., Storm, T., Crosier, K., and Crosier, P. (2007). The zebrafish lysozyme C promoter drives myeloid-specific expression in transgenic fish. BMC Dev Biol *7*, 42.

Hamm, E. E., Voth, D. E., and Ballard, J. D. (2006). Identification of Clostridium difficile toxin B cardiotoxicity using a zebrafish embryo model of intoxication. Proc Natl Acad Sci U S A *103*, 14176-14181.

Hammerschmidt, M., and McMahon, A. P. (1998). The effect of pertussis toxin on zebrafish development: a possible role for inhibitory G-proteins in hedgehog signaling. Dev Biol *194*, 166-171.

Hanington, P. C., Barreda, D. R., and Belosevic, M. (2006). A novel hematopoietic granulin induces proliferation of goldfish (Carassius auratus L.) macrophages. J Biol Chem *281*, 9963-9970.

Harding, G. E., and Smith, D. W. (1977). Host-parasite relationships in experimental airborne tuberculosis. VI. Influence of vaccination with Bacille Calmette-Guerin on the onset and/or extent of hematogenous dissemination of virulent Mycobacterium tuberculosis to the lungs. J Infect Dis *136*, 439-443.

Hart, P. D., Armstrong, J. A., Brown, C. A., and Draper, P. (1972). Ultrastructural study of the behavior of macrophages toward parasitic mycobacteria. Infect Immun *5*, 803-807.

Haugarvoll, E., Thorsen, J., Laane, M., Huang, Q., and Koppang, E. O. (2006). Melanogenesis and evidence for melanosome transport to the plasma membrane in a CD83 teleost leukocyte cell line. Pigment Cell Res *19*, 214-225.

Hauser, A. R., Cobb, E., Bodi, M., Mariscal, D., Valles, J., Engel, J. N., and Rello, J. (2002). Type III protein secretion is associated with poor clinical outcomes in patients with ventilator-associated pneumonia caused by Pseudomonas aeruginosa. Crit Care Med *30*, 521-528.

Herbomel, P., Thisse, B., and Thisse, C. (1999). Ontogeny and behaviour of early macrophages in the zebrafish embryo. Development *126*, 3735-3745.

Herbomel, P., Thisse, B., and Thisse, C. (2001). Zebrafish early macrophages colonize cephalic mesenchyme and developing brain, retina, and epidermis through a M-CSF receptor-dependent invasive process. Dev Biol *238*, 274-288.

Hernandez-Pando, R., Jeyanathan, M., Mengistu, G., Aguilar, D., Orozco, H., Harboe, M., Rook, G. A., and Bjune, G. (2000). Persistence of DNA from Mycobacterium tuberculosis in superficially normal lung tissue during latent infection. Lancet *356*, 2133-2138.

Herraez, M. P., and Zapata, A. G. (1991). Structural characterization of the melano-macrophage centres (MMC) of goldfish Carassius auratus. Eur J Morphol *29*, 89-102.

Honer zu Bentrup, K., and Russell, D. G. (2001). Mycobacterial persistence: adaptation to a changing environment. Trends Microbiol *9*, 597-605.

Hsu, K., Traver, D., Kutok, J. L., Hagen, A., Liu, T. X., Paw, B. H., Rhodes, J., Berman, J. N., Zon, L. I., Kanki, J. P., and Look, A. T. (2004). The pu.1 promoter drives myeloid gene expression in zebrafish. Blood *104*, 1291-1297.

Hsu, T., Hingley-Wilson, S. M., Chen, B., Chen, M., Dai, A. Z., Morin, P. M., Marks, C. B., Padiyar, J., Goulding, C., Gingery, M.*, et al.* (2003). The primary mechanism of attenuation of bacillus Calmette-Guerin is a loss of secreted lytic function required for invasion of lung interstitial tissue. Proc Natl Acad Sci U S A *100*, 12420-12425.

Humphreys, I. R., Stewart, G. R., Turner, D. J., Patel, J., Karamanou, D., Snelgrove, R. J., and Young, D. B. (2006). A role for dendritic cells in the dissemination of mycobacterial infection. Microbes Infect *8*, 1339-1346.

Hung, D. T., Shakhnovich, E. A., Pierson, E., and Mekalanos, J. J. (2005). Small-molecule inhibitor of Vibrio cholerae virulence and intestinal colonization. Science *310*, 670-674.

Ichikawa, J. K., English, S. B., Wolfgang, M. C., Jackson, R., Butte, A. J., and Lory, S. (2005). Genome-wide analysis of host responses to the Pseudomonas aeruginosa type III secretion system yields synergistic effects. Cell Microbiol *7*, 1635-1646.

Igawa, D., Sakai, M., and Savan, R. (2006). An unexpected discovery of two interferon gamma-like genes along with interleukin (IL)-22 and -26 from teleost: IL-22 and -26 genes have been described for the first time outside mammals. Mol Immunol *43*, 999-1009.

Imhof, B. A., and Aurrand-Lions, M. (2004). Adhesion mechanisms regulating the migration of monocytes. Nat Rev Immunol *4*, 432-444.

Isogai, E., Kitagawa, H., Isogai, H., Kurebayashi, Y., and Ito, N. (1986). Phagocytosis as a defense mechanism against infection with leptospiras. Zentralbl Bakteriol Mikrobiol Hyg [A] *261*, 65-74.

Isogai, S., Horiguchi, M., and Weinstein, B. M. (2001). The vascular anatomy of the developing zebrafish: an atlas of embryonic and early larval development. Dev Biol *230*, 278-301.

Ito, A., Mukaiyama, A., Itoh, Y., Nagase, H., Thogersen, I. B., Enghild, J. J., Sasaguri, Y., and Mori, Y. (1996). Degradation of interleukin 1beta by matrix metalloproteinases. J Biol Chem *271*, 14657-14660.

Izzo, A. A., Izzo, L. S., Kasimos, J., and Majka, S. (2004). A matrix metalloproteinase inhibitor promotes granuloma formation during the early

phase of Mycobacterium tuberculosis pulmonary infection. Tuberculosis (Edinb) *84*, 387-396.

Jang, S., Uematsu, S., Akira, S., and Salgame, P. (2004). IL-6 and IL-10 induction from dendritic cells in response to Mycobacterium tuberculosis is predominantly dependent on TLR2-mediated recognition. J Immunol *173*, 3392-3397.

Jault, C., Pichon, L., and Chluba, J. (2004). Toll-like receptor gene family and TIR-domain adapters in Danio rerio. Mol Immunol *40*, 759-771.

Johnson, R. C., and Harris, V. G. (1967). Differentiation of pathogenic and saprophytic letospires. I. Growth at low temperatures. J Bacteriol *94*, 27-31.

Jozefowicz, C., McClintock, J., and Prince, V. (2003). The fates of zebrafish Hox gene duplicates. J Struct Funct Genomics *3*, 185-194.

Kahnert, A., Hopken, U. E., Stein, M., Bandermann, S., Lipp, M., and Kaufmann, S. H. (2007). Mycobacterium tuberculosis triggers formation of lymphoid structure in murine lungs. J Infect Dis *195*, 46-54.

Kamei, M., Isogai, S., and Weinstein, B. M. (2004). Imaging blood vessels in the zebrafish. Methods Cell Biol *76*, 51-74.

Kamei, M., and Weinstein, B. M. (2005). Long-term time-lapse fluorescence imaging of developing zebrafish. Zebrafish *2*, 113-123.

Kaufmann, S. H., and Ladel, C. H. (1994). Role of T cell subsets in immunity against intracellular bacteria: experimental infections of knock-out mice with Listeria monocytogenes and Mycobacterium bovis BCG. Immunobiology *191*, 509-519.

Keane, J., Balcewicz-Sablinska, M. K., Remold, H. G., Chupp, G. L., Meek, B. B., Fenton, M. J., and Kornfeld, H. (1997). Infection by Mycobacterium tuberculosis promotes human alveolar macrophage apoptosis. Infect Immun *65*, 298-304.

Keane, J., Shurtleff, B., and Kornfeld, H. (2002). TNF-dependent BALB/c murine macrophage apoptosis following Mycobacterium tuberculosis infection inhibits bacillary growth in an IFN-gamma independent manner. Tuberculosis (Edinb) *82*, 55-61.

Keller, C., Lauber, J., Blumenthal, A., Buer, J., and Ehlers, S. (2004). Resistance and susceptibility to tuberculosis analysed at the transcriptome level: lessons from mouse macrophages. Tuberculosis (Edinb) *84*, 144-158.

Kemenade, B., Groeneveld, A., Rens, B., and Rombout, J. (1994). Characterization Of Macrophages And Neutrophilic Granulocytes From The Pronephros Of Carp (Cyprinus Carpio). J Exp Biol *187*, 143-158.

Kerr, J. R. (1999). Cell adhesion molecules in the pathogenesis of and host defence against microbial infection. Mol Pathol *52*, 220-230.

Kimmel, C. B., Ballard, W. W., Kimmel, S. R., Ullmann, B., and Schilling, T. F. (1995). Stages of embryonic development of the zebrafish. Dev Dyn *203*, 253-310.

Knaut, H., Werz, C., Geisler, R., and Nusslein-Volhard, C. (2003). A zebrafish homologue of the chemokine receptor Cxcr4 is a germ-cell guidance receptor. Nature *421*, 279-282.

Knowles, M. R., and Boucher, R. C. (2002). Mucus clearance as a primary innate defense mechanism for mammalian airways. J Clin Invest *109*, 571-577.

Ko, A. I., Galvao Reis, M., Ribeiro Dourado, C. M., Johnson, W. D., Jr., and Riley, L. W. (1999). Urban epidemic of severe leptospirosis in Brazil. Salvador Leptospirosis Study Group. Lancet *354*, 820-825.

Koo, I. C., Wang, C., Raghavan, S., Morisaki, J. H., Cox, J. S., and Brown, E. J. (2008). ESX-1-dependent cytolysis in lysosome secretion and inflammasome activation during mycobacterial infection. Cell Microbiol.

Kornfeld, H., Mancino, G., and Colizzi, V. (1999). The role of macrophage cell death in tuberculosis. Cell Death Differ *6*, 71-78.

Krutzik, S. R., and Modlin, R. L. (2004). The role of Toll-like receptors in combating mycobacteria. Semin Immunol *16*, 35-41.

Krutzik, S. R., Sieling, P. A., and Modlin, R. L. (2001). The role of Toll-like receptors in host defense against microbial infection. Curr Opin Immunol *13*, 104-108.

Kuchler, A. M., Gjini, E., Peterson-Maduro, J., Cancilla, B., Wolburg, H., and Schulte-Merker, S. (2006). Development of the zebrafish lymphatic system requires VEGFC signaling. Curr Biol *16*, 1244-1248.

Lammas, D. A., Stober, C., Harvey, C. J., Kendrick, N., Panchalingam, S., and Kumararatne, D. S. (1997). ATP-induced killing of mycobacteria by human macrophages is mediated by purinergic P2Z(P2X7) receptors. Immunity *7*, 433-444.

Langenau, D. M., Ferrando, A. A., Traver, D., Kutok, J. L., Hezel, J. P., Kanki, J. P., Zon, L. I., Look, A. T., and Trede, N. S. (2004). In vivo tracking of T cell development, ablation, and engraftment in transgenic zebrafish. Proc Natl Acad Sci U S A *101*, 7369-7374.

Langenau, D. M., Traver, D., Ferrando, A. A., Kutok, J. L., Aster, J. C., Kanki, J. P., Lin, S., Prochownik, E., Trede, N. S., Zon, L. I., and Look, A. T. (2003). Myc-induced T cell leukemia in transgenic zebrafish. Science *299*, 887-890.

Laskowski, M. A., Osborn, E., and Kazmierczak, B. I. (2004). A novel sensor kinase-response regulator hybrid regulates type III secretion and is required for virulence in Pseudomonas aeruginosa. Mol Microbiol *54*, 1090-1103.

Lawson, N. D., and Weinstein, B. M. (2002). In vivo imaging of embryonic vascular development using transgenic zebrafish. Dev Biol *248*, 307-318.

Lazarevic, V., Nolt, D., and Flynn, J. L. (2005). Long-term control of Mycobacterium tuberculosis infection is mediated by dynamic immune responses. J Immunol *175*, 1107-1117.

Le Guyader, D., Redd, M. J., Colucci-Guyon, E., Murayama, E., Kissa, K., Briolat, V., Mordelet, E., Zapata, A., Shinomiya, H., and Herbomel, P. (2008). Origins and unconventional behavior of neutrophils in developing zebrafish. Blood *111*, 132-141.

Lee, V. T., Smith, R. S., Tummler, B., and Lory, S. (2005). Activities of Pseudomonas aeruginosa effectors secreted by the Type III secretion system in vitro and during infection. Infect Immun *73*, 1695-1705.

Leemans, J. C., Florquin, S., Heikens, M., Pals, S. T., van der Neut, R., and Van Der Poll, T. (2003). CD44 is a macrophage binding site for Mycobacterium tuberculosis that mediates macrophage recruitment and protective immunity against tuberculosis. J Clin Invest *111*, 681-689.

Leemans, J. C., Juffermans, N. P., Florquin, S., van Rooijen, N., Vervoordeldonk, M. J., Verbon, A., van Deventer, S. J., and van der Poll, T. (2001). Depletion of alveolar macrophages exerts protective effects in pulmonary tuberculosis in mice. J Immunol *166*, 4604-4611.

Leemans, J. C., Thepen, T., Weijer, S., Florquin, S., van Rooijen, N., van de Winkel, J. G., and van der Poll, T. (2005). Macrophages play a dual role during pulmonary tuberculosis in mice. J Infect Dis *191*, 65-74.

Lesley, R., and Ramakrishnan, L. (2008). Insights into early mycobacterial pathogenesis from the zebrafish. Curr Opin Microbiol *11*, 277-283.

Levett, P. N. (2001). Leptospirosis. Clin Microbiol Rev *14*, 296-326.

Lewis, K. N., Liao, R., Guinn, K. M., Hickey, M. J., Smith, S., Behr, M. A., and Sherman, D. R. (2003). Deletion of RD1 from Mycobacterium tuberculosis mimics bacille Calmette-Guerin attenuation. J Infect Dis *187*, 117-123.

Li, J., Barreda, D. R., Zhang, Y. A., Boshra, H., Gelman, A. E., Lapatra, S., Tort, L., and Sunyer, J. O. (2006). B lymphocytes from early vertebrates have potent phagocytic and microbicidal abilities. Nat Immunol *7*, 1116-1124.

Li, Q., Park, P. W., Wilson, C. L., and Parks, W. C. (2002). Matrilysin shedding of syndecan-1 regulates chemokine mobilization and transepithelial efflux of neutrophils in acute lung injury. Cell *111*, 635-646.

Lin, B., Chen, S., Cao, Z., Lin, Y., Mo, D., Zhang, H., Gu, J., Dong, M., Liu, Z., and Xu, A. (2007). Acute phase response in zebrafish upon Aeromonas salmonicida and Staphylococcus aureus infection: striking similarities and obvious differences with mammals. Mol Immunol *44*, 295-301.

Linehan, S. A., and Holden, D. W. (2003). The interplay between Salmonella typhimurium and its macrophage host--what can it teach us about innate immunity? Immunol Lett *85*, 183-192.

Lowe, B. A., Miller, J. D., and Neely, M. N. (2007). Analysis of the polysaccharide capsule of the systemic pathogen Streptococcus iniae and its implications in virulence. Infect Immun *75*, 1255-1264.

Lowery, L. A., and Sive, H. (2005). Initial formation of zebrafish brain ventricles occurs independently of circulation and requires the nagie oko and snakehead/atp1a1a.1 gene products. Development *132*, 2057-2067.

Lurie, M. B., Abramson, S., and Heppleston, A. G. (1952). On the response of genetically resistant and susceptible rabbits to the quantitative inhalation of human type tubercle bacilli and the nature of resistance to tuberculosis. J Exp Med *95*, 119-134.

Lyczak, J. B., Cannon, C. L., and Pier, G. B. (2000). Establishment of Pseudomonas aeruginosa infection: lessons from a versatile opportunist. Microbes Infect *2*, 1051-1060.

Mackaness, G. B. (1969). The influence of immunologically committed lymphoid cells on macrophage activity in vivo. J Exp Med *129*, 973-992.

Mahairas, G. G., Sabo, P. J., Hickey, M. J., Singh, D. C., and Stover, C. K. (1996). Molecular analysis of genetic differences between Mycobacterium bovis BCG and virulent M. bovis. J Bacteriol *178*, 1274-1282.

Mahajan-Miklos, S., Tan, M. W., Rahme, L. G., and Ausubel, F. M. (1999). Molecular mechanisms of bacterial virulence elucidated using a Pseudomonas aeruginosa-Caenorhabditis elegans pathogenesis model. Cell *96*, 47-56.

Marshall, R. B. (1976). The route of entry of leptospires into the kidney tubule. J Med Microbiol *9*, 149-152.

Mathias, J. R., Dodd, M. E., Walters, K. B., Rhodes, J., Kanki, J. P., Look, A. T., and Huttenlocher, A. (2007). Live imaging of chronic inflammation caused by mutation of zebrafish Hai1. J Cell Sci *120*, 3372-3383.

Mathias, J. R., Perrin, B. J., Liu, T. X., Kanki, J., Look, A. T., and Huttenlocher, A. (2006). Resolution of inflammation by retrograde chemotaxis of neutrophils in transgenic zebrafish. J Leukoc Biol *80*, 1281-1288.

Matsui, H., Verghese, M. W., Kesimer, M., Schwab, U. E., Randell, S. H., Sheehan, J. K., Grubb, B. R., and Boucher, R. C. (2005). Reduced three-dimensional motility in dehydrated airway mucus prevents neutrophil capture and killing bacteria on airway epithelial surfaces. J Immunol *175*, 1090-1099.

McBride, A. J., Athanazio, D. A., Reis, M. G., and Ko, A. I. (2005). Leptospirosis. Curr Opin Infect Dis *18*, 376-386.

McClellan, S. A., Huang, X., Barrett, R. P., van Rooijen, N., and Hazlett, L. D. (2003). Macrophages restrict Pseudomonas aeruginosa growth, regulate polymorphonuclear neutrophil influx, and balance pro- and anti-inflammatory cytokines in BALB/c mice. J Immunol *170*, 5219-5227.

McDonough, K. A., Kress, Y., and Bloom, B. R. (1993). Pathogenesis of tuberculosis: interaction of Mycobacterium tuberculosis with macrophages. Infect Immun *61*, 2763-2773.

McGrath, H., Adler, B., Vinh, T., and Faine, S. (1984). Phagocytosis of virulent and avirulent leptospires by guinea-pig and human polymorphonuclear leukocytes in vitro. Pathology *16*, 243-249.

McMurray, D. N. (2003). Hematogenous reseeding of the lung in low-dose, aerosol-infected guinea pigs: unique features of the host-pathogen interface in secondary tubercles. Tuberculosis (Edinb) *83*, 131-134.

McQuibban, G. A., Gong, J. H., Wong, J. P., Wallace, J. L., Clark-Lewis, I., and Overall, C. M. (2002). Matrix metalloproteinase processing of monocyte chemoattractant proteins generates CC chemokine receptor antagonists with anti-inflammatory properties in vivo. Blood *100*, 1160-1167.

McShane, H. (2004). Developing an improved vaccine against tuberculosis. Expert Rev Vaccines *3*, 299-306.

Meijer, A. H., Gabby Krens, S. F., Medina Rodriguez, I. A., He, S., Bitter, W., Ewa Snaar-Jagalska, B., and Spaink, H. P. (2004). Expression analysis of the Toll-like receptor and TIR domain adaptor families of zebrafish. Mol Immunol *40*, 773-783.

Meijer, A. H., van der Sar, A. M., Cunha, C., Lamers, G. E., Laplante, M. A., Kikuta, H., Bitter, W., Becker, T. S., and Spaink, H. P. (2007). Identification and real-time imaging of a myc-expressing neutrophil population involved in inflammation and mycobacterial granuloma formation in zebrafish. Dev Comp Immunol.

Merien, F., Baranton, G., and Perolat, P. (1997). Invasion of Vero cells and induction of apoptosis in macrophages by pathogenic Leptospira interrogans are correlated with virulence. Infect Immun *65*, 729-738.

Merien, F., Truccolo, J., Rougier, Y., Baranton, G., and Perolat, P. (1998). In vivo apoptosis of hepatocytes in guinea pigs infected with Leptospira interrogans serovar icterohaemorrhagiae. FEMS Microbiol Lett *169*, 95-102.

Miller, E. A., and Ernst, J. D. (2008). Illuminating the Black Box of TNF Action in Tuberculous Granulomas. Immunity *29*, 175-177.

Miller, J. D., and Neely, M. N. (2004). Zebrafish as a model host for streptococcal pathogenesis. Acta Trop *91*, 53-68.

Miller, J. D., and Neely, M. N. (2005). Large-scale screen highlights the importance of capsule for virulence in the zoonotic pathogen Streptococcus iniae. Infect Immun *73*, 921-934.

Miller, N. G., Allen, J. E., and Wilson, R. B. (1974). The pathogenesis of hemorrhage in the lung of the hamster during acute leptospirosis. Med Microbiol Immunol *160*, 269-278.

Miyasaka, N., Knaut, H., and Yoshihara, Y. (2007). Cxcl12/Cxcr4 chemokine signaling is required for placode assembly and sensory axon pathfinding in the zebrafish olfactory system. Development *134*, 2459-2468.

Miyata, S., Casey, M., Frank, D. W., Ausubel, F. M., and Drenkard, E. (2003). Use of the Galleria mellonella caterpillar as a model host to study the role of the type III secretion system in Pseudomonas aeruginosa pathogenesis. Infect Immun *71*, 2404-2413.

Mohan, V. P., Scanga, C. A., Yu, K., Scott, H. M., Tanaka, K. E., Tsang, E., Tsai, M. M., Flynn, J. L., and Chan, J. (2001). Effects of tumor necrosis factor alpha on host immune response in chronic persistent tuberculosis: possible role for limiting pathology. Infect Immun *69*, 1847-1855.

Molloy, A., Laochumroonvorapong, P., and Kaplan, G. (1994). Apoptosis, but not necrosis, of infected monocytes is coupled with killing of intracellular bacillus Calmette-Guerin. J Exp Med *180*, 1499-1509.

Montanez, G. E., Neely, M. N., and Eichenbaum, Z. (2005). The streptococcal iron uptake (Siu) transporter is required for iron uptake and virulence in a zebrafish infection model. Microbiology *151*, 3749-3757.

Moreira, A. L., Tsenova-Berkova, L., Wang, J., Laochumroonvorapong, P., Freeman, S., Freedman, V. H., and Kaplan, G. (1997). Effect of cytokine modulation by thalidomide on the granulomatous response in murine tuberculosis. Tuber Lung Dis *78*, 47-55.

Mueller-Ortiz, S. L., Wanger, A. R., and Norris, S. J. (2001). Mycobacterial protein HbhA binds human complement component C3. Infect Immun *69*, 7501-7511.

Murayama, E., Kissa, K., Zapata, A., Mordelet, E., Briolat, V., Lin, H. F., Handin, R. I., and Herbomel, P. (2006). Tracing hematopoietic precursor migration to successive hematopoietic organs during zebrafish development. Immunity *25*, 963-975.

Musa, S. A., Kim, Y., Hashim, R., Wang, G. Z., Dimmer, C., and Smith, D. W. (1987). Response of inbred mice to aerosol challenge with Mycobacterium tuberculosis. Infect Immun *55*, 1862-1866.

Myrvik, Q. N., Leake, E. S., and Wright, M. J. (1984). Disruption of phagosomal membranes of normal alveolar macrophages by the H37Rv strain of Mycobacterium tuberculosis. A correlate of virulence. Am Rev Respir Dis *129*, 322-328.

Nasevicius, A., and Ekker, S. C. (2000). Effective targeted gene 'knockdown' in zebrafish. Nat Genet *26*, 216-220.

Nayak, A. S., Lage, C. R., and Kim, C. H. (2007). Effects of low concentrations of arsenic on the innate immune system of the zebrafish (danio rerio). Toxicol Sci *98*, 118-124.

Neely, M. N., Pfeifer, J. D., and Caparon, M. (2002). Streptococcus-zebrafish model of bacterial pathogenesis. Infect Immun *70*, 3904-3914.

Neuenhahn, M., Kerksiek, K. M., Nauerth, M., Suhre, M. H., Schiemann, M., Gebhardt, F. E., Stemberger, C., Panthel, K., Schroder, S., Chakraborty, T.*, et al.* (2006). CD8alpha+ dendritic cells are required for efficient entry of Listeria monocytogenes into the spleen. Immunity *25*, 619-630.

Neumann, N. F., Barreda, D. R., and Belosevic, M. (2000). Generation and functional analysis of distinct macrophage sub-populations from goldfish (Carassius auratus L.) kidney leukocyte cultures. Fish Shellfish Immunol *10*, 1-20.

Neumann, N. F., Stafford, J. L., Barreda, D., Ainsworth, A. J., and Belosevic, M. (2001). Antimicrobial mechanisms of fish phagocytes and their role in host defense. Dev Comp Immunol *25*, 807-825.

Nigou, J., Zelle-Rieser, C., Gilleron, M., Thurnher, M., and Puzo, G. (2001). Mannosylated lipoarabinomannans inhibit IL-12 production by human dendritic cells: evidence for a negative signal delivered through the mannose receptor. J Immunol *166*, 7477-7485.

Nivens, D. E., Ohman, D. E., Williams, J., and Franklin, M. J. (2001). Role of alginate and its O acetylation in formation of Pseudomonas aeruginosa microcolonies and biofilms. J Bacteriol *183*, 1047-1057.

North, R. J., and Jung, Y. J. (2004). Immunity to tuberculosis. Annu Rev Immunol *22*, 599-623.

Novoa, B., Romero, A., Mulero, V., Rodriguez, I., Fernandez, I., and Figueras, A. (2006). Zebrafish (Danio rerio) as a model for the study of vaccination against viral haemorrhagic septicemia virus (VHSV). Vaccine *24*, 5806-5816.

Oddo, M., Renno, T., Attinger, A., Bakker, T., MacDonald, H. R., and Meylan, P. R. (1998). Fas ligand-induced apoptosis of infected human macrophages reduces the viability of intracellular Mycobacterium tuberculosis. J Immunol *160*, 5448-5454.

Ogura, Y., Saab, L., Chen, F. F., Benito, A., Inohara, N., and Nunez, G. (2003). Genetic variation and activity of mouse Nod2, a susceptibility gene for Crohn's disease. Genomics *81*, 369-377.

Ohta, Y., Landis, E., Boulay, T., Phillips, R. B., Collet, B., Secombes, C. J., Flajnik, M. F., and Hansen, J. D. (2004). Homologs of CD83 from elasmobranch and teleost fish. J Immunol *173*, 4553-4560.

Okada, T., Miller, M. J., Parker, I., Krummel, M. F., Neighbors, M., Hartley, S. B., O'Garra, A., Cahalan, M. D., and Cyster, J. G. (2005). Antigen-engaged B cells undergo chemotaxis toward the T zone and form motile conjugates with helper T cells. PLoS Biol *3*, e150.

Orme, I. M., and Collins, F. M. (1994). Mouse Model of Tuberculosis. In Tuberculosis: Pathogenesis, Protection, and Control, B. R. Bloom, ed. (Washington, DC, American Society for Microbiology), pp. 113-134.

Orme, I. M., and Cooper, A. M. (1999). Cytokine/chemokine cascades in immunity to tuberculosis. Immunol Today *20*, 307-312.

Palic, D., Andreasen, C. B., Ostojic, J., Tell, R. M., and Roth, J. A. (2007a). Zebrafish (Danio rerio) whole kidney assays to measure neutrophil extracellular trap release and degranulation of primary granules. J Immunol Methods *319*, 87-97.

Palic, D., Ostojic, J., Andreasen, C. B., and Roth, J. A. (2007b). Fish cast NETs: neutrophil extracellular traps are released from fish neutrophils. Dev Comp Immunol *31*, 805-816.

Palmer, M. F., Waitkins, S. A., Fitzgeorge, R. B., and Baskerville, A. (1987). Experimental infection of monkeys with Leptospira interrogans serovar hardjo. Epidemiol Infect *98*, 191-197.

Pan, H., Yan, B. S., Rojas, M., Shebzukhov, Y. V., Zhou, H., Kobzik, L., Higgins, D. E., Daly, M. J., Bloom, B. R., and Kramnik, I. (2005). Ipr1 gene mediates innate immunity to tuberculosis. Nature *434*, 767-772.

Parichy, D. M., and Turner, J. M. (2003). Temporal and cellular requirements for Fms signaling during zebrafish adult pigment pattern development. Development *130*, 817-833.

Parks, W. C., Wilson, C. L., and Lopez-Boado, Y. S. (2004). Matrix metalloproteinases as modulators of inflammation and innate immunity. Nat Rev Immunol *4*, 617-629.

Pathak, S. K., Basu, S., Basu, K. K., Banerjee, A., Pathak, S., Bhattacharyya, A., Kaisho, T., Kundu, M., and Basu, J. (2007). Direct extracellular interaction between the early secreted antigen ESAT-6 of Mycobacterium tuberculosis and TLR2 inhibits TLR signaling in macrophages. Nat Immunol *8*, 610-618.

Patton, E. E., and Zon, L. I. (2001). The art and design of genetic screens: zebrafish. Nat Rev Genet *2*, 956-966.

Peatman, E., Bao, B., Baoprasertkul, P., and Liu, Z. (2005). In silico identification and expression analysis of 12 novel CC chemokines in catfish. Immunogenetics *57*, 409-419.

Peatman, E., Bao, B., Peng, X., Baoprasertkul, P., Brady, Y., and Liu, Z. (2006). Catfish CC chemokines: genomic clustering, duplications, and expression after bacterial infection with Edwardsiella ictaluri. Mol Genet Genomics *275*, 297-309.

Peatman, E., and Liu, Z. (2006). CC chemokines in zebrafish: evidence for extensive intrachromosomal gene duplications. Genomics *88*, 381-385.

Pederson, K. J., Krall, R., Riese, M. J., and Barbieri, J. T. (2002). Intracellular localization modulates targeting of ExoS, a type III cytotoxin, to eukaryotic signalling proteins. Mol Microbiol *46*, 1381-1390.

Peri, F., and Nusslein-Volhard, C. (2008). Live imaging of neuronal degradation by microglia reveals a role for v0-ATPase a1 in phagosomal fusion in vivo. Cell *133*, 916-927.

Peters, W., and Ernst, J. D. (2003). Mechanisms of cell recruitment in the immune response to Mycobacterium tuberculosis. Microbes Infect *5*, 151-158.

Peters, W., Scott, H. M., Chambers, H. F., Flynn, J. L., Charo, I. F., and Ernst, J. D. (2001). Chemokine receptor 2 serves an early and essential role in resistance to Mycobacterium tuberculosis. Proc Natl Acad Sci U S A *98*, 7958-7963.

Peterson, R. T., Link, B. A., Dowling, J. E., and Schreiber, S. L. (2000). Small molecule developmental screens reveal the logic and timing of vertebrate development. Proc Natl Acad Sci U S A *97*, 12965-12969.

Peterson, R. T., Shaw, S. Y., Peterson, T. A., Milan, D. J., Zhong, T. P., Schreiber, S. L., MacRae, C. A., and Fishman, M. C. (2004). Chemical suppression of a genetic mutation in a zebrafish model of aortic coarctation. Nat Biotechnol *22*, 595-599.

Phelan, P. E., Mellon, M. T., and Kim, C. H. (2005a). Functional characterization of full-length TLR3, IRAK-4, and TRAF6 in zebrafish (Danio rerio). Mol Immunol *42*, 1057-1071.

Phelan, P. E., Pressley, M. E., Witten, P. E., Mellon, M. T., Blake, S., and Kim, C. H. (2005b). Characterization of snakehead rhabdovirus infection in zebrafish (Danio rerio). J Virol *79*, 1842-1852.

Phelps, H. A., and Neely, M. N. (2007). SalY of Streptococcus pyogenes lantibiotic locus is required for full virulence and intracellular survival in macrophages. Infect Immun.

Picard, C., Puel, A., Bonnet, M., Ku, C. L., Bustamante, J., Yang, K., Soudais, C., Dupuis, S., Feinberg, J., Fieschi, C.*, et al.* (2003). Pyogenic bacterial infections in humans with IRAK-4 deficiency. Science *299*, 2076-2079.

Ponta, H., Sherman, L., and Herrlich, P. A. (2003). CD44: from adhesion molecules to signalling regulators. Nat Rev Mol Cell Biol *4*, 33-45.

Post, F. A., Manca, C., Neyrolles, O., Ryffel, B., Young, D. B., and Kaplan, G. (2001). Mycobacterium tuberculosis 19-kilodalton lipoprotein inhibits Mycobacterium smegmatis-induced cytokine production by human macrophages in vitro. Infect Immun *69*, 1433-1439.

Pozos, T. C., and Ramakrishnan, L. (2004). New models for the study of Mycobacterium-host interactions. Curr Opin Immunol *16*, 499-505.

Prajsnar, T. K., Cunliffe, V. T., Foster, S. J., and Renshaw, S. A. (2008). A novel vertebrate model of Staphylococcus aureus infection reveals phagocyte-dependent resistance of zebrafish to non-host specialized pathogens. Cell Microbiol *10*, 2312-2325.

Pressley, M. E., Phelan, P. E., 3rd, Witten, P. E., Mellon, M. T., and Kim, C. H. (2005). Pathogenesis and inflammatory response to Edwardsiella tarda infection in the zebrafish. Dev Comp Immunol *29*, 501-513.

Quiding-Jarbrink, M., Smith, D. A., and Bancroft, G. J. (2001). Production of matrix metalloproteinases in response to mycobacterial infection. Infect Immun *69*, 5661-5670.

Rahme, L. G., Ausubel, F. M., Cao, H., Drenkard, E., Goumnerov, B. C., Lau, G. W., Mahajan-Miklos, S., Plotnikova, J., Tan, M. W., Tsongalis, J.*, et al.* (2000). Plants and animals share functionally common bacterial virulence factors. Proc Natl Acad Sci U S A *97*, 8815-8821.

Ramakrishnan, L., Federspiel, N. A., and Falkow, S. (2000). Granuloma-specific expression of Mycobacterium virulence proteins from the glycine-rich PE-PGRS family. Science *288*, 1436-1439.

Rawls, J. F., Mahowald, M. A., Ley, R. E., and Gordon, J. I. (2006). Reciprocal gut microbiota transplants from zebrafish and mice to germ-free recipients reveal host habitat selection. Cell *127*, 423-433.

Redd, M. J., Kelly, G., Dunn, G., Way, M., and Martin, P. (2006). Imaging macrophage chemotaxis in vivo: studies of microtubule function in zebrafish wound inflammation. Cell Motil Cytoskeleton *63*, 415-422.

Reiling, N., Holscher, C., Fehrenbach, A., Kroger, S., Kirschning, C. J., Goyert, S., and Ehlers, S. (2002). Cutting edge: Toll-like receptor (TLR)2- and TLR4-mediated pathogen recognition in resistance to airborne infection with Mycobacterium tuberculosis. J Immunol *169*, 3480-3484.

Renshaw, S. A., Loynes, C. A., Trushell, D. M., Elworthy, S., Ingham, P. W., and Whyte, M. K. (2006). A transgenic zebrafish model of neutrophilic inflammation. Blood *108*, 3976-3978.

Rhoades, E. R., Cooper, A. M., and Orme, I. M. (1995). Chemokine response in mice infected with Mycobacterium tuberculosis. Infect Immun *63*, 3871-3877.

Rhodes, J., Hagen, A., Hsu, K., Deng, M., Liu, T. X., Look, A. T., and Kanki, J. P. (2005). Interplay of pu.1 and gata1 determines myelo-erythroid progenitor cell fate in zebrafish. Dev Cell *8*, 97-108.

Rich, A. R. (1946). Pathogenesis of Tuberculosis (Springfield, IL, Charles C. Thomas).

Rodriguez, A., Esteban, M. A., and Meseguer, J. (2003). A mannose-receptor is possibly involved in the phagocytosis of Saccharomyces cerevisiae by seabream (Sparus aurata L.) leucocytes. Fish Shellfish Immunol *14*, 375-388.

Rook, G. A., Steele, J., Ainsworth, M., and Leveton, C. (1987). A direct effect of glucocorticoid hormones on the ability of human and murine macrophages to control the growth of M. tuberculosis. Eur J Respir Dis *71*, 286-291.

Roy-Burman, A., Savel, R. H., Racine, S., Swanson, B. L., Revadigar, N. S., Fujimoto, J., Sawa, T., Frank, D. W., and Wiener-Kronish, J. P. (2001). Type III protein secretion is associated with death in lower respiratory and systemic Pseudomonas aeruginosa infections. J Infect Dis *183*, 1767-1774.

Russell, D. G. (1995). Mycobacterium and Leishmania: stowaways in the endosomal network. Trends Cell Biol *5*, 125-128.

Russell, D. G., Mwandumba, H. C., and Rhoades, E. E. (2002). Mycobacterium and the coat of many lipids. J Cell Biol *158*, 421-426.

Salgame, P. (2005). Host innate and Th1 responses and the bacterial factors that control Mycobacterium tuberculosis infection. Curr Opin Immunol *17*, 374-380.

Sanchez-Madrid, F., and del Pozo, M. A. (1999). Leukocyte polarization in cell migration and immune interactions. Embo J *18*, 501-511.

Sanders, G. E., Batts, W. N., and Winton, J. R. (2003). Susceptibility of zebrafish (Danio rerio) to a model pathogen, spring viremia of carp virus. Comp Med *53*, 514-521.

Santos, F., MacDonald, G., Rubel, E. W., and Raible, D. W. (2006). Lateral line hair cell maturation is a determinant of aminoglycoside susceptibility in zebrafish (Danio rerio). Hear Res *213*, 25-33.

Saunders, B. M., and Cooper, A. M. (2000). Restraining mycobacteria: role of granulomas in mycobacterial infections. Immunol Cell Biol *78*, 334-341.

Scanga, C. A., Bafica, A., Feng, C. G., Cheever, A. W., Hieny, S., and Sher, A. (2004). MyD88-deficient mice display a profound loss in resistance to Mycobacterium tuberculosis associated with partially impaired Th1 cytokine and nitric oxide synthase 2 expression. Infect Immun *72*, 2400-2404.

Schlesinger, L. S. (1993). Macrophage phagocytosis of virulent but not attenuated strains of Mycobacterium tuberculosis is mediated by mannose receptors in addition to complement receptors. J Immunol *150*, 2920-2930.

Schlesinger, L. S., Bellinger-Kawahara, C. G., Payne, N. R., and Horwitz, M. A. (1990). Phagocytosis of Mycobacterium tuberculosis is mediated by human monocyte complement receptors and complement component C3. J Immunol *144*, 2771-2780.

Schlesinger, L. S., Kaufman, T. M., Iyer, S., Hull, S. R., and Marchiando, L. K. (1996). Differences in mannose receptor-mediated uptake of lipoarabinomannan from virulent and attenuated strains of Mycobacterium tuberculosis by human macrophages. J Immunol *157*, 4568-4575.

Schmits, R., Filmus, J., Gerwin, N., Senaldi, G., Kiefer, F., Kundig, T., Wakeham, A., Shahinian, A., Catzavelos, C., Rak, J.*, et al.* (1997). CD44 regulates hematopoietic progenitor distribution, granuloma formation, and tumorigenicity. Blood *90*, 2217-2233.

Schorey, J. S., Carroll, M. C., and Brown, E. J. (1997). A macrophage invasion mechanism of pathogenic mycobacteria. Science *277*, 1091-1093.

Schorey, J. S., and Cooper, A. M. (2003). Macrophage signalling upon mycobacterial infection: the MAP kinases lead the way. Cell Microbiol *5*, 133-142.

Schraml, B., Baker, M. A., and Reilly, B. D. (2006). A complement receptor for opsonized immune complexes on erythrocytes from Oncorhynchus mykiss but not Ictalarus punctatus. Mol Immunol *43*, 1595-1603.

Scott, E. W., Simon, M. C., Anastasi, J., and Singh, H. (1994). Requirement of transcription factor PU.1 in the development of multiple hematopoietic lineages. Science *265*, 1573-1577.

Scott, H. M., and Flynn, J. L. (2002). Mycobacterium tuberculosis in chemokine receptor 2-deficient mice: influence of dose on disease progression. Infect Immun *70*, 5946-5954.

Seiler, P., Aichele, P., Bandermann, S., Hauser, A. E., Lu, B., Gerard, N. P., Gerard, C., Ehlers, S., Mollenkopf, H. J., and Kaufmann, S. H. (2003). Early granuloma formation after aerosol Mycobacterium tuberculosis infection is regulated by neutrophils via CXCR3-signaling chemokines. Eur J Immunol *33*, 2676-2686.

Selvaraj, P., Narayanan, P. R., and Reetha, A. M. (1999). Association of functional mutant homozygotes of the mannose binding protein gene with susceptibility to pulmonary tuberculosis in India. Tuber Lung Dis *79*, 221-227.

Shaver, C. M., and Hauser, A. R. (2006). Interactions between effector proteins of the Pseudomonas aeruginosa type III secretion system do not significantly affect several measures of disease severity in mammals. Microbiology *152*, 143-152.

Shepard, C. C. (1957a). Growth characteristics of tubercle bacilli and certain other mycobacteria in HeLa cells. J Exp Med *105*, 39-48.

Shepard, C. C. (1957b). Use of HeLa cells infected with tubercle bacilli for the study of antituberculous drugs. J Bacteriol *73*, 494-498.

Sherman, D. R., Guinn, K. M., Hickey, M. J., Mathur, S. K., Zakel, K. L., and Smith, S. (2004). Mycobacterium tuberculosis H37Rv: Delta RD1 is more virulent than M. bovis bacille Calmette-Guerin in long-term murine infection. J Infect Dis *190*, 123-126.

Shu, X., Shaner, N. C., Yarbrough, C. A., Tsien, R. Y., and Remington, S. J. (2006). Novel chromophores and buried charges control color in mFruits. Biochemistry *45*, 9639-9647.

Sichel, G., Scalia, M., Mondio, F., and Corsaro, C. (1997). The amphibian Kupffer cells build and demolish melanosomes: an ultrastructural point of view. Pigment Cell Res *10*, 271-287.

Sitprija, V., Pipatanagul, V., Mertowidjojo, K., Boonpucknavig, V., and Boonpucknavig, S. (1980). Pathogenesis of renal disease in leptospirosis: Clinical and experimental studies. Kidney Int *17*, 827-836.

Skromne, I., and Prince, V. E. (2008). Current perspectives in zebrafish reverse genetics: moving forward. Dev Dyn *237*, 861-882.

Soanes, K. H., Figuereido, K., Richards, R. C., Mattatall, N. R., and Ewart, K. V. (2004). Sequence and expression of C-type lectin receptors in Atlantic salmon (Salmo salar). Immunogenetics *56*, 572-584.

Sorensen, K. K., Tollersrud, O. K., Evjen, G., and Smedsrod, B. (2001). Mannose-receptor-mediated clearance of lysosomal alpha-mannosidase in scavenger endothelium of cod endocardium. Comp Biochem Physiol A Mol Integr Physiol *129*, 615-630.

Sorokin, S. P., and Hoyt, R. F., Jr. (1987). Pure population of nonmonocyte derived macrophages arising in organ cultures of embryonic rat lungs. Anat Rec *217*, 35-52.

Stafford, J., Neumann, N. F., and Belosevic, M. (1999). Inhibition of macrophage activity by mitogen-induced goldfish leukocyte deactivating factor. Dev Comp Immunol *23*, 585-596.

Stafford, J. L., and Belosevic, M. (2003). Transferrin and the innate immune response of fish: identification of a novel mechanism of macrophage activation. Dev Comp Immunol *27*, 539-554.

Stafford, J. L., Neumann, N. F., and Belosevic, M. (2001). Products of proteolytic cleavage of transferrin induce nitric oxide response of goldfish macrophages. Dev Comp Immunol *25*, 101-115.

Stamm, L. M., and Brown, E. J. (2004). Mycobacterium marinum: the generalization and specialization of a pathogenic mycobacterium. Microbes Infect *6*, 1418-1428.

Stamm, L. M., Morisaki, J. H., Gao, L. Y., Jeng, R. L., McDonald, K. L., Roth, R., Takeshita, S., Heuser, J., Welch, M. D., and Brown, E. J. (2003). Mycobacterium marinum escapes from phagosomes and is propelled by actin-based motility. J Exp Med *198*, 1361-1368.

Stamm, L. M., Pak, M. A., Morisaki, J. H., Snapper, S. B., Rottner, K., Lommel, S., and Brown, E. J. (2005). Role of the WASP family proteins for Mycobacterium marinum actin tail formation. Proc Natl Acad Sci U S A *102*, 14837-14842.

Stanley, S. A., Raghavan, S., Hwang, W. W., and Cox, J. S. (2003). Acute infection and macrophage subversion by Mycobacterium tuberculosis require a specialized secretion system. Proc Natl Acad Sci U S A *100*, 13001-13006.

Stead, W. W. (2001). Variation in vulnerability to tuberculosis in America today: random, or legacies of different ancestral epidemics? Int J Tuberc Lung Dis *5*, 807-814.

Stevens, E. J., Ryan, C. M., Friedberg, J. S., Barnhill, R. L., Yarmush, M. L., and Tompkins, R. G. (1994). A quantitative model of invasive Pseudomonas infection in burn injury. J Burn Care Rehabil *15*, 232-235.

Stoll, S., Delon, J., Brotz, T. M., and Germain, R. N. (2002). Dynamic imaging of T cell-dendritic cell interactions in lymph nodes. Science *296*, 1873-1876.

Stossel, T. P., and Babior, B. M. (2003). Structure, function, and functional disorders of the phagocyte system. In Blood: Principle and Practice of Hematology, R. I. Handin, S. E. Lux, and T. P. Stossel, eds. (Philadelphia, PA, Lippincott), pp. 531-568.

Sturgill-Koszycki, S., Schlesinger, P. H., Chakraborty, P., Haddix, P. L., Collins, H. L., Fok, A. K., Allen, R. D., Gluck, S. L., Heuser, J., and Russell, D. G. (1994). Lack of acidification in Mycobacterium phagosomes produced by exclusion of the vesicular proton-ATPase. Science *263*, 678-681.

Sugawara, I., Yamada, H., Li, C., Mizuno, S., Takeuchi, O., and Akira, S. (2003). Mycobacterial infection in TLR2 and TLR6 knockout mice. Microbiol Immunol *47*, 327-336.

Sun, J., and Barbieri, J. T. (2003). Pseudomonas aeruginosa ExoT ADP-ribosylates CT10 regulator of kinase (Crk) proteins. J Biol Chem *278*, 32794-32800.

Swaim, L. E., Connolly, L. E., Volkman, H. E., Humbert, O., Born, D. E., and Ramakrishnan, L. (2006). Mycobacterium marinum infection of adult zebrafish causes caseating granulomatous tuberculosis and is moderated by adaptive immunity. Infect Immun *74*, 6108-6117.

Tabel, H., and Karstad, L. (1967). The renal carrier state of experimenal Leptospira pomona infections in skunks (Mephitis mephitis). Am J Epidemiol *85*, 9-16.

Tailleux, L., Pham-Thi, N., Bergeron-Lafaurie, A., Herrmann, J. L., Charles, P., Schwartz, O., Scheinmann, P., Lagrange, P. H., Blic, J., Tazi, A.*, et al.* (2005). DC-SIGN Induction in Alveolar Macrophages Defines Privileged Target Host Cells for Mycobacteria in Patients with Tuberculosis. PLoS Med *2*, e381.

Tailleux, L., Schwartz, O., Herrmann, J. L., Pivert, E., Jackson, M., Amara, A., Legres, L., Dreher, D., Nicod, L. P., Gluckman, J. C.*, et al.* (2003). DC-SIGN is the major Mycobacterium tuberculosis receptor on human dendritic cells. J Exp Med *197*, 121-127.

Tan, B. H., Meinken, C., Bastian, M., Bruns, H., Legaspi, A., Ochoa, M. T., Krutzik, S. R., Bloom, B. R., Ganz, T., Modlin, R. L., and Stenger, S. (2006). Macrophages acquire neutrophil granules for antimicrobial activity against intracellular pathogens. J Immunol *177*, 1864-1871.

Tanji, T., and Ip, Y. T. (2005). Regulators of the Toll and Imd pathways in the Drosophila innate immune response. Trends Immunol *26*, 193-198.

Thomas, D. D., and Higbie, L. M. (1990). In vitro association of leptospires with host cells. Infect Immun *58*, 581-585.

Tobin, D. M., and Ramakrishnan, L. (2008). Comparative pathogenesis of Mycobacterium marinum and Mycobacterium tuberculosis. Cell Microbiol *10*, 1027-1039.

Tone, S., Sugimoto, K., Tanda, K., Suda, T., Uehira, K., Kanouchi, H., Samejima, K., Minatogawa, Y., and Earnshaw, W. C. (2007). Three distinct stages of apoptotic nuclear condensation revealed by time-lapse imaging, biochemical and electron microscopy analysis of cell-free apoptosis. Exp Cell Res *313*, 3635-3644.

Tonjum, T., Welty, D. B., Jantzen, E., and Small, P. L. (1998). Differentiation of Mycobacterium ulcerans, M. marinum, and M. haemophilum: mapping of their relationships to M. tuberculosis by fatty acid profile analysis, DNA-DNA hybridization, and 16S rRNA gene sequence analysis. J Clin Microbiol *36*, 918-925.

Traver, D., Herbomel, P., Patton, E. E., Murphey, R. D., Yoder, J. A., Litman, G. W., Catic, A., Amemiya, C. T., Zon, L. I., and Trede, N. S. (2003). The zebrafish as a model organism to study development of the immune system. Adv Immunol *81*, 253-330.

Trede, N. S., Langenau, D. M., Traver, D., Look, A. T., and Zon, L. I. (2004). The use of zebrafish to understand immunity. Immunity *20*, 367-379.

Trede, N. S., Medenbach, J., Damianov, A., Hung, L. H., Weber, G. J., Paw, B. H., Zhou, Y., Hersey, C., Zapata, A., Keefe, M.*, et al.* (2007). Network of coregulated spliceosome components revealed by zebrafish mutant in recycling factor p110. Proc Natl Acad Sci U S A *104*, 6608-6613.

Trede, N. S., Zapata, A., and Zon, L. I. (2001). Fishing for lymphoid genes. Trends Immunol *22*, 302-307.

Tu, V., Adler, B., and Faine, S. (1982). The role of macrophages in the protection of mice against leptospirosis: in vitro and in vivo studies. Pathology *14*, 463-468.

Ulrichs, T., and Kaufmann, S. H. (2006). New insights into the function of granulomas in human tuberculosis. J Pathol *208*, 261-269.

Ulrichs, T., Kosmiadi, G. A., Trusov, V., Jorg, S., Pradl, L., Titukhina, M., Mishenko, V., Gushina, N., and Kaufmann, S. H. (2004). Human tuberculous granulomas induce peripheral lymphoid follicle-like structures to orchestrate local host defence in the lung. J Pathol *204*, 217-228.

Valdivia, R. H., Hromockyj, A. E., Monack, D., Ramakrishnan, L., and Falkow, S. (1996). Applications for green fluorescent protein (GFP) in the study of host-pathogen interactions. Gene *173*, 47-52.

van Crevel, R., Ottenhoff, T. H., and van der Meer, J. W. (2002). Innate immunity to Mycobacterium tuberculosis. Clin Microbiol Rev *15*, 294-309.

van der Sar, A. M., Appelmelk, B. J., Vandenbroucke-Grauls, C. M., and Bitter, W. (2004). A star with stripes: zebrafish as an infection model. Trends Microbiol *12*, 451-457.

van der Sar, A. M., Musters, R. J., van Eeden, F. J., Appelmelk, B. J., Vandenbroucke-Grauls, C. M., and Bitter, W. (2003). Zebrafish embryos as a model host for the real time analysis of Salmonella typhimurium infections. Cell Microbiol *5*, 601-611.

van der Sar, A. M., Stockhammer, O. W., van der Laan, C., Spaink, H. P., Bitter, W., and Meijer, A. H. (2006). MyD88 innate immune function in a zebrafish embryo infection model. Infect Immun *74*, 2436-2441.

van der Wel, N., Hava, D., Houben, D., Fluitsma, D., van Zon, M., Pierson, J., Brenner, M., and Peters, P. J. (2007). M. tuberculosis and M. leprae translocate from the phagolysosome to the cytosol in myeloid cells. Cell *129*, 1287-1298.

Vance, R. E., Rietsch, A., and Mekalanos, J. J. (2005). Role of the type III secreted exoenzymes S, T, and Y in systemic spread of Pseudomonas aeruginosa PAO1 in vivo. Infect Immun *73*, 1706-1713.

Vigliano, F. A., Bermudez, R., Quiroga, M. I., and Nieto, J. M. (2006). Evidence for melano-macrophage centres of teleost as evolutionary precursors of germinal centres of higher vertebrates: an immunohistochemical study. Fish Shellfish Immunol *21*, 467-471.

Volkman, H. E., Clay, H., Beery, D., Chang, J. C., Sherman, D. R., and Ramakrishnan, L. (2004). Tuberculous granuloma formation is enhanced by a mycobacterium virulence determinant. PLoS Biol *2*, 1946-1956.

von Bernuth, H., Picard, C., Jin, Z., Pankla, R., Xiao, H., Ku, C. L., Chrabieh, M., Mustapha, I. B., Ghandil, P., Camcioglu, Y.*, et al.* (2008). Pyogenic bacterial infections in humans with MyD88 deficiency. Science *321*, 691-696.

Voth, D. E., Hamm, E. E., Nguyen, L. G., Tucker, A. E., Salles, II, Ortiz-Leduc, W., and Ballard, J. D. (2005). Bacillus anthracis oedema toxin as a cause of tissue necrosis and cell type-specific cytotoxicity. Cell Microbiol *7*, 1139-1149.

Wakae, K., Magor, B. G., Saunders, H., Nagaoka, H., Kawamura, A., Kinoshita, K., Honjo, T., and Muramatsu, M. (2006). Evolution of class switch recombination function in fish activation-induced cytidine deaminase, AID. Int Immunol *18*, 41-47.

Wakamatsu, Y., Pristyazhnyuk, S., Kinoshita, M., Tanaka, M., and Ozato, K. (2001). The see-through medaka: a fish model that is transparent throughout life. Proc Natl Acad Sci U S A *98*, 10046-10050.

Wang, Z., Zhang, S., and Wang, G. (2008). Response of complement expression to challenge with lipopolysaccharide in embryos/larvae of zebrafish Danio rerio: acquisition of immunocompetent complement. Fish Shellfish Immunol *25*, 264-270.

Waskiewicz, A. J., Rikhof, H. A., and Moens, C. B. (2002). Eliminating zebrafish pbx proteins reveals a hindbrain ground state. Dev Cell *3*, 723-733.

Webb, S. E., Pollard, J. W., and Jones, G. E. (1996). Direct observation and quantification of macrophage chemoattraction to the growth factor CSF-1. J Cell Sci *109 (Pt 4)*, 793-803.

Westerfield, M. (2000). The Zebrafish Book. A guide for the use of Zebrafish (*Danio rerio*) (Eugene, University of Oregon Press).

White, R. M., Sessa, A., Burke, C., Bowman, T., LeBlanc, J., Ceol, C., Bourque, C., Dovey, M., Goessling, W., Burns, C. E., and Zon, L. I. (2008). Transparent adult zebrafish as a tool for in vivo transplantation analysis. Cell Stem Cell *2*, 183-189.

Wilkinson, R. J., Patel, P., Llewelyn, M., Hirsch, C. S., Pasvol, G., Snounou, G., Davidson, R. N., and Toossi, Z. (1999). Influence of polymorphism in the genes for the interleukin (IL)-1 receptor antagonist and IL-1beta on tuberculosis. J Exp Med *189*, 1863-1874.

Willett, C. E., Cortes, A., Zuasti, A., and Zapata, A. G. (1999). Early hematopoiesis and developing lymphoid organs in the zebrafish. Dev Dyn *214*, 323-336.

Willett, C. E., Zapata, A. G., Hopkins, N., and Steiner, L. A. (1997). Expression of zebrafish rag genes during early development identifies the thymus. Dev Biol *182*, 331-341.

Worley, M. J., Nieman, G. S., Geddes, K., and Heffron, F. (2006). Salmonella typhimurium disseminates within its host by manipulating the motility of infected cells. Proc Natl Acad Sci U S A *103*, 17915-17920.

Yahr, T. L., Vallis, A. J., Hancock, M. K., Barbieri, J. T., and Frank, D. W. (1998). ExoY, an adenylate cyclase secreted by the Pseudomonas aeruginosa type III system. Proc Natl Acad Sci U S A *95*, 13899-13904.

Yang, C. W. (2007). Leptospirosis renal disease: understanding the initiation by Toll-like receptors. Kidney Int *72*, 918-925.

Yaniv, K., Isogai, S., Castranova, D., Dye, L., Hitomi, J., and Weinstein, B. M. (2006). Live imaging of lymphatic development in the zebrafish. Nat Med *12*, 711-716.

Young, D. B., and Stewart, G. R. (2002). Tuberculosis vaccines. Br Med Bull *62*, 73-86.

Zaffran, Y., and Ellner, J. J. (1997). A coat of many complements. Nat Med *3*, 1078-1079.

Zhang, Y. X., Geng, Y., Yang, J. W., Guo, X. K., and Zhao, G. P. (2008). Cytotoxic activity and probable apoptotic effect of Sph2, a sphigomyelinase hemolysin from Leptospira interrogans strain Lai. BMB Rep *41*, 119-125.

Zimmerli, S., Edwards, S., and Ernst, J. D. (1996). Selective receptor blockade during phagocytosis does not alter the survival and growth of Mycobacterium tuberculosis in human macrophages. Am J Respir Cell Mol Biol *15*, 760-770.

Zolfaghar, I., Evans, D. J., Ronaghi, R., and Fleiszig, S. M. (2006). Type III secretion-dependent modulation of innate immunity as one of multiple factors regulated by Pseudomonas aeruginosa RetS. Infect Immun *74*, 3880-3889.

Zuasti, A., Jara, J. R., Ferrer, C., and Solano, F. (1989). Occurrence of melanin granules and melanosynthesis in the kidney of Sparus auratus. Pigment Cell Res *2*, 93-99.